UNIVERSITY
OF TRENTO - Italy
DEPARTMENT OF INDUSTRIAL ENGINEERING

Doctoral School in Materials Science and Engineering

Bone Tissue Engineering: structures and strategies for functional scaffold design and evaluation

Matteo Stoppato

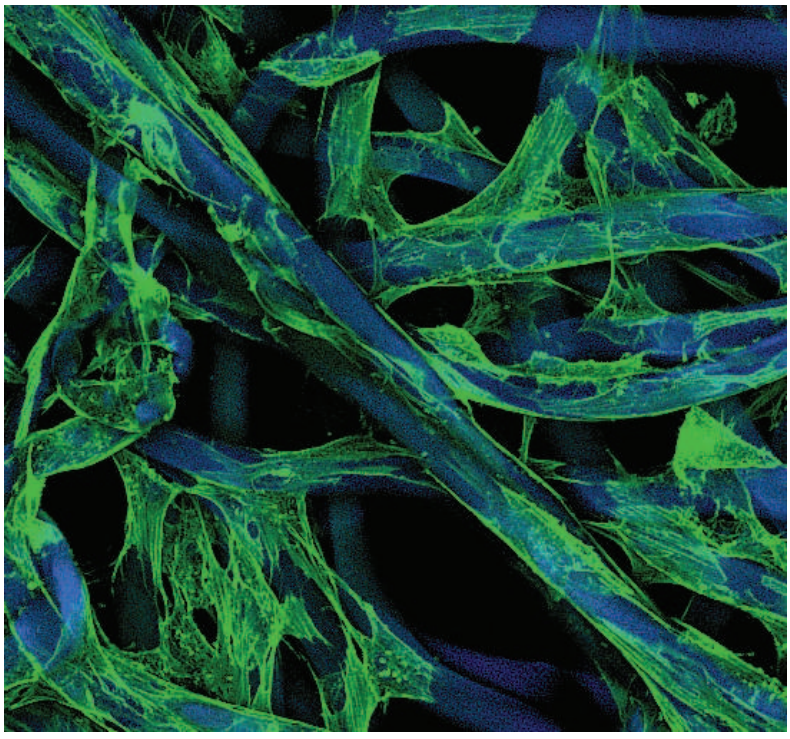

April 2013

Bone Tissue Engineering: structures and strategies for functional scaffold design and evaluation

Matteo Stoppato

E-mail: matteo.stoppato@gmail.com

Advisors:
Dr. Antonella Motta
Dr. Eleonora Carletti
Prof. Robert E. Guldberg

Ph.D. Commission:
Prof. Claudio Migliaresi
Dr. Pranesh Aswath
Prof. Orfeo Sbaizero
Dr. Arthur J Coury

University of Trento,

Department of Industrial Engineering

April 2013

.. to the people who made me live a dream. And to the people who supported me when it crashed.

Contents

List of Figures

List of Tables

Abstract

Skeletal tissue has a good ability to self-regenerate after injury through the processes of bone healing. However, bone can suffer from a wide range of pathologies, cancers or congenital defects which lead to loss of bone mass and density.

Current progresses in tissue engineering have shown great potential for creating biological alternatives and new perspectives for the treatment of bone damage and defects. In this approach, scaffolding plays a pivotal role. In particular, the principles of biomimesis have to be followed and the scaffolds have to be designed to this purpose. Furthermore, these tissue engineered systems have not only to support and guide the new tissue formation, but they have to induce a complete tissue functionality.

The aim of this research work was the application of these advanced principles to produce and evaluate scaffolds for bone regeneration.

Starting from the idea to mimic the extracellular matrix (ECM), template that characterizes the early step of the bone healing process, we design scaffolds for the evaluation of biological outputs considering the initial ECM produced by cells. We used two polymers, naturally (silk fibroin) or synthetically (poly-d,l-lactic acid) derived, and we modulated scaffold geometry (random vs ordered pore distribution), pore size and chemical composition, combining spongy and fibrous structures.

The scaffolds were indeed considered as models, to investigate if they control cell production of type I collagen, principle component of the natural template for the final mineralization. Moreover, due to the key role of vessel formation in tissue engineering and the correlation between osteoblasts and endothelial cells, the influence of the scaffolds on angiogenesis and vascularisation was assessed.

The innovation of this study consists in the evaluation shift from the final healing stage to the earlier stages. In fact, the results emphasize the possibility to correlate the scaffold morphology to type I collagen assembly, which in turn affects the final mineralization process, allowing to evaluate the tissue produced by osteoblasts from

the first steps of bone formation. Moreover, we were able to control some cell behaviours changing construct properties.

In a future research, a segmental bone defect models should be considered to better characterize the role of scaffold features during bone healing process and to determine if it would be better to use scaffolds which favour angiogenesis or mineralization to speed up a physiological bone regeneration process.

1 Introduction[1]

1.1 Extracellular matrix

The extracellular matrix (ECM) is the major component of the cellular microenvironment, or niche. The principal constituents of ECM are fibrous proteins with a support function (i.e. collagens, fibronectin, laminins, vitronectin, elastin), other specific proteins (i.e. growth factors, small matricellular proteins and small integrin-binding glycoproteins), proteoglycans (PGs) and water. Physical, mechanical and biochemical properties of tissues depend on the specific assembling and concentration of these constituents [3]. ECM undergoes to a continuous remodeling driven by cells that cleave, rearrange and deposit the different components and define the tissue architecture, with reciprocal interactions.

All cells are in connection with their ECM, either continuously or at certain stage of their life, such as at stem or progenitor cell phase or during cell migration and proliferation.

ECM most evident role is related to its scaffolding/template function for cells and tissues. In fact it can guide and regulate cell activity (i.e. proliferation, adhesion, migration, differentiation, apoptosis and gene expression) through patterned chemical signals (ligands) properly exposed to cell receptor (transmembrane proteins) as well as mechanical and structural stimuli [4].

The complex mechanism of ECM remodeling allows regulation of stem cell differentiation and it is central during growth and wound healing. Moreover, anomalous ECM dynamics generate a deregulation of cell activities, resulting in congenital defects and causing pathological tissue growths (fibrosis and cancer). Understanding and regulating the remodeling mechanisms of ECM is strategic for tissue engineering and regenerative medicine perspectives [5].

[1] Part of this chapter has been submitted as a book chapter: Carletti, E., Stoppato, M., et al. The functional role of Extra Cellular Matrix. *Scaffolds for Tissue Engineering: Biological Design, Materials and Fabrication.*

1.1.1 ECM functions

ECM defines the functional organ architecture while acting as bioactive substrate for cell adhesion, migration, growth and differentiation. Moreover, ECM serves as storage for molecules and growth factors, transmits and distributes the loads preventing mechanical failure, partitions and distributes cells in specific functional units [6].

The chemical composition, architecture, physical and mechanical properties of ECM vary according to the tissues and their specific developmental stage, age, pathological state and during the wound healing process.

1.1.2 Biochemical properties

ECM is typically a highly hydrated macromolecular network composed of various amounts of proteins and proteoglycans.

All macromolecular components of the ECM are synthesized by cells and subsequently secreted in the extracellular space where further physical-chemical modifications can take place.

Nearly all of the proteins are glycoproteins [7], characterized by oligosaccharide chains covalently attached. Most of them are fibrous structural proteins and include the large family of collagens, laminins, fibronectins and nidogens. Elastin is also a protein but without chains of carbohydrate residues attached. Proteoglycans are other proteins but consist of big clusters of carbohydrate chains, glycosaminoglycans (GAGs), attached to a core protein. Some examples are heparin sulphate (which regulates a wide variety of biological activities, including developmental processes, angiogenesis and blood coagulation), chondroitin sulphate (which is considered to stabilize brain synapses), and keratin sulphates (which are involved in various tissues development and wound healing). Among the GAGs, hyaluronic acid (HA) does not have a protein component. HA has many functions: it stimulates cytokine and angiogenesis, attracts water, influences damaged or growing tissues and allows nutrients and metabolites diffusion. Moreover, particularly during embryogenesis, hyaluronic acid creates cell-free space filled with water into which cells can proliferate and migrate.

As a highly charged protein network, rich in polysaccharide modifications, the ECM shows a wide variety of unique functions reflecting buffering, hydration, binding and

force-resistance properties [8].

GAGs can bind to a myriad of growth factors and they can control the diffusive range and accessibility of ligands to their receptors. Heparan sulphate proteoglycan, for example, facilitates interactions between ligands and their receptors and has the capability to bind to various growth factors [9].

ECM acts as a molecular "reservoir" binding to ligands and creating a concentration gradient of many growth factors produced by cells, such as bone morphogenetic proteins (BMPs), fibroblast growth factors (FGFs), hedgehogs (HHs), and Wnt proteins (signaling molecules that control cell-cell communication) [10, 11].

It is widely recognized that the unique chemical composition of each tissue, due to the mix of the components described, maintains biological and biochemical information, guiding cells behavior and tissue organization.

1.1.3 Physical properties

The physical properties of ECM refer to its morphology (i.e. shape, structure, porosity, pattern), topography (related to the surface), water content, and biomechanical characteristics. ECM has a clear structural function, fundamental in connective tissues, but still significant in all the other tissues where a support for cell is provided.

Some of the ECM proteins, such as collagens and elastin, are organized in fibrils/fibers forming the ECM skeletal structure and providing the tensile strength and viscoelasticity of the tissue. The network solidity is instead guaranteed by linking proteins, working as natural crosslinkers, including collagens, fibronectin, laminin, and nidogen [3, 4, 11].

The most evident role of ECM is related to its scaffolding/template support function. More generally, ECM supports tissues structure, ensuring their integrity and favoring cell anchorage and migration or, in the case of basement membrane, creating a barrier for cells and factors migration [4, 10, 12, 13, 14, 15]. The cell-ECM constant interaction is fundamental to maintain the proper ECM composition and assembling, which, in turn, can promote cell movement and orientation. It has been demonstrated the importance of the ECM structure on the formation of tissue during its healing process and, in particular, that the orientation of collagen fibrils can significantly impact on cell arrangement and, consequently, on matrix formation [16, 17].

ECM is a composite material which comprises a fibrous structural net (fibrillar and

elastic proteins) embedded in a of porous hydrated gels matrix of glycosaminoglycans (GAGs). The ratio between the constituents varies according to the tissue.

GAGs and proteoglycans can combine to form huge polymeric complexes, and they are also connected with fibrous matrix proteins (i.e. collagen) and with protein networks (i.e. basal lamina), creating a continuous complex fiber arrangement [18, 19, 20]. GAGs tend to arrange in a highly extended conformations that occupy a large volume, forming gels even at low concentrations. The high density of negative charges in the chain attracts cations, Na^+, that are osmotically active, thus forcing a large amounts of water into the matrix. This creates a swelling pressure, that enables the matrix to withstand compressive forces (in contrast to collagen fibrils, which resist stretching forces). As mentioned before, one of the main glycosaminoglycans is the hyaluronic acid, also important for its resistance to compressive forces due to its capacity to attract water. Chondroitin sulphate is another glycosaminoglycan that contributes to the tensile strength of cartilage, tendons, ligaments and walls of the blood vessels.

The ECM biomechanical behavior describes the reaction of ECM to loads, such as compressive, tensile, bending, torsion and shear stresses applied by cells or external forces [21]. These loads have a great impact on the ECM characteristics, influencing its elasticity/rigidity. ECM mechanical properties range from those of soft and compliant structures, as in adipose tissue, brain, or muscles, to those of stiff and rigid tissues, as bones [22, 23]. Tissues clinical studies suggest that ECM elasticity plays a significant role in organ homeostasis and function, recognizing that diseased tissues have markedly altered elasticity compared to the healthy ones and that changes in tissue stiffness may indicate a pathologic condition [24, 25]. Indeed, the extent of tissue stiffness is often considered a good prognostic indicator for disease [8].

1.1.4 Mechanical transduction

It is widely accepted that mechanical stimuli have an important role in tissue-organ development and physiological processes. In fact, cells and ECM have a dynamic 3D interrelationship that is kept in balance and influenced by internal and external stimuli, to control cell phenotype and matrix maintenance process. Local mechanical cross-talk between cells and the surrounding environment is described by Provenzano et al. [26] as a unifying principle that connects ECM micro- and nano-scale structure with cell shape, distribution and differentiation.

Cells have indeed developed sophisticated mechanosensors and systems, such as filaments, integrins and cytoskeleton, connecting cells with ECM. In this way, external forces can modify nuclear architecture, chromatin organization and, consequently, gene expression and cell differentiation [27, 28, 29].

This means that external mechanical stimuli are transduced to cells through the ECM that they are connected to, then cells are able to convert sensed mechanical stimuli into biochemical pathways leading to different cell activities.

Part of such bidirectional communication between ECM and cells, is a result of a direct mechanical connection between fibrous protein in the ECM and cell cytoskeleton via integrins. Integrin-mediated cell-ECM interactions promote the assembly of cytoskeletal and signaling molecule complexes at focal adhesion sites. These complexes include Src-family members, focal adhesion kinase (FAK), phosphatidylinositol-3´-kinase (PI3K), and phospholipase C (PLC) [30, 31]. Accordingly, cells do not only exert forces, but also respond to the resistance sensed through cytoskeleton organization/tension, triggering several intracellular signaling pathways [32].

In coordination, it seems that there is a synergy between mechanical stimuli and hormones, growth factors, and inflammatory mediators which collectively activate the same signalling pathways [29, 30, 33, 34, 35].

During development, ECMs are able to adapt to the higher mechanical demands, by increasing the size of the necessary tissue components [34, 36].

Furthermore, mechano-chemical transduction is altered in aging connective tissues. In fact, recent evidence suggests that tension applied by cells to ECM is reduced or lost during aging and diseases such as osteoarthritis [37]. The reduction observed is similar to changes that occur as a result of disuse [38].

Mechanical transduction seems to be particularly important even during wound healing. In this case, cells that are moving into a wounded area to synthesize new ECM produce cellular contractile forces, and, simultaneously, in the final phases of the process, the ECM tension transmitted through integrins can modulate cell fate, removing the unneeded cells and organizing the new tissue.

1.2 Bone composition and morphology

Bone is a dynamic and highly specialized form of connective tissue. The main function of bone is to sustain and protect the soft tissues of the body, and it acts as a storage facility for systemic mineral homeostasis. Bone tissue is characterized by a unique composition which gives a marked rigidity and strength while still maintaining a good degree of elasticity.

The bone structure consists of approximately 65-70%w mineral, 20-25% protein, 8-9% water, and less than 1% cell amount [39]. Collagen constitutes approximately 95% of the organic matrix (which 99% is type I Collagen); the remaining 5% is composed of proteoglycans and numerous non-collagenous proteins.

The major component of bone is, however, mineral. The main bone mineral components are calcium phosphates, especially hydroxyapatite ($Ca_5(PO_4)_3(OH)$). It forms prism crystals, with a length of 20 nm and a thickness of 2 nm. The presence of minerals combined with an appropriate distribution of collagen fibers in the extracellular matrix provides strong mechanical properties in terms of hardness, and compressive, tensile, and torsion strength. From a material science perspective, it is possible to describe the bone properties as if it was a composite material due to its organic and inorganic components [40].

The relatively cell-free bone tissue comprises 4 different kinds of cells: osteoprogenitor cells, osteoblasts, osteocytes, and osteoclasts. Osteoprogenitor cells, deriving from periosteum, present a high proliferative ability and are able to differentiate in bone cells [41]. Osteoblasts tend to form sheets on the bone surface during tissue formation and their role is to secrete the type I collagen and the non-collagenous proteins, synthesizing and mineralizing new ECM. After the appropriate bone deposition, osteoblasts decrease their metabolism and finally differentiate into osteocytes. The osteocyte is the most abundant cell type of bone and is responsible for its maintenance and remodeling [42]. These cells have the capacity not only to synthesize, but also to resorb matrix to a limited extent. Each osteocyte occupies a space, or lacunae, within the matrix. Instead, osteoclasts are large (100-200 μm), multi-nucleated cells, developed from hemopoietic cells of the monocyte–macrophage lineage, that resorb bone. Active osteoclasts exhibit a characteristic polarity with nuclei typically locate in the part closer to the removed bone surface [43].

Bones can be classified as long bones (e.g. femur, tibia), short (e.g. carpal, tarsal), and flat (e.g. cranium, irregular bones). The resulting structure of the skeleton

is influenced heavily by the individual's mechanical loading history, acting both as constraints and as driving forces in its architecture [44, 45].

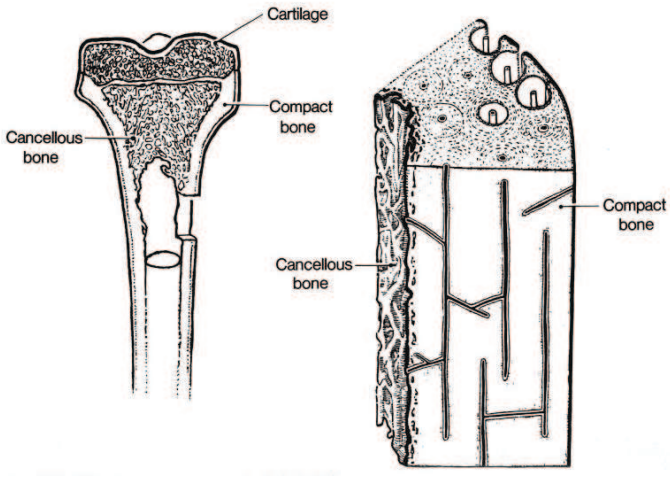

Figure 1.1: Bone morphology

Morphologically, there are two main types of bone: compact (cortical) and trabecular (cancellous or spongy). In compact bone, densely packed collagen fibrils form concentric lamellae, and the fibrils in adjacent lamellae run in perpendicular planes as in plywood. Trabecular bone has a loosely organized, porous matrix. Differences in the structural arrangements of the two bone types are related to their primary functions: cortical bone, more solid, provides mechanical and protective functions and trabecular bone, more porous, provides metabolic functions [39, 46].

Thanks to cell activity, bone tissue undergoes a continuous renewal in a delicate equilibrium between synthesis and degradation of the extracellular matrix. Its metabolism and regeneration are under the influence of a variety of molecules and local factors, such as Insulin-like Growth Factor (IGF), Fibroblast Growth Factor (FGF) and Bone Morphogenetic Protein (BMP).

There are two principal physiologic processes of bone production: intramembranous and endochondral ossification. Intramembranous ossification is the direct laying down of bone into the primitive connective tissue occurs during embryonic development by the direct transformation of mesenchymal cells into osteoblasts. Endochondral ossification provides a mechanism for the formation and growth of the skeleton during growth of the individual and it involves cartilage as a precursor [47]. Both require a solid base and a well-developed vascular supply for the modification and mineralization of the extracellular matrix.

1.2.1 Collagen

Collagen is the most abundant family of proteins constituting the extracellular matrix in animals and it represents one third of the total protein in humans [48, 49, 50]. Collagens are the major structural elements of all connective tissues and they provide stability and structural integrity of tissues and organs [51].

Collagen molecules form the characteristic fibrillar and micro-fibrillar networks contributing to the basement membrane structure as well as other structures of the extracellular matrix. If originally it was widely accepted that all collagens were secreted by fibroblasts in connective tissue, in the last decade, the knowledge on the collagen family increased considerably identifying that osteoblasts, numerous epithelial cells and other cell type are able to produce certain types of collagens [52].

So far, 28 genetically distinct collagen types have been described in vertebrates [53, 54, 55, 56]. The different collagen types are characterized by considerable complexity and diversity in their structure, their splice variants, the presence of additional, non-helical domains, their assembly and their function. Based on their structure and supramolecular organization, they can be grouped in different families. The most widespread family of collagens with about 90% of the total collagen is represented by the fibril-forming collagens, comprising collagen types I, II, III, V, and XI. These collagens are characterized by their ability to assemble into highly orientated supramolecular aggregates with a characteristic suprastructure, with diameters between 25 and 400 nm. Type I contributes to the structural backbone of bone [57, 58] and it is the most abundant and best known.

The central feature of collagen is characterized by three parallel polypeptide chains (which generally consists of two identical chains and an additional chain that differs slightly in its chemical composition) arranged in a helical conformation. The amino acid composition of collagen results in a repeating X-Y-Gly sequence, where X and Y can be any amino acid (often proline and hydroxyproline) and Glycine is found at almost every third residue.

Collagen, as other secreted protein, follows a standard biosynthesis pathway. Collagen chains are synthesized as longer precursors called procollagens, delivered and packaged within the Golgi apparatus into secretory vesicles and released into the extracellular space, where they are finally assembled and cross-linked. The resultant protein consists almost completely of a triple-stranded helix, which is 1.5 nm in diameter and 300 nm long [52, 59].

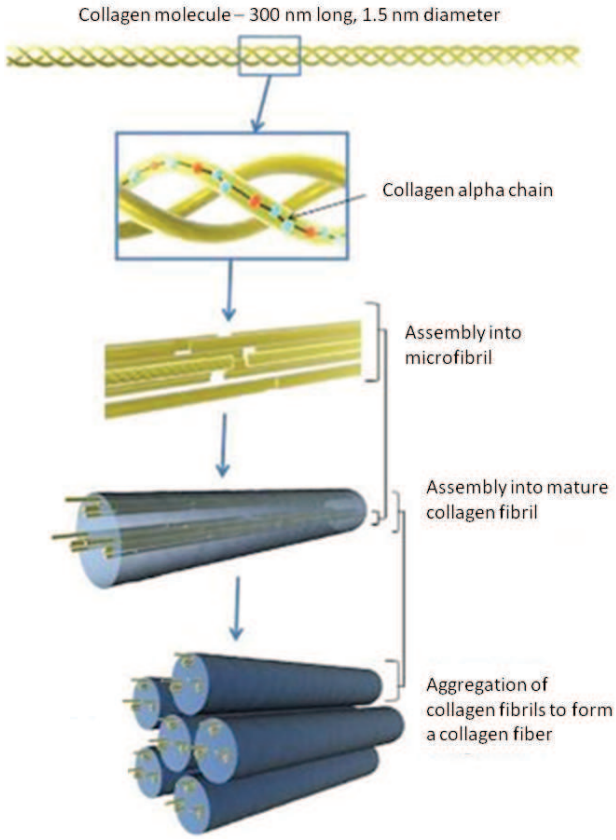

Figure 1.2: Representation of collagen assembly.

The importance of collagen is attributed to many of its essential characteristics, including thermal stability, mechanical strength and the ability to interact with other biomolecules and cells. These properties are derived from the triple-helix structure with its interstrand hydrogen bonds, hydroxylation of Proline residues in the Y position and covalent crosslinking within the triple helices. The hierarchical nature of collagen organization permits the assessment of its mechanical properties at different levels of structural complexity, including the tropocollagen monomer, individual collagen fibrils, and collagen fibers [50]. For example it was determined that the fracture strength of a tropocollagen monomer is higher than that of a collagen fibril, 11 Gpa versus 0.5 Gpa, probably due to the covalent bonds breakage necessary in the first case. Another measure of the strength is through the quantification of shear modulus, connected to the rigidity. Hydration of collagen fibrils reduced their shear modulus significantly, whereas cross-linking increased their shear modulus. It is significant that a certain level of cross-linking is favorable for the mechanical properties of collagen fibrils, however, high cross-linking results in a brittle collagen

fibrils structure, a general symptom of aging [60]. In fact, an excessive high crosslink density does not permit a high energy dissipation during deformation and leads to a dehydrated collagen that results strong but not tough [61].

1.3 Bone healing

Bone healing is a process that combine certain aspects of skeletal development and growth involving a complex interplay of cells, growth factors and extracellular matrix. Conventionally the process is explained in four stages. In the early step, the cellular inflammatory reaction is followed by fibrocartilage tissue production (soft callus tissue). This is the natural fingerprint for the formation of hard callus, that is physiologically replaced by the final bone, either cortical or trabecular, remodeled and completed in an ultimate stage. During the repair process every newly formed tissue evolves from the previous and the entire healing mechanism results from the development of these overlapped stages [1, 62, 63, 64, 65, 66].

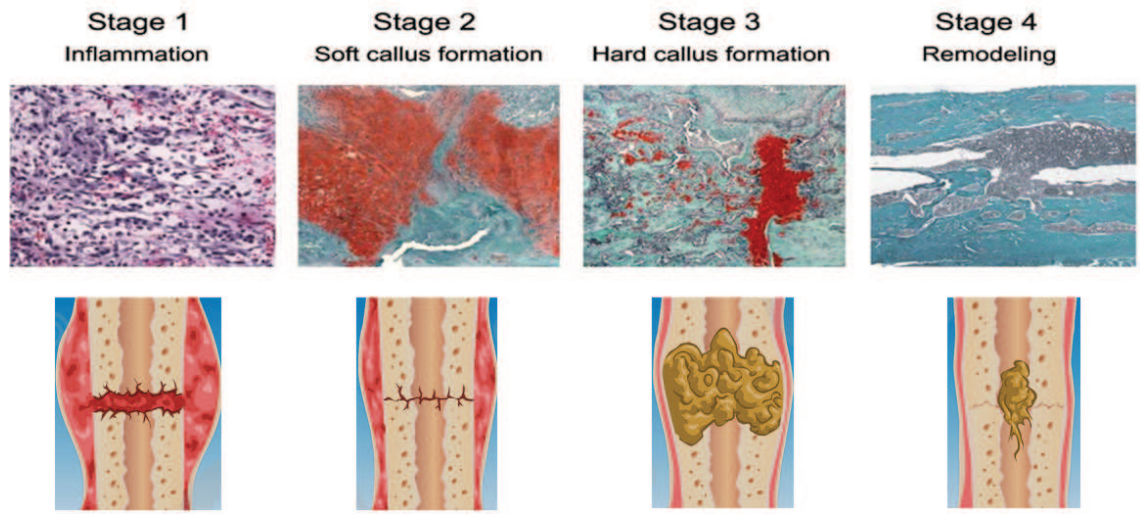

Figure 1.3: A representative series of images of the four-stage model of fracture healing. Adapted from Schindeler et al.[1]

1.3.1 Stage 1: inflammation

A bone damage is typically associated with disruption of the local soft tissue integrity, causing the bleeding within the site and the development of a hematoma. The initial phase of wound healing is non-specific and it is characterized by an up regulation of inflammatory mediators. Degranulating platelets, macrophages and inflammatory cells are recruited in the site of tissue injury to combat infection, secrete cytokines and growth factors, and advance clotting into a fibrinous thrombus. Over time, endothelial cells produce new capillaries into the clot, which is

reorganized into granulation tissue. Macrophages, giant cells and other phagocytic cells clear degenerated cells and other debris. This cellular response is coordinated by the secretion of a range of cytokines and growth factors. The in situ scenery, when an inflammation condition is present, is extremely complex and not only cells and molecules are interested but also the ECM with its biophysical features and geometrical characteristics [1, 62, 67, 68, 69, 70].

1.3.2 Stage 2: soft callus formation

Fractures are usually characterized by some level of mechanical instability. Ossification is therefore preceded by a cartilaginous template, a soft callus, that provides a semi-rigid support to the fracture. Chondrocytes and fibroblasts are the cells responsible for the synthesis of the cartilaginous matrix, temporary plug between the fractured fragments, that is subsequently replaced. Chondrocytes, derived from mesenchymal progenitors, before going through apoptosis undergo hypertrophy and mineralize the cartilaginous matrix. An important role is played by the growth factors that guide fibroblast proliferation, chondrocyte behavior and regulate vascular morphogenesis of larger vessels and collateral branches from existent vessels [1, 62, 66].

1.3.3 Stage 3: hard callus formation

This stage is dominated on a cellular level by osteoblasts which differentiate from osteoprogenitors in the presence of osteogenic factors. The progenitor cells originate from many sources such as periosteum, bone marrow, vasculature and surrounding local tissues. During this step osteoblasts produce the woven mineralized bone matrix, starting in the stable areas of the soft callus. In order for bridging new hard callus, the unstable soft callus is gradually removed, concomitant with revascularization. The vasculature is a key point for formation of the hard callus because it increases oxygen tension in the local region that seems necessary for progenitor cells that develop into osteoblasts [1, 62, 66].

1.3.4 Stage 4: bone remodeling

This final stage is characterized by bone remodeling, a process where hard callus is replaced and new cortical or trabecular bone is formed. The key cell type involved

are osteoclasts which resorb the surface of the bone and osteoblasts, which secrete new bone. In particular, osteoclasts pump acid and proteinases into the resorption domain to demineralise the matrix and to degrade the organic components, such as collagen. Contemporary, osteoblasts lay down new bone, and secrete cytokines that influence osteoclast behavior and are responsible for the coordination of bone formation and bone resorption. During this stage vascularization is sustained [1, 62, 66].

1.4 Bone damage, degeneration and clinical treatment

In general, bone has a good ability to self-regenerate. However, bone can suffer from a wide range of disorders. Among all the disorders, fractures, which lead to delayed or non-union defect, are common. When the critical size is exceeded, a surgery procedure is required for complete recovery. Moreover, in the orthopedic field, extensive bone reconstruction is needed in case of widespread loss, as resulting by severe congenital malformations, trauma, hypoplasia, ischemic necrosis, primary neoplastic lesions (osteosarcoma, benign bone tumors) or secondary (metastases). Due to the aging of the population and the spread of these disorders, socioeconomic considerations of possible treatments are a major concern [71].

Internal or external fixator are commonly used to provide bone transfer along the defect, to support functions and finally to adjust the bone length and alignment. However, the process rate is relative slow, leading to complications in prolonged treatment, such as infections, contractures and edema.

Currently, bone-grafting plays a predominant role. The current gold standard for bone graft is the autograft, which involves harvesting bone from the patient's own body. This strategy is commonly considered a safe solution in terms of compatibility and immune response absence, but also uncomfortable for patient in which a second surgery is needed. Furthermore, the graft availability may limit the application of this technique.

Another strategy uses allograft bone, derived from humans and harvested from an individual other than the one receiving the graft. When the defect size exceeds the homologous donor possibility, allografts may be a good alternative. Anyway, several studies have demonstrated how allograft transplantation results in poor and inadequate remodeling, reabsorption and revascularization, with problems concerning the graft rejection and the risk of infections.

As alternative, the use of synthetic bone grafts has been explored, producing bone graft substitutes made from ceramics or metals. They are used to provide a replication of the missing bone segment or joint, but poor integration, high probability of infections and rejections can occur, as well as technical problems involving breakage, friction wear and loosening, precluding their general use in orthopedic field.

All of these options, each having its own advantages and drawbacks, are still not

able to provide an adequate replacement for full recovery of the patients. Therefore, tissue engineering may result as a viable alternative with the progression in this field [72, 73, 74].

1.5 Tissue Engineering

In 1988, during a conference organized by the National Science Foundation, the term tissue engineering (TE) was for the first time introduced and defined as the "application of the principles and methods of engineering and life sciences in order to understand the fundamental relationships between the structure and functions in mammalian tissues (both normal and pathological) and to develop biological substitutes to restore, maintain and improve tissue functions" [75]. The idea of this interdisciplinary field is to replace or regenerate tissues which have been compromised by trauma or pathologies allowing cell growth and thus restoring the original tissue.

The main approach consists in producing a functional tissue starting from a scaffold. Scaffolds are three dimensional structures made of natural and/or artificial materials and populated by cells, before or after implantation. The chemical, physical and biological properties of the scaffold have to be designed carefully, to guide the tissue regeneration. To improve tissue development specific signals can be conjugated to the material to engineer the construct. These signals can be chemical (i.e. growth factors) or mechanical (i.e. hydrostatic pressure or compressive stimulation) and their aim is to help processes such as tissue morphogenesis, ECM functional distribution throughout the scaffold and cell differentiation [75].

The main challenge of this strategy is to control the 3D tissue development in a functional way. The achievement of this goal is dependent on many variables: the use of a cell-free or a pre-seeded scaffold, the choice of the most appropriate cell source, the material of the scaffold, the design of the morphological, chemical and physical properties of the scaffold, the parameters of the in vitro culture, the concentration of growth factors, and so on.

The strategy generally followed consists in mimicking characteristics and properties of the biological system to be regenerated. This principle is well known as biomimetics. After all these considerations, the complexity of the tissue engineering approach appears evident.

Nevertheless, applications are today commercially available, for instance for skin regeneration to heal burns or diabetic ulcers and many studies are currently in progress in the field of cardiovascular, urologic, neurologic, orthopedic and muscular diseases. Results remain indeed promising and more and more benefits will soon be available for patients.

1.5.1 Scaffolds

Nowadays the importance of the extracellular matrix structure is well known. For this reason, in a TE perspective, considerable effort has been devoted to obtain 3D functional scaffolds. It is in fact recognized how cells in conventional culture plates do not retain normal behavior due to the lack of in vivo 3D environment.

Scaffolds should be designed to have a high reproducibility and appropriate characteristics such as porosity, interconnected geometry, elasticity and chemical composition, giving the material the right degradable or resorbable rate [76, 77]. These requirements make the production of artificial substrates very challenging.

A scaffold can be developed by modulating different properties which in turn determine its biocompatibility, defined exhaustively by Williams [78]: "Biocompatibility refers to the ability of a biomaterial to perform its desired function with respect to a medical therapy, without eliciting any undesirable local or systemic effects in the recipient or beneficiary of that therapy, but generating the most appropriate beneficial cellular or tissue response in that specific situation, and optimizing the clinically relevant performance of that therapy".

Scaffolds have mainly a structural role, supporting cell growth and allowing a certain scaffold integrity during tissue regeneration [77]. At the same time the scaffold porosity should permit nutrient supply, waste removal, cell migration and vascularisation.

A growing variety of techniques have been developed to manipulate natural and synthetic materials and, scaffold design, has become increasingly precise, from the macro to the nanoscale level. This multi-scale approach of structural design allows to control scaffold characteristics and it is considered especially important because nature often derives properties from multi-scale or hierarchical structures.

Natural ECM is a fully hydrated matrix and for this reason wettability is a key property to be taken into account [79]. Synthetic bulk materials with a hydrophilic behavior are indeed better at mimicking the aqueous physiologic environment. Consequently, hydrogels, networks of hydrophilic polymer chains, have been used as 3D matrix materials [80, 81] even if lack of mechanical properties and cell binding motifs are common drawbacks.

Another possibility extensively studied was to design scaffolds based on the characteristic fiber conformation of ECM proteins. Nano and micro structured fibrous constructs to support and guide cells have been produced, mimicking the physical

structure of the extracellular matrix.

In addition to mimic the mechanical and morphological properties of the ECM, scaffolds can also mimic some aspects of molecular recognition. A strategy consists to mix natural molecules to the scaffold, either adding the ECM components in an appropriate ratio while creating the synthetic polymer scaffold; or covalently attaching the desired ECM protein/peptide or glycosaminoglycan to the backbone polymer [82]; or impregnating an already created polymeric scaffold with an appropriate combination of ECM macromolecules [83, 77].

3D biomimetic scaffolds can be also obtained isolating the main constituents of the ECM and using them after purification without further modifications. The idea is to utilize decellularised and sterilized natural extracellular matrix with biomolecules of the natural ECM maintaining the physiological information. This would help to overcome the lack of cell recognition signals usually noticed using synthetic matrix.

In addition, the goal to mimic the complex structures and regulation processes within the living tissue has been persecuted using scaffolds in coordination with more complex co-culture systems and/or bioreactors, tools to analyze cellular interactions in different biological and environmental conditions [84].

1.5.2 Materials

To fabricate a scaffold, several so-called biomaterials have been proposed and used: polymers, metals, ceramics and composites.

For bone tissue engineering, the most commonly used materials are natural and synthetic polymers, due to their degradation properties; while in some other bone applications, ceramic materials (i.e. calcium phosphate, glass ceramic, chalk calcium carbonate, coralline hydroxyapatite) are also used, especially combined with polymers as composites, due to their mechanical properties.

Natural derived polymers are obtained by extraction from living organisms and include agarose [85, 86], alginate [81, 87], chitosan, collagen, glycosaminoglycan (GAG) [88], hyaluronic acid [89, 90, 91], silk fibroin [92, 93, 94, 95], and finally starch [96, 97]. They possess usually a good interaction cell-material, low toxicity, low chronic inflammatory response and an ideal environment for cell growth but exhibit poor engineering properties and are characterized by a certain variability. Moreover, the main problem is to understand which are the induced stimuli. In fact, cell response may not be what expected or desired.

Synthetic polymers, such as polycaprolactone (PCL) [98, 99], poly(glycolic acid) (PGA) [100, 101], poly(lactic acid) (PLA), or their copolymers (i.e. PLGA poly(lactic-co-glycolic acid) [102, 103, 104, 105] or PCLLA Poly(ε-caprolactone-co-lactide)), or blends, are generally less biocompatible than the natural polymers and it is necessary to evaluate the possible toxicity of the released monomers. On the other hand they have high and tunable properties, they are easily processed and adapted and the results are usually more reproducible.

1.5.3 Process techniques

Bioartificial scaffolds are porous, degradable structures fabricated from polymers. They can be nets, sponges, sheets, gels, or highly complex structures with intricate pores and channels, fabricated using materials processing technologies. The fabrication techniques must provide the correct design for cell support, adhesion, migration, proliferation, differentiation and subsequently ECM biosynthesis. The commonly used techniques can be divided in two main categories; in the first case, scaffolds are generated with a random structure, in the second category porous scaffolds are produced with predetermined design and architecture, normally using a computer-assisted device and with the material deposited layer by layer.

SOLVENT CASTING/PARTICULATE LEACHING

To produce thin films, polymer solution is casted on a support until the volatile solvent evaporates. This well exploited technique allows to obtain good film quality, desired thickness, and uniformity controlling process parameters, such as solution viscosity, chemistry of the solvent, and process conditions. Solvent casting is often used in combination with particulate leaching to obtained 3D porous scaffolds. Porogen agents such as ammonium bicarbonate, glucose, and sodium chloride, are added to the polymer solution and, after solvent evaporation, leached out.

FREEZE DRYING

This process is based on the competition between solute interfacial concentration gradient and surface energy and consists in the solvent sublimation under proper pressure and temperature conditions. By controlling parameters such as polymer

concentration, quenching temperature and cooling rate it is possible to tune pore size, distribution, and alignment as well as mechanical properties [106].

PHASE INVERSION

A polymer solution is cast in a proper support and a second, non-miscible solvent is subsequently added. Under specific conditions, the solvent and the non-solvent induce the solution to phase-separate, obtaining a porous scaffold. Important parameters are solution viscosity, polymer density, interfacial energy and mechanical stirring. In tissue engineering, supercritical carbon dioxide is recently become an attractive non-solvent due to its non-toxic properties [107, 108, 109].

ELECTROSPINNING

A high voltage is applied to a polymeric solution that is extruded from a needle. The solution becomes charged, the electrostatic repulsion counteracts the surface tension and a liquid jet is formed. The jet dries in flight and the resulting submicrometric fibers are collected on the grounded collector. The main parameters which govern this process are solution properties, electric field strength, distance between collector and needle, temperature and humidity. The final result is a nonwoven fibrous structure in which fiber orientation, morphology, thickness, and mesh spacing can be controlled [88, 110, 111, 112].

STEREOLITHOGRAPHY

A photopolymerizable polymer solution is cast, layer by layer, using a specific light source (generally UV) to selectively polymerize it. When the structure is concluded, the extra solution is washed away and it is cured. This technique shows some limitations such as a low resolution and a limited availability of biocompatible photopolymers.

SELECTIVE LASER SINTERING

A CO2 laser beam is used to activate a sinterization process of polymeric powder. The temperature is increased locally, fusing polymer particle to each other. Also in this case, scaffolds are built up layer by layer.

3D PRINTING

3D printing use an additive process, where successive layers of material are laid down in different shapes, using digital technology. The three-dimensional printing technology was developed at the MIT [113]. Scaffolds were produced by stacking different layers in which a binder solution was injected into selected areas of sequentially deposited layers of powder [96, 114]. Another strategy, known as fused deposition modeling, is based on the use of a micro-extruder, which deposits successive layers of a polymer solution or a melt on a support substrate. The micro-extruder or the substrate can move in the x-y-z directions at a proper speed directed by a computer-controlled mechanism. Scaffolds geometry and properties depend on the viscosity of the polymer melt or solution, pressure applied to the extruder, temperature, and humidity [115].

1.6 Bone tissue engineering

The limitations associated with clinical use of autografts and allografts continue to drive efforts to develop bone graft substitutes using the principles of biomaterials and tissue engineering.

As mentioned before, tissue engineering requires a scaffold with proper physical, chemical and mechanical properties. In this contest, osteogenic, osteoconductive, and osteoinductive properties have to be taken in considerations. Osteogenic refers to the capacity of bone cells to contribute to develop bone tissue in the construct, osteoconductive to the material capacity to guide the reparative growth of the natural bone, and osteoinductive to the property of encouraging undifferentiated cells to become active osteoblasts.

Numerous types of synthetic scaffolds have been fabricated and investigated trying to understand how different scaffold design variables can influence the biologic response. Structural scaffolds with adequate mechanical properties must often be surface modified or combined with bioactive components to achieve good biological properties. In the last decade advances in biomaterial synthesis and characterization have been exploited to create a multitude of possible choices for the selection of scaffold materials.

Many researchers are focusing their attention among the many possible combinations of growth factors, cells, and genes to promote bone tissue formation. In spite of these impressive efforts, biomaterials that precisely control the survival, proliferation and fate of stem cell populations in vitro and in vivo are still not well developed. Moreover, it is not completely clear how physical and morphological properties interact with cells and tissues. Nevertheless it is nowadays recognized that a scaffold for bone tissue engineering, to be attractive, has to be biomimetic and designed to control cell behavior [72, 116, 117].

1.7 Angiogenesis in tissue engineering

Engineered tissues of relevant sizes that exceed the diffusion limit (1-2 mm), require a vascular network capable of supplying oxygen, nutrients, signaling molecules and removing waste. Insufficient blood vessels cause a decrease of cell viability and function as well as tissue formation and ischemia, leading to the failure of the engineered tissue [118, 119, 120]. For this reason, the growth and development of vessels in the engineered constructs has become a major goal in tissue engineering.

New blood vessels are formed through two main processes:

- angiogenesis: new vessels sprout from pre-existing blood vessels or, in the case of intussusception, the lumen of an existing blood vessel splits to form two separate vessels;
- vasculogenesis: new blood vessels are formed by recruited endothelial cells differentiated from endothelial progenitor cells (EPCs).

In order to develop and establish a functional vascularization, a variety of approaches are currently used.

The use of scaffolds alone made with angiogenic biomaterials can be used to recruit endogenous cells to vascularize the scaffold in situ. This is a simple, cost effective and versatile method of inducing angiogenesis, exploiting the vascular response induced by inflammation during scaffold implantation.

Decellularized scaffolds have been also used to provide a natural template for recreating the vascular network.

Current approaches to therapeutic angiogenesis focus on the angiogenic growth factor released from biomaterial scaffolds, permitting a localized and sustained delivery of these molecules. The challenge in this case consists in controlling the right delivery rate profile of more growth factors and in using the proper dose of each one of them [121].

Scaffolds can be also used to deliver specific cells (i.e cells transfected with genes that allow over-expression of angiogenic factors).

Another strategy focuses on scaffold prevascularization. In this case endothelial cells can be seeded onto the scaffolds to create tube-like structure. Alternatively, scaffolds can be implanted subcutaneously *in vivo* until they are vascularized and, subsequently, relocated in the desired site. In both case anastomosis (the capacity of the scaffold vasculature to connect to the host vasculature) is fundamental [121, 122].

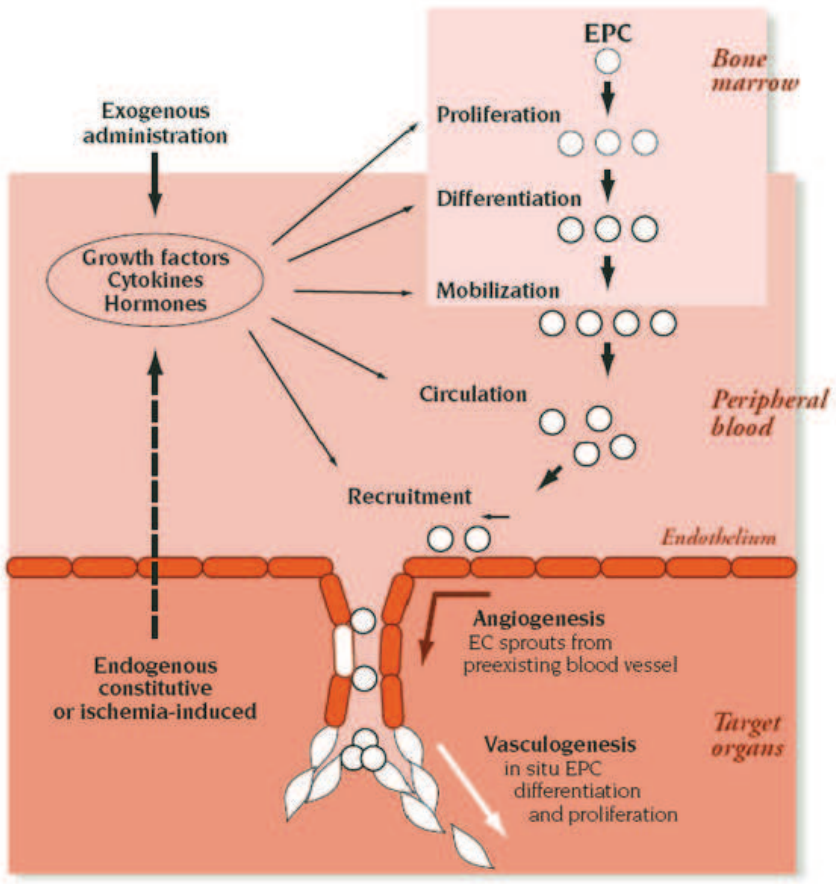

Figure 1.4: Neovascularization encompasses both angiogenesis and vasculogenesis. Angiogenesis represents the classic paradigm for new vessel growth, as mature, differentiated endothelial cells form sprouts from parental vessels. Vasculogenesis involves participation of endothelial progenitor cells that, recruited, form new blood vessels. Images adapted from Isner at al.[2].

In coordination to the creation of vascularized tissue, it is finally essential that the formed vessels are functional and persist over time [119].

2 Research strategies and objectives

2.1 Thesis rationale

In the previous chapter, the skeletal system and the key role of ECM were introduced. Then, it was described with particular attention the leading strategies employed today and the issues remained open in the field of bone healing and regeneration. Finally, the principles of tissue engineering were defined, focusing on how their application can potentially overcome the limits of the current treatments for bone defects.

The final objectives of the presented research work were the production and the evaluation of scaffolds for bone regeneration.

Starting from the concept of biomimicry a multicomponent scaffold to regenerate bone was design. We hypothesized to be more efficient to try mimicking the ECM template that characterized the early step of the bone healing process, rather than the final bone tissue. In this way the normal regeneration progression would be supported by scaffolds able to support cells and to trigger their response in a physiologic way. The reference ECM chosen was therefore the one present in the soft callus and not the final mineralized matrix.

Contemporary, the research focused on the evaluation of the cell response to the scaffold properties. We decided to modify scaffold features and to investigate carefully the type I collagen network production and assembling because it represents the natural template for the final mineralization.

Moreover, due to the key role of vessel formation in TE and the correlation between osteoblasts and endothelial cells, the influence of the scaffolds on angiogenesis and vascularization was assessed.

For those reasons different scaffolds were proposed, modifying geometries, morpholo-

gies and chemical compositions. The produced constructs were used as model to understand the strict relation between cell behavior, scaffold properties and ECM production/assembling.

In the next sections materials, structures and setups used are introduced and described.

2.1.1 Scaffold fabrication

2.1.1.1 Materials

In this work scaffolds were produced using two polymers: one from synthetic origin, poly-d,l-lactic acid (PdlLA), and one from natural origin, silk fibroin (SF).

PdlLA

Poly-d,l-lactic acid is a aliphatic polyester. This is a very interesting category of synthetic polymer because of their good mechanical properties, tailorability and controlled degradation rate [123, 124, 125]. Due to the chiral nature of lactic acid, two stereoisomeric forms are possible and distinct polymers can be obtained: the two stereoregular polymer PdLA, PlLA, and the PdlLA. Poly-l-lactide (PlLA) is the product resulting from the ring-opening polymerization of l-lactide; it presents a crystallinity of about 37% with glass transition temperature between 50°C and 80°C and fusion temperature between 180°C and 190°C. Poly-d-lactide (PdLA) is analogous to PlLA but it is derived from polymerization of d-lactide. Poly-d,l-lactide is the racemic polymer obtain from a mixture of d- and l-lactic acids; it has an amorphous structure presenting a glass transition temperature at about 60°C.

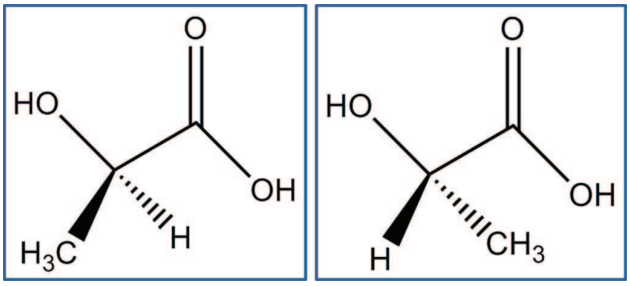

Figure 2.1: The two stereoisomeric forms of lactic acid: PdLA and PlLA.

The degree of crystallinity strongly affects the water uptake and the degradation kinetic; in fact, amorphous regions offer a better accessibility and mobility to water

molecules and degradation occurs at higher rate. Differences in crystallinity also influence the mechanical properties with semicrystalline materials characterized by higher performance [126].

The material itself and its degradation products were studied to verify the biocompatibility and toxicity. Publications report good biocompatibility results, with only some few inflammatory responses [127]. Among polyester family, PLA is very interesting because it is soluble in many different solvents, it is easy to process in different 3D structures and, depending on the process story, it degrades in 2 to 12 months [128].

Poly-d,l-lactic acid (PdlLA, type RESOMER® 207, MW= 252 kDa) was purchased from Boehringer Ingelheim, Germany. The polymer was used without further purification. The two solvent used, dichloromethane (DCM) and dimethylformamide (DMF), were obtained from BDH Chemicals (UK) and J.T.Baker (Holland), respectively.

Silk fibroin

The term silk indicates the protein polymers synthesized by epithelial cells in specialized glands of Arachnids and some Lepidoptera. According to their animal origin, silk proteins differ in composition and final configuration, but some general properties can be identified: their primary structure is usually simple and repetitive, while the secondary structure is mostly β-sheet because of the predominance of amino acids with a short lateral chain in hydrophobic domains. These domains allow the

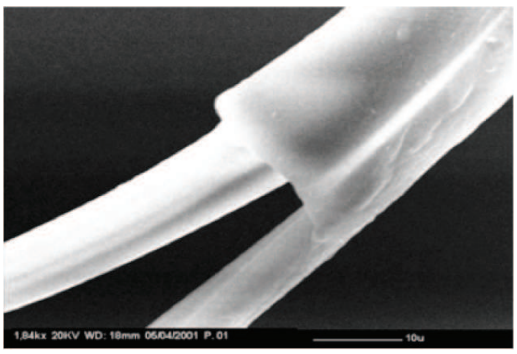

Figure 2.2: Scanning electron micrograph of a partial degummed silk filament.

formation of a packed tertiary structure thanks to the establishment of hydrogen bonds along protein chains. This assembly gives silk high resistance and resilience, which are needed during the formation of cocoons or spider webs [129].

Silk from Bombyx mori cocoons has been widely utilized as biomaterial. The fibers have a diameter of 10-25 µm and consist of two inner filaments of fibroin coated by a layer of sericin, which acts as a glue and represents 25-30% of the whole fiber [130]. A fibroin molecule is made of two protein chains, a light chain (about 26 kDa) and a heavy chain (about 390 kDa) in a ratio 1:1. They are joined by disulfide bonds between two cysteine amino acids and by a glycoprotein called P25 that is non-covalently linked to both fibroin and sericin [129]. Amino acid composition of fibroin from Bombyx mori consists mainly of glycine (43%), alanine (30%) and serine (12%). The heavy chain is formed by 12 domains which compose the crystalline regions of the silk fiber: they are repetitions of sequences Gly-X, where X can be one of the following amino acids: alanine, serine, valine or threonine. As previously indicated, the formation of crystalline structures is due to the short lateral chains of the amino acids in these regions, which allow protein folding in a β-sheet conformation [131]. The secondary structure of the less crystalline portions of the heavy chain is random coil because the bigger lateral chains, which cause a steric effect [129].

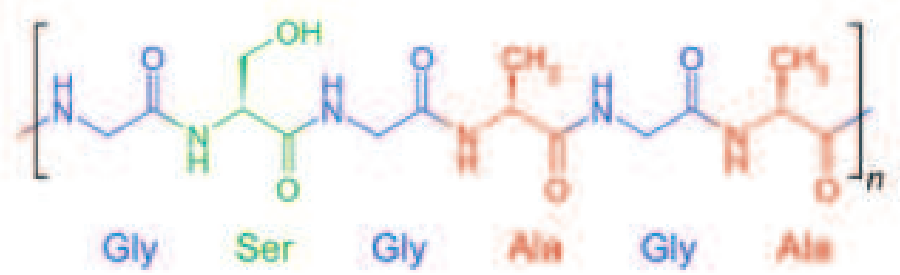

Figure 2.3: Typical amino acid sequence of fibroin.

Silk fibroin exists in two different polymorphisms: the glandular state before crystallization (Silk I) and the state which follows its extrusion with the formation of β-sheet secondary structures (Silk II). When fibroin is in a Silk I state, it is water soluble and can be easily crystallized by heat or shear stresses. Fibroin can be in a Silk I state also in the aqueous solution obtained *in vitro*. After crystallization, β-sheet structures are asymmetric: one side is occupied by the hydrogen atoms of glycine residues, while methyl groups of alanines populate the other side. Strong hydrogen bonds and van der Waals forces form a structure which is thermodynamically stable [129].

Degradation of fibroin is proteolytic and usually mediated by a foreign body response. During degradation less crystalline regions of the protein are broken in

peptides which can be phagocytized by cells more easily.

Biocompatibility of this natural polymer has been extensively established. It was observed that silk sutures could elicit hypersensitivity in some cases, but it was demonstrated that the major cause of these responses was sericin. Once sericin is removed by degumming, the biological response of fibroin is comparable to all biomaterials [129, 130].

In addition, silk fibroin has the nature of a multifunctional material which possesses active domains in the linkers among hydrophobic blocks, which can be recognized by cell receptors and demonstrated to stimulate cell adhesion and growth [132].

2.1.1.2 3D structures

Microfabricated scaffold

The microfabrication system, developed and optimized in our laboratories is able to fabricate scaffolding supports of controlled geometry.

The microfabrication system consists of three independent slides (National Instrument, Austin, Texas, US), that move a platform where the polymer solution is extruded and the scaffold is built on. The extrusion system is composed by a glass

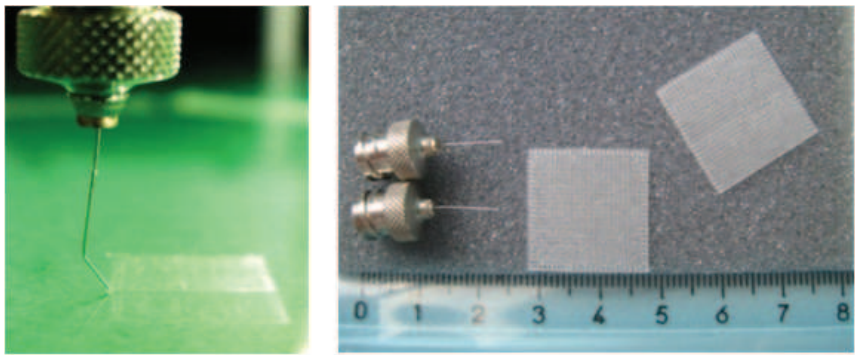

Figure 2.4: On the left the polymer extrusion from the metal micro-needle. On the right typical microfabricated scaffolds.

syringe fixed up on an automatic pumping system (11 Plus, Harvard Apparatus, Massachusetts, US) by which it is possible to set the proper flow rate; a metal micro-needle (HamiltonTM, 34 gauge - 60 microns inner diameter; 1 cm length, 90º point style) is connected to the glass syringe by a luer-lock mechanism.

The polymer solution is deposited from the needle of the glass syringe with a constant flow rate on a polyethylene terephthalate (PET) platform. Scaffold is built on layer

by layer in the vertical direction. Each layer is composed by a series of parallel fibers, deposited by the syringe through a back-and-forward movement. The distance between the fibers, which influences the properties of the scaffold, is a parameter controlled with the software (LabVIEW). Once a layer is completed, the support moves down, then, another layer is deposited, whose fibers are perpendicular to those of the previous one.

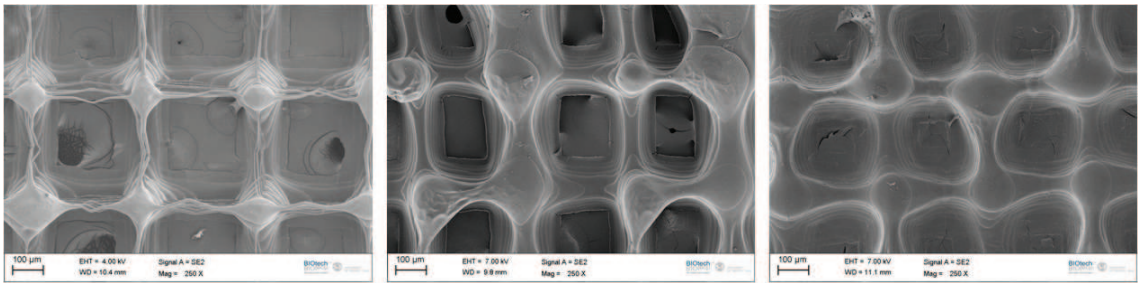

Figure 2.5: Scanning electron microscopy images of PdlLA microfabricated scaffolds obtained changing polymer solution concentrations.

The process strongly depends on environmental variables (such as temperature and humidity) and parameters such as number of layers, distance between fibers, pressure applied to the syringe, viscosity of the solution, motor speed and dimensions of the needle.

Some examples of PdlLA scaffolds obtained changing some parameters are reported Fig. 2.5.

Sponge

Sponges are one of the most used scaffolds in bone Tissue Engineering, especially because of their high porosity.

Several techniques can be employed, such as solvent casting particulate leaching (with salt or glucose as porogen) and freeze-drying, which may be eventually combined with gas foaming.

In particular, solvent casting particulate leaching, the technique selected, allows the formation of a more interconnected porosity and a higher control on pore dimension. Briefly, porogen agents are added to the polymer solution and, after solvent evaporation, leached out. In this work NaCl was selected as porogen and the polymer was first dissolved in (70:30 v/v) dichloromethane/dimethylformamide solvent. The final suspension of polymer solution and porogen was then dried under hood

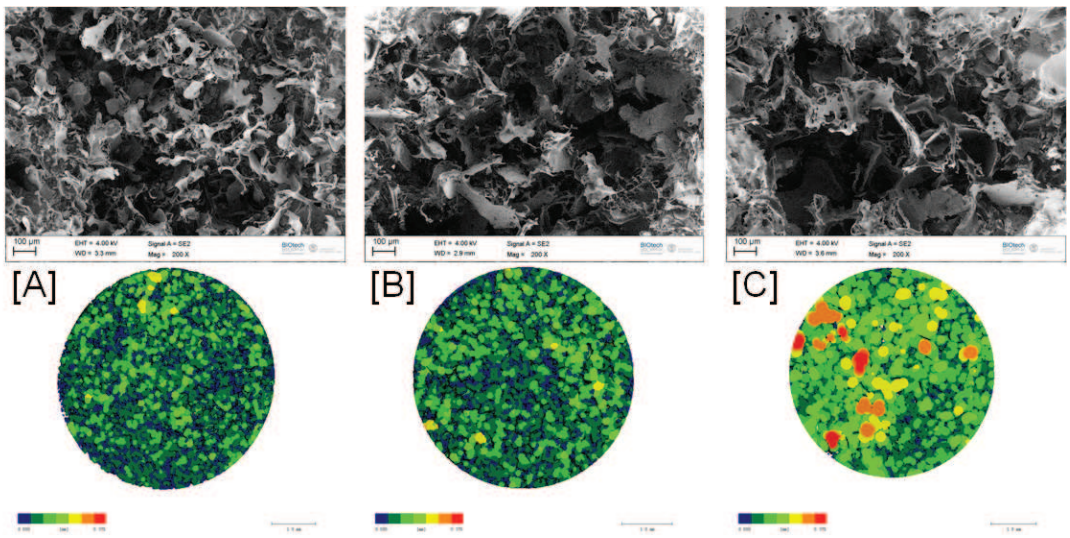

Figure 2.6: On the top scanning electron microscopy images of PdlLA sponges. Scale bars = 100 μm. On the bottom micro-CT color-coded pore diameter scale images. NaCl particulates with three different dimensional ranges were used: (A) 240-315 μm, (B) 315-425 μm, and (C) 425-1180 μm

overnight and washed into distilled water for 3 days to eliminate both the residual solvent and the salt.

The obtained sponges were finally air dried at room temperature Setting the proper combination of process parameters was very important to produce porous, well interconnected and homogeneous scaffolds. Therefore, parameters such as polymer concentration, NaCl amount and range size were optimized to obtained the specific properties requested each times.

Images of sponges produced varying NaCl range size are shown in Fig. 2.6, while in Fig. 2.7 there are some quantitative data obtained to characterize the same scaffolds. In each chapter there are the specifications of the scaffolds produced.

Sponge with SF fibers

The fibers were obtained from Bombyx mori silkworm cocoons.

The idea was to use fibrous elements with active domains producing a scaffold more similar to the natural ECM. Cocoons were boiled in two aqueous alkaline baths of Na2CO3 (1.1 and 0.4 g/l, respectively), 1 hour each, in order to remove from the fiber the external sericin coating and obtain fibroin. Degummed silk fibers were then washed several times in distilled water and dried at room temperature. Then 0.05 g

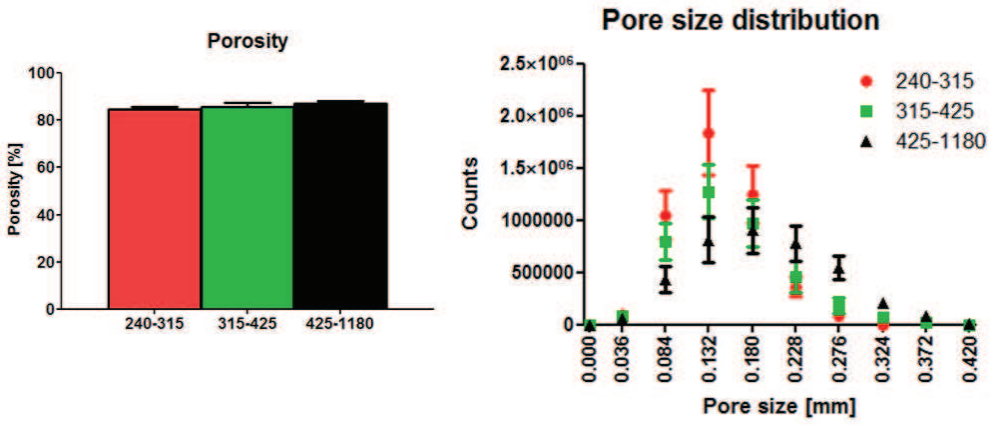

Figure 2.7: On the left porosity of the three scaffolds. On the right pore size profile of the three scaffolds.

of these spread fibers was mixed with sieved NaCl particulates, ranging from 425 to 1180 µm as before, and the PdlLA solution (see chapter 2.1.1.2.2), obtaining a 1:14 w/w polymer/porogen final concentration. The mixture was air dried (24-36 hours) and immersed in deionized water (dH2O) for 3 days with changes every 6 hours for the removal of the porogen.

The parameters (PdlLA concentration, NaCl and SF fibers amount, porogen range size) were chosen after several attempts, trying to optimize porosity and interconnectivity. Images of scaffold with different PdlLA concentration and SF fibers amount are shown in Fig. 2.8.

2.1.2 Cells

In this work three main type of cells were used: MG63, hMSC and HUVEC.

2.1.2.1 MG63

Human osteosarcoma-derived osteoblasts (MG63) are derived from malignant bone tumor and have properties consistent with the characteristics of normal osteoblast line. These osteoblast-like cells are often used as model of osteoblasts, especially in studies testing biomaterials. Despite of gene expression profile has some differences respect to primary osteoblast, MG63 are considered a good model due to the constant properties they show. Moreover these cells, as osteoblast cells, express alkaline phosphatase, osteocalcin and type I collagen.

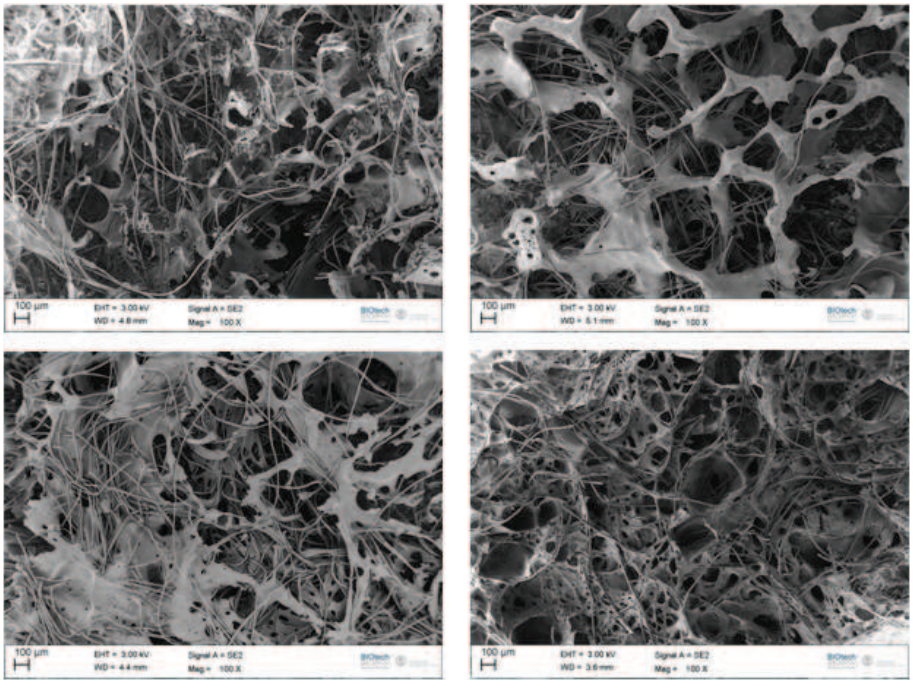

Figure 2.8: Scanning electron microscopy images of PdlLA sponges with SF fibers. The concentration of the initial polymer solution is different as the amount of the SF fibers.

2.1.2.2 hMSC

Human mesenchymal stem cells (hMSC) are multipotent stromal cells with the ability to differentiate into osteoblasts (bone cells), chondrocytes (cartilage cells), adipocytes (fat cells) and neurons (nervous system cells). They were originally identified in the bone marrow stroma, where they regulate key stages of haematopoiesis. MSCs have a great capacity for self-renewal while maintaining their multipotency. The degree to which the culture will differentiate varies among individuals and how differentiation is induced. The capacity of cells to proliferate and differentiate is known to decrease with the age of the donor, as well as the time in culture.

2.1.2.3 HUVEC

Human umbilical vein endothelial cells (HUVECs) are cells isolated from the vein of the umbilical cord. They therefore have the characteristics of venous endothelial cells. They express specific venous markers and they also express all specific markers of endothelial cells, whose surface antigens PECAM-1, CD144 and KDR, and vWF factor, expressed in an intra-cytoplasmic manner. HUVECs are used as a laboratory

model system for the study of the function and pathology of endothelial cells.

2.1.3 Animal model

A rat model in which each animal received four dorsal subcutaneous implants was selected for its simplicity and its capability of responding by producing angiogenesis. The experiment was performed at Georgia Institute of Technology (Atlanta, US), under approval of the Georgia Institute of Technology Institutional Animal Care and Use Committee. All animals were treated humanely per the guidelines outlined in the Guide for the Care and Use of Laboratory Animals by the National Institutes of Health (US).

2.2 Outline and objectives

The skeletal system is unique in its capacity to regenerate after injury through the processes of bone healing.

Factors that influence the repair process, particularly in situations of challenging trauma or disease, include proper biological signals and sufficient vascularization.

The regenerative processes of osteogenesis and angiogenesis are strictly linked at both cellular and molecular levels, and the responses of osteoblasts and endothelial cells have been shown to be correlated *in vitro*.

Despite the knowledge on the bone healing, characterized by different steps, the evaluation of the cell response at the first stages has not been deeply studied.

The overall objective of this work was therefore to investigate the role of scaffold properties in osteogenesis and angiogenesis. The strategy was to design constructs with the proper morphology and to evaluate the results focusing on the early step of bone healing and not only on the final mineralization. This objective was evaluated in the following specific aims.

CHAPTER 3 - AIM I

Determine the efficiency of different scaffold geometries exploring the relationship among them and collagen 3D organization.

Two scaffolds, made with the same chemical composition but different 3D architecture (a random versus a ordered structures), were used as model to verify different influence on biological outputs. In particular the analysis of the collagen distribution was performed to evaluate if different morphology lead to different collagen assembling and organization. The results show that scaffolds with random porosity distribution seem to allow a collagen organization similar to the natural callus matrix.

CHAPTER 4 - AIM II

Evaluate the effects of in vitro scaffold pore size on ECM matrix produced by MG63.

In this *in vitro* study we compared three different salt leached PdlLA scaffolds obtained by varying the pore size range. This work is targeted to the intermediate stage of bone healing and collagen I assembling evaluation was combined with gene expression measures of common genes involved in the osteogenesis. Results showed that

pore size plays an important role in cell behavior and ECM development. Moreover, a strict relation between collagen I assembly and mineralization was demonstrated.

CHAPTER 5 - AIM III

Evaluate angiogenic effects of SF fibers on a PdlLA engineered constructs.

The development of an extracellular matrix in most tissues, including bone, is dependent upon the establishment of a well developed vascular supply to provide oxygen and nutrients to regenerating tissues. We hypothesized that incorporation of silk fibroin fibers to a PdlLA sponge enhances the construct capacity to better support endothelial cell colonization *in vitro* and to promote *in vivo* vascularization.

CHAPTER 6 - AIM IV

Evaluate angiogenic and osteogenic response of hMSC in a co-culture model onto different functionalized engineered constructs.

In vitro studies have shown that endothelial cells regulate the function of osteoblast cells and vice versa. In this study we check the ability to support endothelial cells and bone regeneration, testing two different scaffolds and two different setups: hMSC and a co-culture of hMSC and HUVEC. The goal was to underline the influence of endothelial cells and if the results are dependent on the scaffold properties.

Chapter 3 has been temporarily removed due to copyright restrictions. It was an already published articles. Original source: Stoppato M, et al., Functional role of scaffold geometries as a template for physiological ECM formation: evaluation of collagen 3D assembly. Journal of Tissue Engineering and Regenerative Medicine (2013), 7(2), 161–8.

4 Influence of scaffold pore size on type I collagen development: a new in vitro evaluation perspective[1]

4.1 Abstract

Bone tissue engineering takes part in the complex process of bone healing by combining cells, chemical/physical signals and scaffolds with the scaffolds providing an artificial ECM network. The role of the support template for cell activity is crucial to guide the healing process. This in vitro study compared three different PdlLA scaffolds obtained by varying the pore size generated by applying different salt leaching processes. The influence of pore dimensions on the ECM matrix produced by human osteosarcoma-derived osteoblasts (MG63 cell line) seeded on these different materials was analyzed. This work is targeted on the intermediate stage of the bone healing process, where a collagen network is beginning to develop by the growing osteoblasts representing the template for the ultimate stage of bone formation. Imaging analyses assessed by confocal laser microscopy were combined with gene expression measures of the most common genes involved in the bone healing process. Furthermore, in vitro evaluations were carried out to investigate cell morphology, proliferation and viability. Results showed that different pore size matrixes can affect ECM development and that cell organization, collagen I assembly and mineralization are strictly correlated.

[1]The work presented in this chapter was published in Journal of Bioactive and Compatible Polymers as Stoppato M, et al., Influence of scaffold pore size on collagen I development: A new in vitro evaluation perspective. Journal of Bioactive and Compatible Polymers (2013), 28(1), 16–32.

4.2 Introduction

Tissue engineering for bone regeneration is based on developing scaffolds, which are structural supports able to mimic the native tissue-like environment, and to assist, once combined with cells, a complete healing process. The main idea is to reproduce the natural Extracellulalar matrix (ECM) with scaffolds able to simulate the physiological ECM features and to interact biomolecularly with cells tuning their functions and guiding the entire multicellular events of ECM formation and tissue regeneration [75, 169].

ECM of connective tissues is a fibrous composite that surrounds cells comprising many biological components. It is the main component of bone combining inorganic and organic parts. Osteoblasts are responsible for ECM synthesis and mineralization. ECM components are central to every phase of wound healing. In the early step, the cellular inflammatory reaction is followed by a fibrocartilage tissue production (soft callus tissue). This is the natural fingerprint for the formation of hard callus, that is physiologically substituted by the final bone, either cortical or trabecular, remodeled and completed in an ultimate stage. During the repair process every newly formed tissue evolves starting from the previous and the entire healing mechanism results from the development of these overlapped stages [1, 62, 63, 64, 65, 66].

Tissue engineering efforts to create functional biological tissues relies on 3D scaffolds as temporary artificial ECM frameworks [170]. 3D constructs are currently produced by different techniques using biocompatible polymers, either of synthetic or natural origin. Different features can be achieved and have to be taken into account when designing a scaffold for bone tissue reconstruction. Therefore, mechanical properties and geometrical features (pore size, pore morphology and interconnectivity) should be selected considering the mechanisms of biocompatibility described by Williams [78, 171], that is the ability of a material to perform with an appropriate host response during the regenerative phase.

In the present study, implications of scaffold geometry and collagen assembling on the ultimate stage of mineralization of bone tissue were assessed. In a previous work [16] a comparison between constructs with a regular ordered structures (microfabricated scaffolds [144]) versus constructs with random morphologies (salt leached sponges) was carried out to evaluate which architecture was more efficient as scaffold to promote osteoblast-like cell activity. Particular attention was paid on the collagen 3D organization, the natural template for the subsequent mineralization.

The study demonstrated that a scaffold with a randomly organized structure, rather than an ordered porous matrix, was more favorable as a template for a physiological collagen assembly from a bone tissue regeneration perspective.

Based on this previous study and beginning with a salt leached scaffold morphology from poly-d,l-lactic acid) (PdlLA) polymer [148, 163, 172], three different pore size ranges were obtained by varying the porogen granulometry. The goal was to develop an in vitro model to evaluate how different scaffold pore sizes can affect cell behavior in terms of collagen I production, development, arrangement and mineralization. A human osteosarcoma-derived osteoblast (MG63) cell line was used for a preliminary in vitro biological evaluations [173]. Cell growth, distribution, proliferation and activity were studied. Imaging analysis by confocal laser microscopy, after marking collagen I with a specific antibody, was combined with collagen quantification as well as gene expression assessment by the reverse transcription quantitative polymerase chain reaction (RT-qPCR) analyses. The expression of the most significant osteogenic genes (RUNX2, Decorin and Alp) was evaluated [174]. AlizarinRed staining was finally used to determine the degree of mineralization.

4.3 Materials and Methods

Production of the salt-leached scaffolds

Sponges with randomly distributed pores were produced by solvent casting particulate leaching technique [126, 136, 150]. PdlLA (Resomer R207S, Boehringer Ingelheim Germany) was dissolved in dichloromethane:dimethylformamide (70:30 v/v) to obtain a 7% (w/v) solution. Sieved NaCl particulates with three different dimensional ranges (240-315 µm, construct S1; 315-425 µm, construct S2; and 425-1180 µm, construct S3) were mixed into the PdlLA, obtaining a 1:25 w/w polymer/porogen final concentration. The mixture was air dried (24-36 hours) and immersed in deionized water (dH_2O) for 3 days with changes every 6 hours for the removal of the porogen.

All the scaffolds were prepared with a thickness ranging from 2 up to 3 mm by casting into glass petri dishes, then, once detached, they were cut into discs with 6 mm diameter. Before use in in vitro cell culture studies, scaffolds were sterilized with aqueous ethanol solution 70% (v/v) at 4°C for 24 hours and dried under a sterile hood at room temperature. Scaffold modifications due to the sterilization process were not detected.

Scaffold characterization

Scanning electron microscopy (Supra 40 Zeiss, operating mode: high vacuum, secondary electron detector) was used for the evaluation of scaffold surface morphologies. Samples were previously sputter-coated with a thin gold layer under argon atmosphere (SEM Coating Unit PS3, Assing S.p.A., Rome, Italy).

Scaffold pore size ranges were estimated by SEM imaging analyses using ImageJ software. Three different scaffolds of each type (S1, S2 and S3) were analyzed and a total of 150 pores per sample were considered.

Sponge porosity was assessed by a liquid displacement method similar to a previously described technique [161, 162, 163]. Briefly, scaffolds were immersed into a 5 ml graduated cylinder containing a known volume of ethanol (V_1). After evacuation of the air from the pores and ethanol penetration into them the volume of ethanol was recorded as V_2. The ethanol-impregnated scaffold was taken from the cylinder and the remaining ethanol volume was measured as V_3. The scaffold porosity was given

by the formula
$p = \frac{V_1 - V_3}{V_2 - V_3}$.
The measures of porosities resulted from a triplicate analysis.

In vitro cell culture

After sterilization, scaffolds were placed in 96-well plates and washed several times with sterile, distilled water. Samples were seeded with 20 µl media containing 5·104 cells, human osteosarcoma-derived osteoblasts (MG63 cells). After 1.5 hours media were added and after 24 hours, scaffolds were moved from the original well plate to a new one and incubated for a total of 28 days. Results were evaluated at six experimental time points: 2, 5, 9, 14, 20 and 28 days. Minimum essential medium (MEM) supplemented with 10% Fetal Bovine Serum (FBS), 1% Penicillin, 1% Glutamax, 1% Vitamin, 1% non-essential amino acids comprised the culture medium. The culture medium was further supplemented with ascorbic acid (50 µg/ml) and 10 mM ß-glycerophosphate after nine days. Cells were incubated at 37ºC in a 5% CO2 atmosphere incubator, with medium changes every 2-3 days.

Proliferation

Cell number and its variations during the culturing time was measured through the DNA quantification, using the PicoGreen assay (Quant-iT PicoGreen dsDNA Assay Kit, Invitrogen). At predetermined time points the medium was removed from wells and the scaffolds washed with PBS. 500 µl of 0.05% Triton-X was used to completely cover the scaffold before freezing and storing at -20°C until analysis. Each thawed sample was then sonicated for 10 seconds using a tip of an ultrasonic processor (UP400S Hielscher Germany). Samples were aliquoted in triplicate (100 µl each) into a 96 Nunclon delta black microwell and 100 µl of PicoGreen working solution was added to each well. Fluorescence was read by a spectrophotometer (excitation wavelength: 485 nm, emission wavelength: 538 nm, Tecan Infinite M200 Pro, Switzerland). To correlate fluorescence to DNA concentration, a calibration curve was generated using DNA standards at a known concentration, provided with the assay. The DNA amount of each sample was divided by 7.7 pg of DNA, the average amount of DNA in a human cell according to literature [175], to finally obtain the cell number.

Cell viability

The cellular metabolic activity was measured using alamarBlue assay kit (Biosource International Inc., USA) at each culturing time. AlamarBlue is reduced by metabolically active cells. The assay was performed according to the manufacturer's instructions. In brief, the seeded scaffolds were incubated for 3 hours at 37°C with fresh culture medium (with reduced serum) supplemented with alamarBlue diluted, simply adding the alamarBlue reagent as 10% of the sample volume. The references were taken from wells with unseeded scaffolds, also incubated with the alamarBlue solution. The resulting fluorescence was read on a fluorescence spectrophotometer (excitation wavelength: 565 nm; emission wavelength: 595 nm, Tecan Infinite M200 Pro, Switzerland).

In addition, to visualize viable cells, they were stained with CalceinAM (Invitrogen C3099). According to the manufacturer's instructions, cells were incubated with medium containing 0.1 mM of the reagent for 15 min and then examined by confocal laser microscopy system (Nikon Eclipse, Ti-E).

Cell morphology and distribution, collagen I fibers assembling

Cell attachment, growth, distribution and migration as well as collagen I fiber formation were detected using specific stainings and visualized by confocal laser microscope (Nikon Eclipse, Ti-E). The surface figures result from stacking multiple horizontal images corresponding to different focused planes.

Cell growth and distribution were visualized by Oregon Green 488 phailloidin (Biosource International, Invitrogen) and DAPI (Sigma Aldrich) staining. To detect collagen I a primary rabbit antibody to human type I collagen was used (Meridian Life Science, Saco, ME, USA). Briefly, fixation with a formaldehyde solution (4% formaldehyde in PBS solution) was performed. After rinses with PBS, samples were incubated with the primary antibody (in PBS containing 1% bovine serum albumin, BSA) overnight at 4°C. The seeded scaffolds were then rinsed with PBS/BSA and incubated with Alexa Fluor 546 goat anti-rabbit secondary antibody (Biosource International, Invitrogen) for 1.5 h at room temperature. Cells were permeabilized with TritonX (0.2% TritonX in PBS solution) and stained with Oregon Green 488 phailloidin and DAPI, according to the manufacturer's protocol. After the final rinses with PBS, samples were examined by confocal microscopy.

Collagen quantification

The Sircol Collagen Assay kit (Biocolor Ltd., Belfast, United Kingdom) was used to analyze the amount of collagen produced by MG63, according to the manufacturer's instructions. Briefly, scaffolds were incubated overnight at 4°C in pepsin (0.1 mg/ml 0.5 M acetic acid) to obtain the collagen into solution. Sircol Dye Reagent was added and mixed for 30 minutes. The collagen–dye complex was precipitated by centrifugation, washed with ice-cold Acid-Salt Wash Reagent, centrifuged and drained. Finally, Alkali Reagent was added to recover the dye and 200 µl of each sample were transferred to a 96 micro well plate. The absorbance at 555 nm was measured by a microplate reader (Tecan Infinite M200 Pro, Switzerland).

ECM mineralization

ECM mineralization was viewed after specific staining, AlizarinRed (Sigma Aldrich), by a stereo microscope (Leica Wild M3Z Stereozoom Microscope). Samples were washed with PBS and fixed in a 99% methanol solution at room temperature for 10 min. The seeded constructs were then washed with dH2O prior to addition of 750 µl of 1% AlizarinRed in 1/100 diluted ammonia per well and incubated at room temperature for 3 min. Samples were washed with dH2O, dried at room temperature and visualized by stereo microscopy.

RNA isolation and RT-qPCR

Total RNA was extracted using the RNeasy MINI kit (Qiagen) according to the manufacturer's instructions. Briefly, at each experimental time, scaffolds were minced and put in a QIAshredder column with 600 µl of lysis buffer, then centrifuged. 600 µl of ethanol were added to the lysate and the solution was transferred in a spin column. After centrifugation and discard of the flow-through, different buffers were added and each time the columns were centrifuged.

The total RNA was eluted in 30 µl of RNase-free water. At each culturing time the RNA was extracted from three constructs of the same scaffold type. The total RNA was quantified using spectrophotometry (Nanodrop, Thermo Scientific) and ranged from 400 ng to 5 µg with an average of 2 µg total RNA. The quality of the RNA, expressed as RNA integrity number (RIN), was checked for randomly selected

samples by automated electrophoresis (Bioanalyser 2100, Agilent) and ranged from 6.0 to 9.9 with a median of 8.6.

Reverse transcriptase–quantitative polymerase chain reaction (RT-qPCR) was performed according to the protocol from the iScript cDNA synthesis kit (BioRad). In brief, a reaction mixture consisting of 1× iScript Reaction Mix, 1 µl iScript Reverse Transcriptase, 400-500 ng total RNA, and nuclease-free water was prepared in 20 µl of total volume. The single-strand cDNA synthesis occurred by incubating the complete reaction mixture 5 min at 25°C, followed by 30 min at 42°C, and terminated by incubation at 85°C for 5 min. Subsequently, the cDNA was diluted with nuclease-free water to 2.5 ng/µl cDNA.

All qPCRs were performed in a 10 µl reaction volume containing 5 ng template cDNA (2 µl), 2× SYBR FAST qPCR Master Mix Universal (5 µl) (KAPA) and 300 nM forward and reverse primers (Eurofins MWG Operon, Germany). Primer sequences are listed in Tab. 4.1.

All reactions were carried out in duplicates in 96-well plates (Hard-Shell Low-Profile 96-Well Skirted PCR plates, Bio-Rad) on the CFX96 real-time PCR detection system (Bio-Rad), followed by a regression Cq value determination method. The cycling conditions comprised 2 min polymerase activation at 95°C and 40 cycles at 95°C for 10 sec, 60°C for 30 sec and 72°C for 10 sec, followed by a dissociation curve analysis from 65 to 95°C. PCR efficiencies were calculated using a relative standard curve derived from a cDNA mixture of 5 randomly selected samples (a ten-fold dilution series with four measuring points).

Calculation of normalized relative expression levels was done in Excel as described by Hellemans [176]. Normalization was performed using the SDHA reference gene.

Gene symbol	Reference sequence	Forward primer	Reverse primer
COL1A1	NM_000088	CCACCAATCACCTGCGTACAGAA	GGGCAGTTCTTGGTCTCGTCAC
DCN	NM_001920	GTTACTTTCAATGGACTGAACCAGATGA	GTATCAGCAATGCGGATGTAGGAGAG
RUNX2	NM_001024630	GTGCCTAGGCGCATTTCA	GCTCTTCTTACTGAGAGTGGAAGG
ALPL	NM_000478	CCAAGAATAAAACTGATGTGGAGTATGAGAGT	TCCAGATGAAGTGGGAGTGCTTGTATC
SDHA	NM_004168	TGGGAACAAGAGGGCATCTG	CCACCACTGCATCAAATTCATG

Table 4.1: Sequences of qPCR primers

Statistical analysis

The data are expressed as mean ± standard deviation (mean ± SD). Statistic analyses were performed using a statistical software (Prism 5, GraphPad Software). To determine the statistical significance of differences among the results two-way or one-way ANOVA test was performed (if the interaction term was significant). F-test of the equality of the variances was conducted with a significance level of 0.05. Significance was assigned at p-values less than 0.05.

4.4 Results

Scaffold morphology

Porogen granulometry is one of the salt leaching process variables in which it is possible to modify the final scaffold structure. By varying this parameter matrix pore size variations can be obtained. Fig. 4.1 shows morphology of the scaffolds selected for this study (indicated with S1, S2 and S3, inherently with an increase of NaCl crystal size).

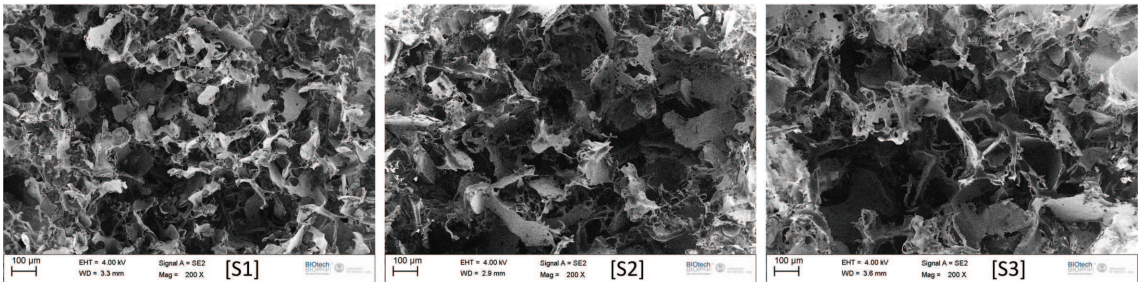

Figure 4.1: Scanning electron microscopy images of PdlLA scaffolds. Sieved NaCl particulates with three different dimensional ranges were used: (S1) 240-315 µm, (S2) 315-425 µm, and (S3) 425-1180 µm. Scale bars = 100 µm.

The pores were highly interconnected and randomly distributed in each scaffold. In general, scaffold architectures were very similar with only variation in pore size, increasing with the varying NaCl crystal sizes used in the different sponges. Through imaging analysis it was found that scaffold pore size range were different on analyzed samples: between nanometers up to 275 µm in S1, nanometers and 325 µm in S2, nanometers and 420 µm in S3. However, the scaffolds open porosity, calculated by liquid displacement method, was comparable and ranges from 85% to 88% (S1=87±2%, S2=88±4%, and S3=85±2%).

Cell proliferation, viability, and distribution

Biological evaluations were performed at predetermined time points after seeding osteoblast-like cells on the three different salt leached sponges.

Fig. 4.2A shows the cell proliferation trend, obtained by DNA content measurements. Cells on all of the scaffolds increased rapidly in cell number up to 9 days, followed by a more constant trend. Furthermore, S2 and S3 had a significantly higher prolif-

eration compared to S1. Cell viability was determined during the cell culture period using alamarBlue assay (Fig. 4.2B). The highest metabolic activity was reached after day 9, when the osteogenic medium was added.

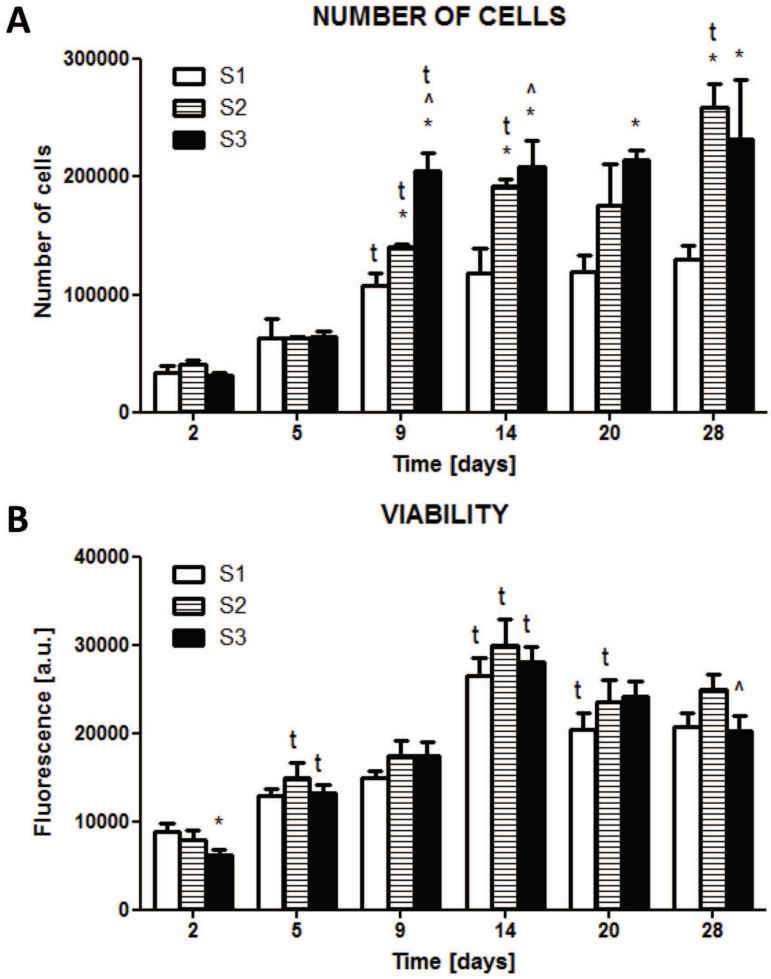

Figure 4.2: (A) Cellular proliferation of MG63 on PdlLA scaffolds. (B) Viability for MG63 cell culture on PdlLA scaffolds. t, $p < 0.05$ vs the same scaffold at the previous time point; *, $p < 0.05$ vs S1 at the same time point; ^, $p < 0.05$ vs S2 at the same time point.

By normalizing the metabolic activity per cell number (data not shown) it was found that single cell viability was higher at day 2 and 5, during cell proliferation and ECM production, and a further second smaller peak was evident at day 14, after the addition of osteogenic medium.

These observations were further confirmed by CLM imaging analyses after staining

the seeded scaffold with CalceinAM. Cell attachment, proliferation and viability are shown in Fig. 4.3.

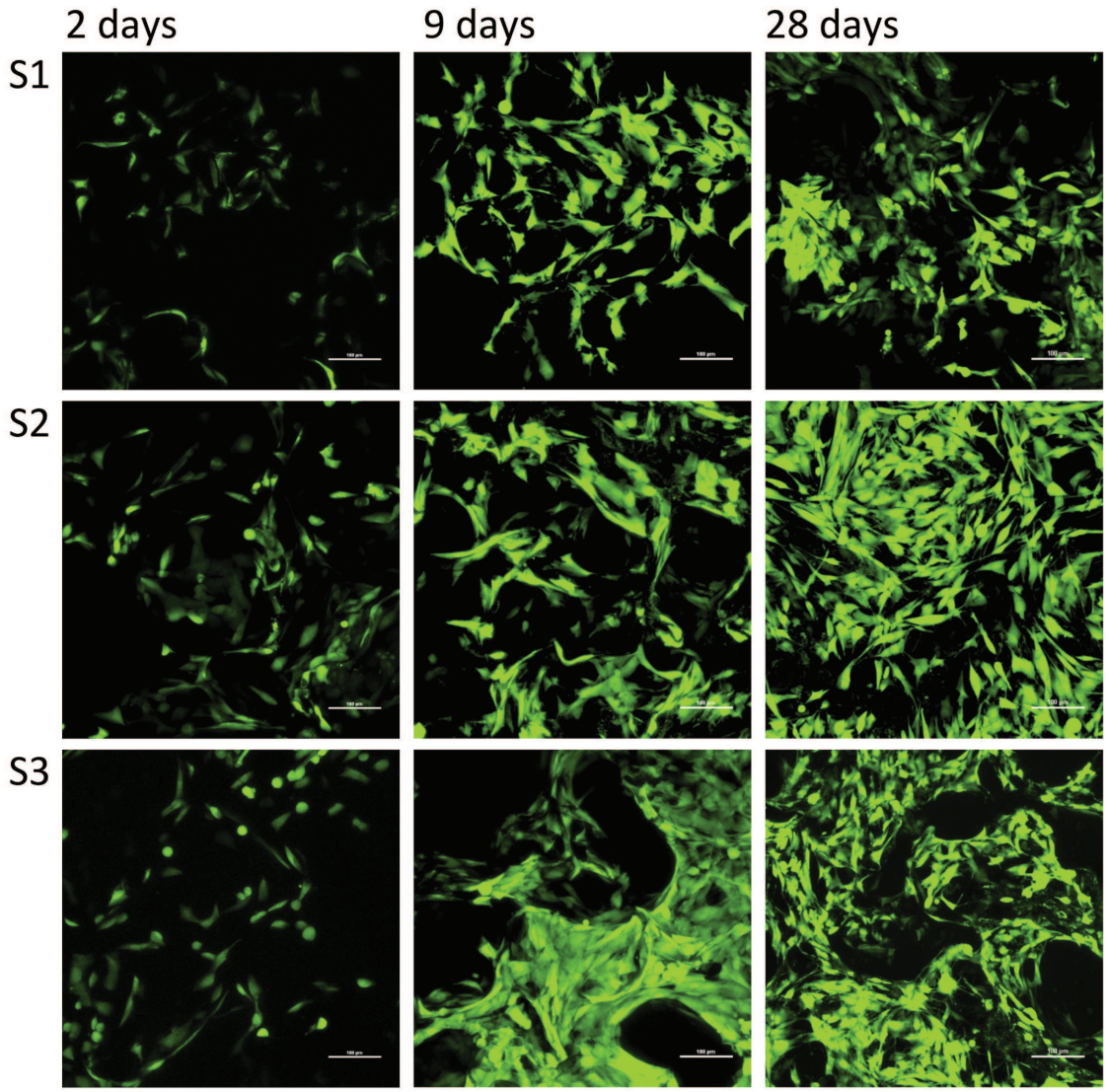

Figure 4.3: Confocal Laser Scanning Microscopy images of MG63 cells stained with CalceinAM. S1, S2 and S3 at 2, 9 and 28 days after cell seeding are shown. Scale bars = 100 µm.

In all samples proliferation and cell migration increased with incubation time. Pore sizes were large enough to permit cells to invade the matrix and sponge surface geometry acted as a template for cell distribution. At early time points scaffolds showed single, unorganized cells. At later time points, cells started to interact (Fig. 4.3) and to create a connected network. On S1, cells appeared less spread out

and always in lower numbers. Cell morphology and distribution among the PdlLA scaffolds were evaluated after staining with DAPI and Oregon Green 488 phailloidin (Fig. 4.4).

Cells attached on all the constructs. On scaffolds S2 and S3, cells showed a more developed and spread out cytoskeleton compared with S1 where they were more isolated and had primarily spherical shapes.

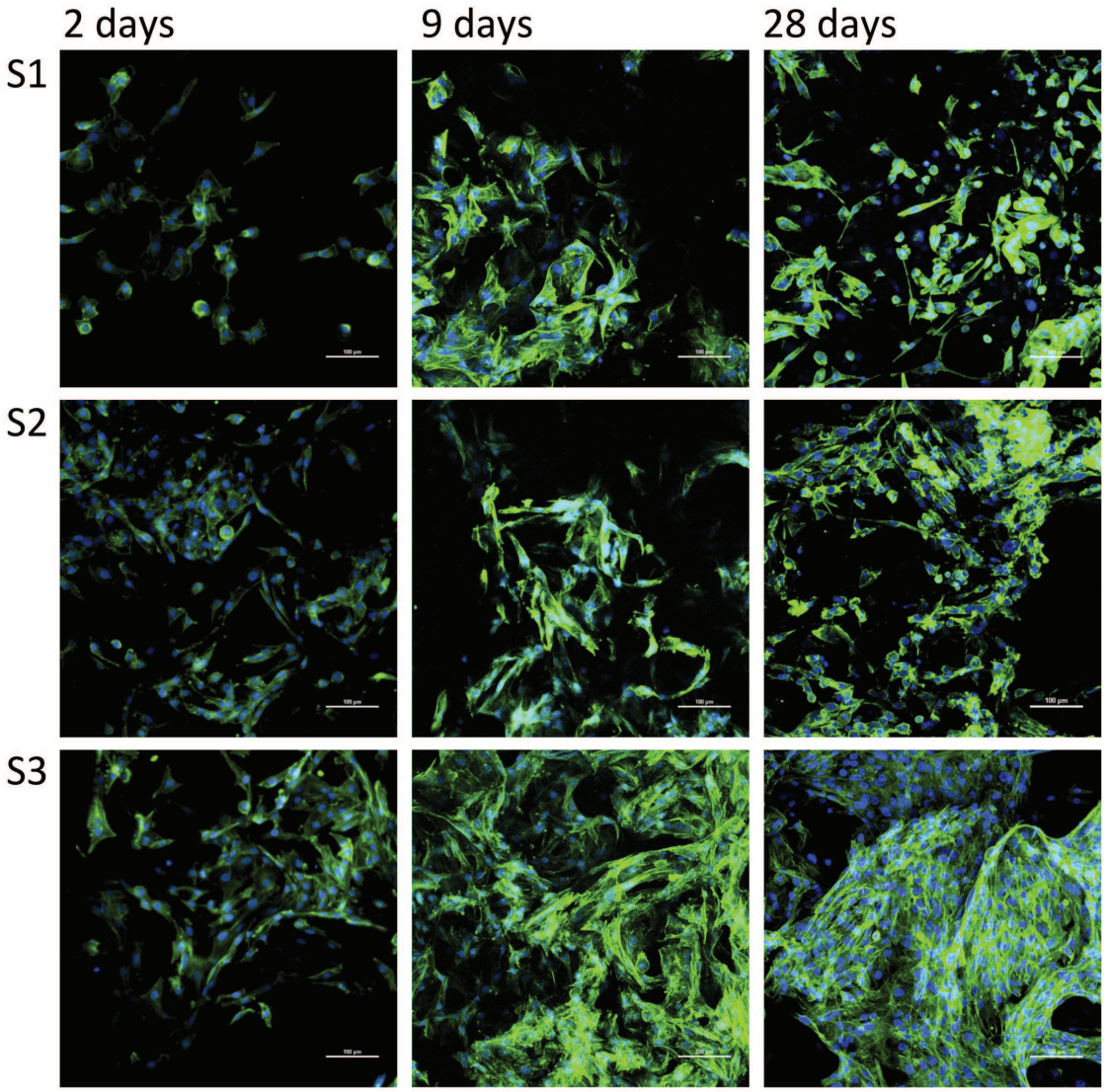

Figure 4.4: Confocal Laser Scanning Microscopy images of MG63 cells stained with Dapi and Oregon Green 488 Phalloidin. S1, S2 and S3 at 2, 9 and 28 days after cell seeding are shown. Scale bars = 100 µm.

Gene expression, collagen production, assembling, and mineralization

Collagen amount as well as collagen I gene expression were quantified and further characterized by imaging analyses. The amount of collagen over the culture time was almost constant (Fig. 4.5A) with a higher collagen amount on S3 and S2 compared to S1 at day 14 and 28.

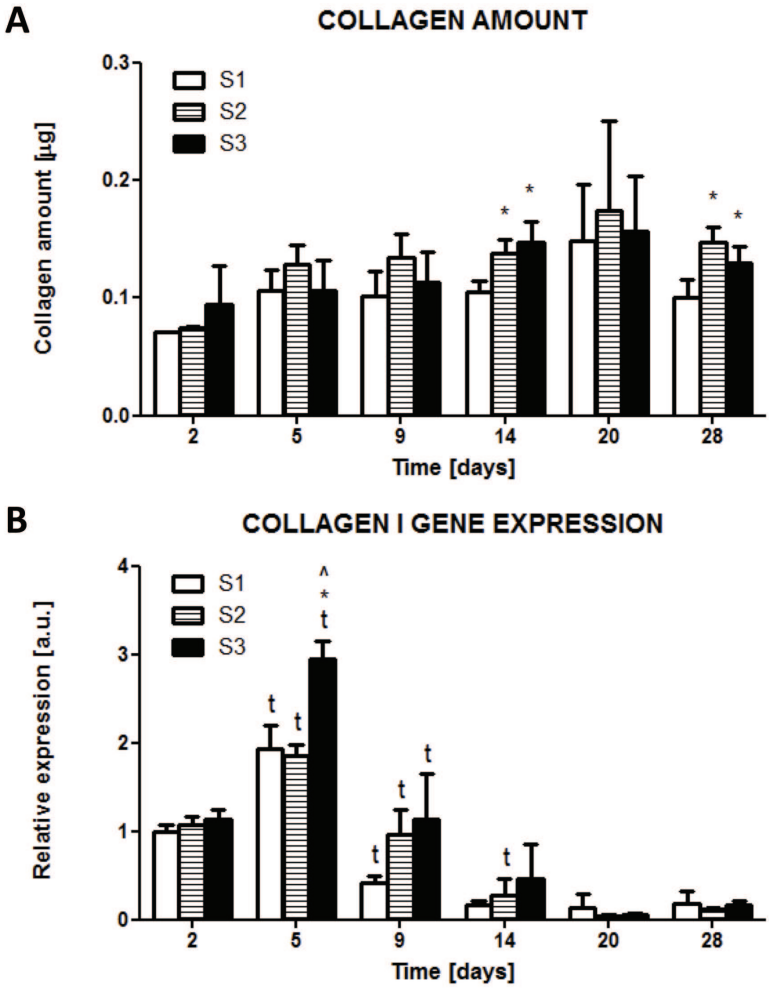

Figure 4.5: (A) Collagen amount in the three scaffolds at the different time points (B) Quantitative PCR analysis of Collagen I gene expression in cells cultured into the three scaffolds at the different time points. t, $p < 0.05$ vs the same scaffold at the previous time point; *, $p < 0.05$ vs S1 at the same time point; ^, $p < 0.05$ vs S2 at the same time point.

The high values at day 20 were not statistically significative.

Quantitative analyses (Fig. 4.5B) showed that at day 5 collagen I gene expression exhibited a consistent up-regulation for all samples. Afterwards, the expression decreased. Collagen I gene expression did not show significant differences between the three constructs, but at day 5, cells on S3 had a higher gene expression compared to cells on the other two scaffolds. These results were validated by CLM images after staining collagen I with a specific antibody.

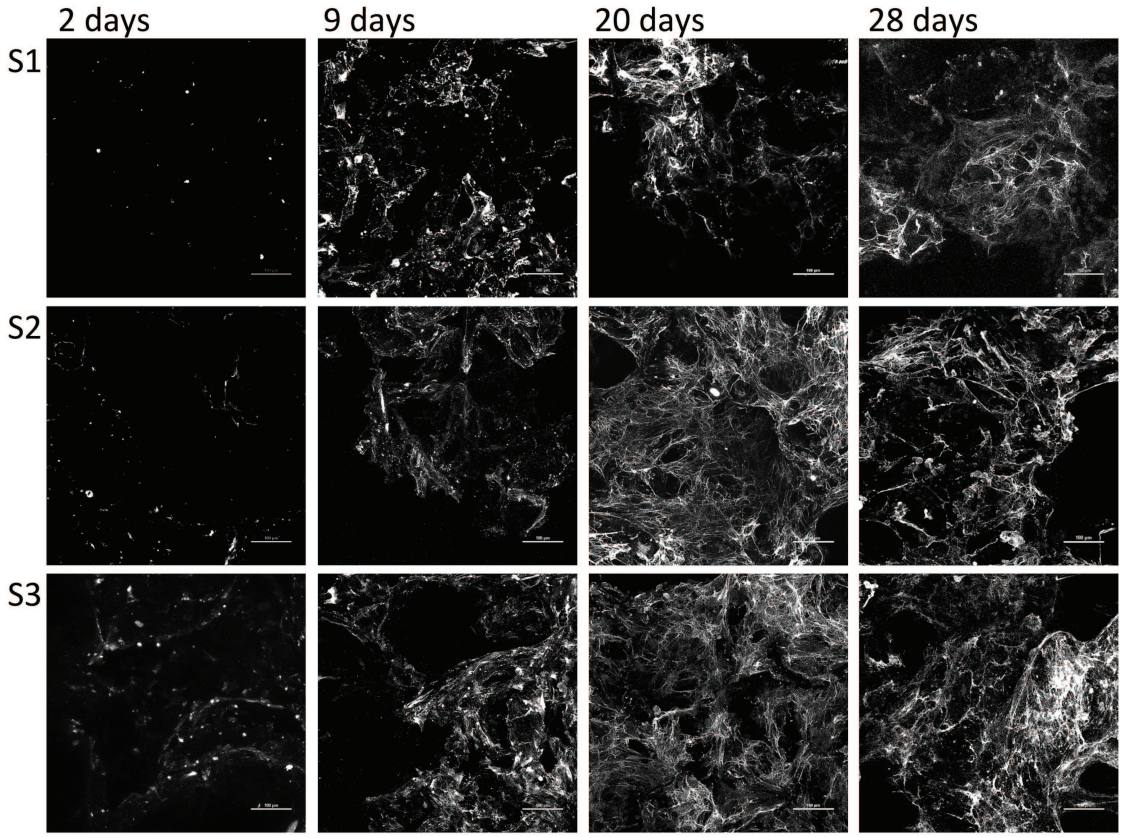

Figure 4.6: Confocal Laser Scanning Microscopy images of the three constructs (S1, S2 and S3) stained with a specific antibody for collagen I. Images of 2, 9, 20 and 28 days after cell seeding are reported. Scale bars = 100 µm.

Fig. 4.6 shows the increases in the collagen I with increased culture time that induced a higher three dimensional organization (every image is the result of a maximum intensity projection of a 3D stack). Collagen structures at early time points appeared unorganized and quite similar on the three different scaffolds. Differences were clearly visible from day 14, when a more complex collagen organization could be observed in S2 and S3. In fact, on scaffold S1, a fiber-like collagen network was detectable only at day 28, while for S2 and S3, a clear fibrous structure was already

visible from day 14 and 21. At the same time it was apparent that the collagen amount for S2 and S3 was higher than for S1. Gene expression of RUNX2 and Decorin, two genes involved in osteogenesis, were also investigated (Fig. 4.7) [177, 178, 179, 180].

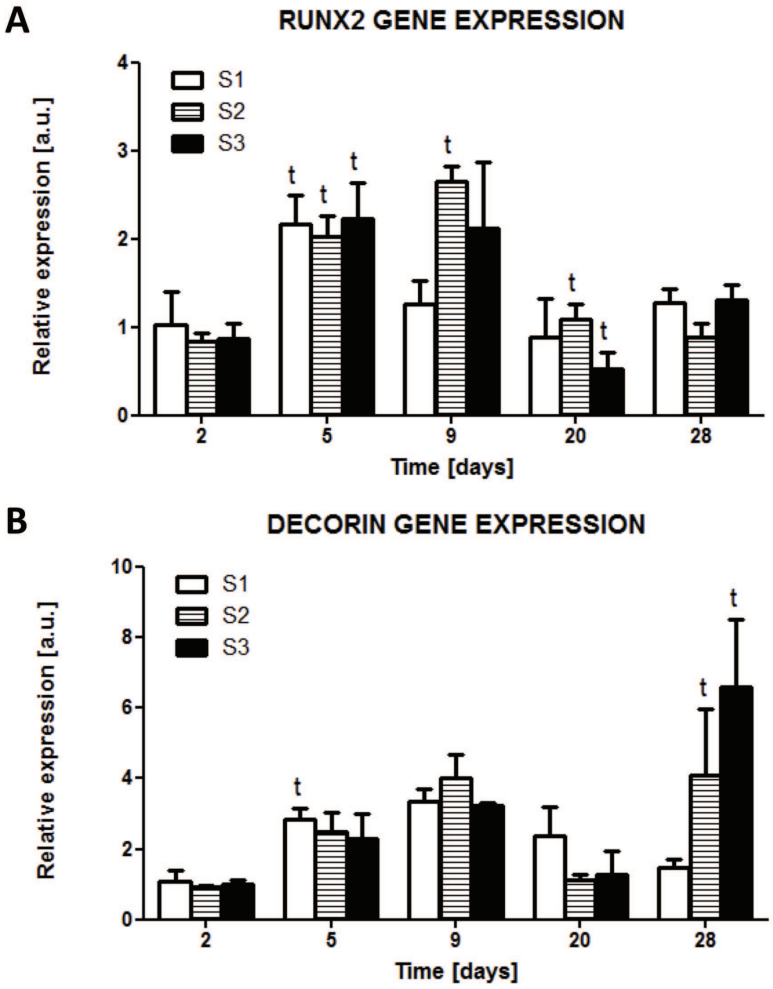

Figure 4.7: RT-qPCR analysis of RUNX2 (A) and Decorin (B) gene expression in cells cultured into the three scaffolds at the different time points. t, $p < 0.05$ vs the same scaffold at the previous time point.

In particular, RUNX2 is a well-known gene, downregulated during the differentiation into mature osteoblasts which form mature bone. Downregulation of RUNX2 gene was particularly evident for samples S2 and S3 after the addition of osteogenic medium (after day 9), while on S1 this trend occurred earlier, between day 5 and 9. The changes in Decorin expression were significant. At day 20 in S2 and S3 a

low value was shown and in the same constructs a subsequent rapid increase was detectable. In constructs S2 and S3 between day 20 and 28, the expression of alkaline phosphatase, an important osteogenic marker corresponding to calcium phosphate deposition, was nearly doubled compared to S1 (data not shown).

To further assess these data and detect the presence of calcium phosphate, samples were stained with AlizarinRed (Fig. 4.8). At day 28, S2 showed clearly visible red spots while S3 continuous red lines. Few traces of mineralization were evident in S1.

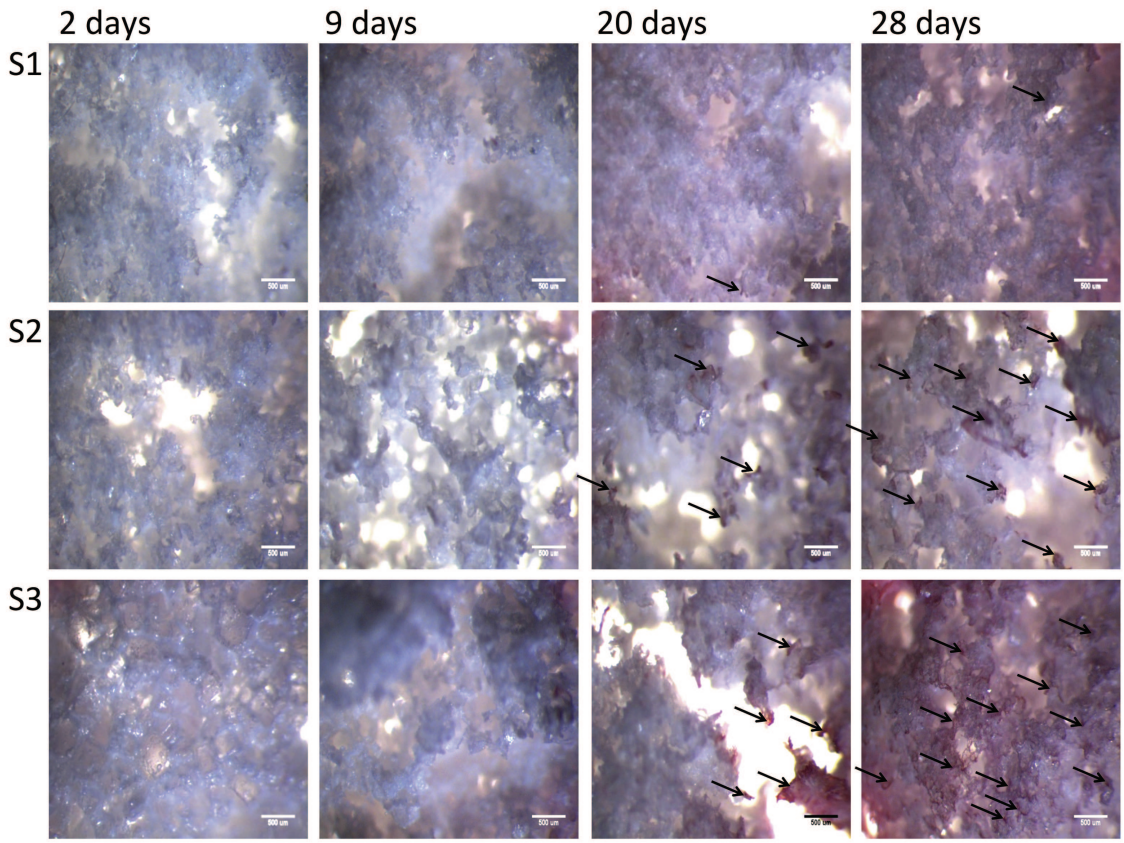

Figure 4.8: Stereo microscopy images of the three constructs (S1, S2 and S3) stained with AlizarinRed (calcium deposition stained red). Images of 5, 9, 20, and 28 days after cell seeding are reported. Arrows indicate calcium deposition. Scale bars = 500 µm.

4.5 Discussion

The key to understanding the mechanisms of biocompatibility, as defined by Williams [78, 171], is the determination of which material variables influence the host response, throughout the regenerative process. Unique combinations of chemical, biochemical, physiological, physical or other characteristics can influence how contact and interaction between biomaterials and the cells or the tissues occur.

The role of scaffold morphology and its features as a bioactive template for cell activities, targeted to regenerate damaged tissues, is therefore one of the main subjects of tissue engineering research. Scaffolds should guide cell functions creating a temporary matrix until the biological ECM produced is mature enough to substitute for the artificial structures. Therefore, different scaffold parameters should be considered in designing a suitable matrix for cell support because every tissue and/or cell type requires a scaffold with specific morphological and physical characteristics [181]. Among the several characteristics that have to be considered, it has been shown that larger porosity and pore size increase the ability of a scaffold to be penetrated by cells and subsequently vascularized [95, 182], but, conversely, its mechanical properties are lower. The best balance between these properties has to be chosen, also considering the material, its degradation profile and the final site of interest [41, 183]. The minimum recommended pore size in order for osteoblasts migration into a scaffold has been shown to be 100 µm [184]. In addition, numerous studies have shown better osteogenesis in implants with pores larger than 300 µm [185, 186, 187].

In this study, targeted at bone tissue regeneration, the attention was focused on understanding how a single scaffold variable, pore size, can influence MG63 activity, in particular regarding ECM development. Three PdlLA salt leached sponges were generated using diverse salt granulometries, resulting in scaffolds having a similar open porosity but different pore size ranges. Scaffolds show a pore size ranging between nanometers up to 275 µm (S1), 325 µm (S2) and 420 µm (S3). Such a broad pore size distribution is suitable for bone regeneration allowing cells penetration, vessel growth, nutrient transport and waste removal. An innovative approach to evaluate the influence of scaffold morphology on the MG63 activity was used, accordingly, ECM production and its development were considered with respect to the scaffold pore size. The major goal of the work was to use the developed scaffolds differing in pore structures as in vitro models to look at the mechanism of ECM formation

in the early stage of regenerative process. All the phases of bone development were characterized examining the expression of different genes. Among them, collagen I, the main structural protein involved in the early stage of bone regeneration, was analyzed quantitatively, via gene expression analysis, and qualitatively, via imaging analysis.

An increased proliferation and a higher level of cell organization were found for sample S2 and S3, when compared to scaffold S1, by DNA quantification and confocal laser microscopy evaluations (Fig. 4.2, Fig. 4.3 and Fig. 4.4). A reasonably more difficult cell migration into the smaller pores may be an explanation of these differences.

Gene expression of collagen I assessed by RT-qPCR analyses showed an up-regulation at day 5 (Figure 5B). These results agree with early steps in bone healing: ECM matrix begins to be produced usually during the first stage of bone formation corresponding in an up-regulation of the Type I collagen. Collagen I gene expression is also linked to the osteogenic gene expression of RUNX2, essential for osteoblasts differentiation and bone formation. It has been shown that RUNX2 is a positive regulator that can up-regulate the expression of bone matrix protein genes such as collagen I [179]. Furthermore, down-regulation of RUNX2 promotes osteoblasts maturation. Considering the gene expression profile (Fig. 4.7) and the confocal images (Fig. 4.6) we can assume that cells on scaffold S1 matured prematurely around day 9 without producing the right amount of organized collagen I necessary for ECM development. Conversely, on S2 and S3, RUNX2 is down regulated later, allowing a functional collagen I production and assembling. Furthermore, Decorin downregulation is connected to collagen I assembling [178] and its increase for S2 and S3 at day 28 may represent that cells were not organizing collagen I anymore but they were mineralizing the ECM already synthesized. A further evidence of these findings was given by the up-regulation of the ALP gene only for sample S2 and S3 at day 28, suggesting that only on these scaffolds the mineralization event was finalized. Those RT-qPCR results are compatible with imaging analyses after Alizarin red staining (Fig. 4.8) in which it was possible to notice mineralization trace only in S2 and S3.

Based on the results observed in Figures 6 and 8 it appears that S2 is characterized by thicker collagen I fibers and calcified spots, S3 by a well-organized net of thin collagen I fibers and slight lines of calcium while no clear mineralization is detectable on S1, where collagen I seems less abundant and packed. This corroborates the connection between the final mineralized bone and the previous phases of ECM developments,

confirming the importance to evaluate each single phase of tissue formation.

4.6 Conclusions

This in vitro study demonstrates that pore size plays an important role in cell behaviour, focusing on ECM production and organization. In fact, a small pore size appears to prevent an efficient cell migration and proliferation and, more interesting, to induce MG63 to mature earlier without however producing a functional ECM. Sponges with a pore size ranging up to 325 µm or to 420 µm lead instead to a well organized collagen I network and to the subsequent calcium deposition. Moreover, the evaluation of collagen I assembling could be a useful tool to predict the degree of the final mineralization as regards the regenerative process. Indeed, this work results interesting and innovative because it emphasizes the possibility to connect scaffold morphology to collagen I assembly, which in turn affects the final mineralization process, allowing to evaluate the tissue produced by osteoblasts from the first steps in bone formation. Further investigations will consider the use of human primary osteoblasts and results will be finally validates by in vivo studies.

5 Effects of silk fibroin fiber incorporation on mechanical properties, endothelial cell colonization and vascularization of PdlLA scaffolds[1]

5.1 Abstract

Attainment of functional vascularization of engineered constructs is one of the fundamental challenges of tissue engineering. However, the development of an extracellular matrix in most tissues, including bone, is dependent upon the establishment of a well developed vascular supply. In this study a poly-d,l-lactic acid (PdlLA) salt-leached sponge was modified by incorporation of silk fibroin fibers to create a multicomponent scaffold, in an effort to better support endothelial cell colonization and to promote in vivo vascularization. Scaffolds with and without silk fibroin fibers were compared for microstructure, mechanical properties, ability to maintain cell populations in vitro as well as to permit vascular ingrowth into acellular constructs in vivo. We demonstrated that adding silk fibroin fibers to a PdlLA salt-leached sponge enhanced scaffold properties and heightened its capacity to support endothelial cells in vitro and to promote vascularization in vivo. Therefore refinement of scaffold properties by inclusion of materials with beneficial attributes may promote and shape cellular responses.

[1]The work presented in this chapter was published in Biomaterials as Stoppato M, et al., Effects of silk fibroin fiber incorporation on mechanical properties, endothelial cell colonization and vascularization of PdlLA scaffolds, Biomaterials (2013), http://dx.doi.org/10.1016/j.biomaterials.2013.02.009

5.2 Introduction

Tissue engineering aims to restore, regenerate or replace tissues functionally compromised by injury or disease. The main strategy comprises scaffolds for tissue support combined with cells or growth factors to exploit physical cues [118, 188, 189].

Use of engineered tissues is becoming commonplace in clinics for thin tissues and for tissues characterized by limited metabolic demand (e.g. cornea [190], skin [191, 192], cartilage [193, 194, 195]). For tissue engineering to be a viable treatment option for more complex tissues, it is imperative that they can become vascularized. In fact the lack of functional vascularization of the engineered constructs can be an indicator of clinical failure [119, 196, 197, 198, 199, 200, 201].

Bone is a highly vascularized tissue. Physiologically, osteogenesis is preceded by angiogenesis, the growth of new blood vessels from pre-existing vessels. It is therefore important to achieve rapid development of an adequate blood supply, considering the central role that the vasculature plays in tissue healing. Limited oxygen and nutrient diffusion is associated with decreased cell growth and survival. Moreover, the vasculature is involved in the production of growth factors, fundamental in the recruitment, differentiation and behavior of cells that are crucial for bone formation and bone healing [121, 202, 203, 204, 205].

To overcome these problems, two main strategies have been proposed to promote vascularization of tissue constructs [119, 122, 202]. The first is scaffold-based and takes advantage of biological [206, 207] or synthetic [208, 209, 210] scaffolds. In the scaffold-based strategy, materials and structures determine biological outcomes. A promising approach is biomimicry, a scientific design discipline that emulates natural morphologies and architectures. The second strategy is cell-based and constitutes two different approaches: one is to prevascularize the scaffold [95, 211, 212, 213, 214] and the other is to promote angiogenesis in vivo [215]. The cell-based strategies include in vitro pre-vascularization, in which the constructs are seeded with endothelial cells and in vivo pre-vascularization, where constructs are implanted into a primary host to vascularize before implantation into the secondary host. Other cell based approaches exploit the addition of growth factors (e.g. vascular endothelial growth factor, fibroblast growth factor) [216, 217] or peptides derived from adhesion proteins or extracellular matrix molecules (e.g. laminin, fibronectin, osteopontin) [218, 219] or co-culture systems [182, 220, 221]. The challenge is always to promote tissue healing and regeneration, while preventing ischemia and nutrient loss.

The aim of this work was to refine a bone tissue engineering baseline scaffold, enhancing its capacity to support endothelial cells and to promote vascularization. In recent years biomimesis, the mimicking of the architecture of the extracellular matrix (ECM), has been a major approach explored for 3D scaffold development. The ECM is a fibrous composite of nano and micro fibrils which surrounds cells and comprises many biological components. The biomimetic matrix should ideally provide cell adhesion sites to maintain cell phenotype and function, mechanical strength, a biodegradation rate compatible with tissue generation and a controlled degree of inflammation [118, 211, 222, 223, 224]. In particular, biomaterial implants should influence the host inflammatory and reparative response [68].

The idea to combine different structures and materials to produce multicomponent scaffolds to improve the control of mechanical properties and metabolic cell activity has been recently exploited. To satisfy these demands, among all the strategies, multi-layered composite scaffolds, embed textile materials within hydrogels or bulk polymers were proposed [225, 226].

In our study a multicomponent scaffold was developed, combining the properties of a synthetic porous scaffold with the properties of a natural fibrous structure to enhance bioactivity. Silk fibroin fibers were incorporated into salt-leached sponge without modifying scaffold porosity. The baseline scaffold, composed of poly-d,l-lactic acid (PdlLA), was specifically designed to promote ECM production and mineralization providing a perfect 3D porous structure as support [16, 17]. Silk fibroin fibers were selected for their ability to support endothelial cell attachment and growth. Unger et al. demonstrated the capability of silk fibroin fibers to favor the formation of microcapillary-like structures in vitro. The authors also reported a rapid anastomosis of preformed capillaries with the host vasculature and a rapid vasculature growth into the silk construct thus leading to the vascularization in vivo [182, 221, 227]. Moreover silk fibroin fibers have been characterized by a gradual degradation attributable to macrophages and multinucleated giant cells, which in turn can produce pro-angiogenic molecules [223, 228]. Our hypothesis was that the capacity of PdlLA sponge to support endothelial cells in vitro and to promote vascularization in vivo could be improved by addition of silk fibroin fibers. In addition, the properties of both scaffolds were investigated.

5.3 Materials and Methods

Scaffold production

Two experimental groups were established; Group 1 (control scaffold) and Group 2 (scaffold with fibers).

Group 1 was produced by the solvent casting particulate leaching technique [126]. PdlLA (Resomer R207S, Boehringer Ingelheim, Germany) was dissolved in dichloromethane: dimethylformamide (70:30 v/v) and a 7% (w/v) solution was prepared. Sieved NaCl particulates, ranging from 425 to 1180 µm, were mixed with PdlLA, obtaining a 1:25 w/w polymer/porogen final concentration. The mixture was air dried (24-36 hours) and immersed in deionized water (dH2O) for 3 days with changes every 6 hours for the removal of the porogen.

In parallel, fibers were introduced into the scaffold (Group 2). The fibroin nets were produced from Bombyx mori silkworm cocoons. Briefly, cocoons were degummed by boiling twice, 1 hour each, in an aqueous solution of Na2CO3 (1.1 and 0.4 g/l, respectively), in order to remove sericin. Degummed silk fibers were then washed several times in distilled water and dried at room temperature. Then 0.05 g of these spread fibers were mixed with sieved NaCl particulates, ranging from 425 to 1180 µm as before, and the PdlLA solution (as above), obtaining a 1:14 w/w polymer/porogen final concentration. The mixture was air dried (24-36 hours) and immersed in deionized water (dH2O) for 3 days with changes every 6 hours for the removal of the porogen. Before use, scaffolds were cut into discs of 8 mm diameter, sterilized with aqueous ethanol solution 70% (v/v) and dried under a sterile hood at room temperature.

Scaffold characterization

Scanning electron microscopy (Supra 40, operating mode: high vacuum, secondary electron detector, Carl Zeiss, Europe) was used for the evaluation of scaffold morphologies. Samples were previously sputter-coated with a thin gold layer under argon (SEM Coating Unit PS3, Assing S.p.A., Rome, Italy).

A micro-CT system (µCT 40, Scanco Medical, Bassersdorf, Switzerland) was used to image and quantify the 3D microstructure of each sample as previously described [229]. Briefly, the samples (n=4/group) were scanned at 12 µm voxel resolution with

an integration time of 250 ms. Isotropic slice data were obtained and reconstructed into 2D images. These slice images were compiled and analyzed to render 3D images and obtain quantitative architectural parameters. Regions of interest were selected in each slice image and thresholded to eliminate background noise. A threshold to distinguish polymer material from pore space and background noise was chosen and kept consistent throughout all evaluations. Porosity, pore size distribution and degree of anisotropy were evaluated.

After measuring the cross-sectional area, wet scaffolds (n=4/group) soaked in PBS for 30 minutes were mechanically tested. Compressive mechanical testing was performed using a uniaxial electromechanical testing device (Info 650R, DDL, Eden Prairie, MN). Initial scaffold height was measured using a micrometer. Samples were tested to failure at a rate of 1 mm/minute. Standard solid compression plates were used for testing. A preload of approximately 1N was applied to the samples before initiating compression testing. Stress vs strain data were computed from load and displacement measurements, and compressive modulus was determined based on the slope of the entire linear-elastic region of the stress–strain curve.

In vitro cell culture

After sterilization, scaffolds were placed in 48 well plates and washed with PBS. Each sample was seeded with 20µl media containing 75,000 Human Umbilical Vein Endothelial Cells (HUVEC CC-2517, Lonza, Walkersville, MD) expanded to passage 4. After 24 hours, scaffolds were moved to 24 well plates and incubated in EGM-2 media (Lonza). All scaffolds were cultured in complete endothelial growth media (EGM-2 media) with FBS, bFGF, VEGF, insulin-like growth factor (IGF), ascorbic acid, epidermal growth factor (EGF), gentamycin sulfate and amphotericin-B (GA-1000) and heparin (all from Lonza SingleQuots) at 37ºC, 5% CO2. Media were replaced every 2 days for a total of 21 days. Scaffolds were harvested at different experimental time points.

Proliferation

Cell number variations over time in culture were determined using a Picogreen DNA quantification assay (Quant-iT PicoGreen dsDNA Assay Kit, Invitrogen, Grand Island, NY). At pre-determined time points, medium was removed from wells and

scaffolds washed three times with PBS. 500 µl of 0.05% Triton-X/PBS was used to completely submerge the scaffold before freezing and storing at -20°C until analysis. Each thawed sample was then sonicated for 10 s using a Virsonic ultrasonic cell disrupter (Virtis, Warminster, PA). Samples (100 µl, in triplicate) were aliquoted into a black 96 well plate and 100 µl PicoGreen working solution added to each well. The plate was read on a Perkin Elmer HTS 7000 fluorescent plate reader (excitation wavelength: 485 nm, emission wavelength: 535 nm). To calculate DNA concentrations, a calibration curve was generated using the double stranded DNA standard provided with the kit. Results were divided by 7.7 pg DNA, (the average amount of DNA in a cell [175]), to obtain estimates of cell number.

Cell viability

The cellular metabolic activity was measured using the CellTiter Blue assay (Promega, Madison, WI) which is based on the ability of living cells to reduce the non-fluorescent compound resazurin to the fluorescent compound resorufin. The assay was performed according to the manufacturer's instructions. In brief, the seeded scaffolds were incubated for 3 hours at 37°C with phenol red free culture medium supplemented with Titer Blue diluted 1:5. The resulting fluorescence was read on a fluorescence reader (excitation wavelength: 550 nm; emission wavelength: 595 nm).

Immunofluorescent localization of PECAM-1 expression on endothelial cells

Cells were fixed with formaldehyde (4% w/v in PBS) for 15 min at room temperature, washed with PBS and incubated in blocking buffer (6% BSA / 10% donkey serum / PBS) for an hour. Subsequently the samples were incubated with primary antibody against Platelet Endothelial Cell Adhesion Molecule (1:100, PECAM-1, Santa Cruz Biotechnology, Inc., Santa Cruz, CA) overnight at 4°C. After washes in PBS, the samples were incubated in secondary antibody (1:1000, donkey anti-rabbit Alexa Fluor 568, Molecular Probes, Grand Island, NY) for 1.5 h at room temperature. The scaffolds were washed again in PBS and permeabilized with 0.25% Triton-X 100 in PBS for 20 min. This was followed by a brief rinse in PBS and a nuclear counterstain (DAPI, Sigma Aldrich, St Louis, MO), according to the manufacturer's protocol. After the final rinses with PBS, samples were examined by

confocal microscopy (Zeiss LSM 510 UV).

RNA isolation and reverse transcriptase–quantitative PCR

VWF (Von Willebrand Factor) and PECAM-1 genes were assessed by RT-qPCR using a Custom PCR Array (RT2 Profiler PCR Array CAPH10845; SABiosciences, Qiagen, Valencia, CA).

Total RNA from scaffolds (3 replicates for each group) was extracted using the RNeasy MINI kit and QIAshredder columns (Qiagen) according to the manufacturer's instructions. The total RNA was quantified using spectrophotometry (Nanodrop ND-1000,Thermo Scientific, Wilmington, DE) and ranged from 1.2 to 6 μg. For best results on the PCR array, all RNA samples were selected for purity using an A260/A280 UV spectrophotometry ratio greater than 1.99. 250 ng RNA was used for cDNA synthesis, performed using the RT2 First Strand Kit (SABiosciences, Qiagen) according to the manufacturer's protocol. The cDNA was then amplified using RT2 qPCR Mastermix with RT2 Profiler PCR Arrays (SABiosciences, Qiagen). The results were normalized to 3 housekeeping genes (HPRT1, GAPDH and RPL13A). Relative gene expression values were analyzed using the RT2 Profiler PCR Array Data Analysis version 3.5 web-based software package.

Subcutaneous implants, Microfil perfusion, and micro-CT images

All animal procedures were approved by the Georgia Institute of Technology Institutional Animal Care and Use Committee (IACUC # A10021). Female 9-10 week-old Sprague Dawley rats (Charles River, Wilmington, MA) were housed two per cage and had access to chow and water ad libitum. All scaffolds used for implantation were prepared in a sterile biosafety cabinet and equilibrated in alpha MEM medium (no additives) for 12 h. Each of 20 rats received four randomized dorsal subcutaneous implants. This was performed by making two lateral incisions on the dorsal region and using a custom made tunneling tool to position the implant at a distance from the incision site. After surgery the animals were given a single dose of 0.03 mg/kg buprenorphine for pain relief. In all instances, the implantation sites healed without complications.

The vascular network in the scaffold area was investigated at 3 and 6 weeks post

surgery using a modified version of a previously described micro CT-based angiography technique [230]. After induction of anesthesia using 5% isoflurane, rats were maintained at 2% isoflurane and the thoracic cavity was opened to insert an 18 gauge catheter (SURFLO ® Teflon IV catheter, Terumuo Medical) through the left heart ventricle into the ascending aorta. The inferior vena cava was cut and 0.9% saline was perfused through the vasculature using a peristaltic pump (Masterflex, Cole-Parmer, Vernon Hills, IL) until complete clearance was achieved. Then 0.9% saline containing 0.4% (w/v) papaverin hydrochloride was perfused. The rats were then perfused with 10% neutral buffered formalin (NBF) for 5 minutes to fix the vasculature. Then polymerizable, lead chromate-based, radiopaque contrast agent (Microfil MV-122, Flow Tech, Carver, MA) was syringe-injected. The contrast agent was prepared according to manufacturer instructions but diluted to 66 % (vol/vol) with diluent and curing agent. Samples were stored at 4oC overnight to allow polymerization of the contrast agent before implant retrieval. Explants were rinsed in PBS, immersion fixed in 10% neutral buffered formalin for 48h prior to imaging in the Viva-CT system (Scanco Medical).

As previously described, isotropic slice data were obtained and reconstructed into 2D images. These slice images were compiled and analyzed to render 3D images and obtain quantitative architectural parameters. Regions of interest were globally thresholded based on X-ray attenuation and 3D images of the vascular network segmented from the surrounding tissues. Harvested scaffolds were evaluated to quantify the vessel volume, connectivity, number, thickness, and degree of anisotropy.

Histological analysis

Rats that were not perfusion fixed were euthanized by CO2 asphyxiation. Explants (from perfused rats and fresh tissue) were immersion fixed in 10% NBF. The tissues were processed and paraffin embedded for histological analysis. Sections, cut at 5 µm, were deparaffinized and rehydrated to stain with hematoxylin and eosin (H&E) and imaged with brightfield microscopy to assess cellular organization. Representative sections were stained with 1% picrosirius red and observed under polarized light to identify collagen fiber organization and maturation.

Statistical analysis

The data are expressed as mean ± standard deviation (mean ± SD). Statistical analyses were performed using Prism 5 (GraphPad, San Diego, CA). To determine the statistical significance of the results one-way and two-way ANOVA tests were performed (if the interaction term was significant). F-tests of the equality of the variances were conducted with a significance level of 0.05. Significance was assigned at p values less than 0.05. For RT-qPCR analysis, the RT2 Profiler PCR Array Data Analysis version 3.5 web-based software package was used.

5.4 Results

Scaffold morphology and mechanical properties

The two scaffold typologies were produced by the solvent casting particulate leaching technique with or without silk fibroin fibers. NaCl concentration was adjusted between the two groups to achieve the same porosity.

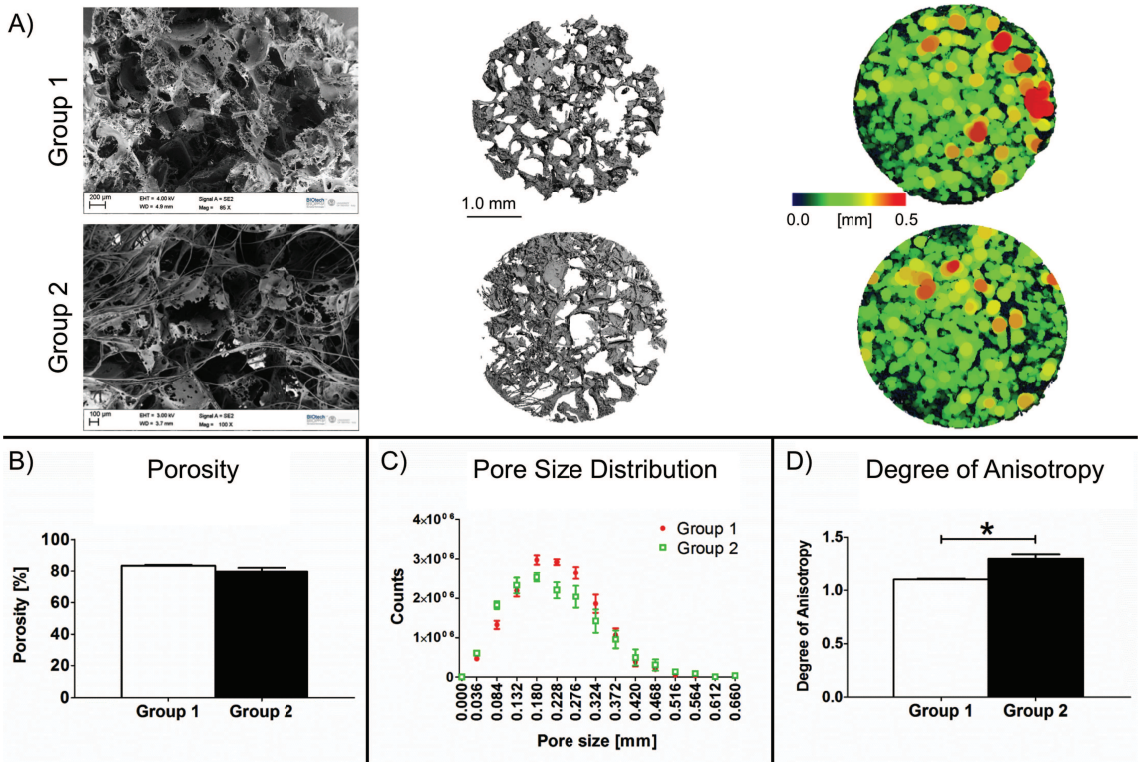

Figure 5.1: (A) From left to right: Scanning electron microscopy images, cross-sectional micro-CT slices and color-coded pore diameter scale images of the two scaffolds. (B) Porosity of the two scaffolds. (C) Pore size profile of the two scaffolds. (D) Degree of anisotropy of the two scaffolds. Group 1: PdlLA salt-leached sponge; Group 2: PdlLA salt-leached sponge with silk fibroin fibers.

Ultimately a concentration of 1:25 w/w polymer/porogen in group 1 (PdlLA) and 1:14 w/w polymer/porogen in group 2 (PdlLA + silk fibroin fibers) was considered optimal. Resulting structures are shown in Fig. 5.1A.

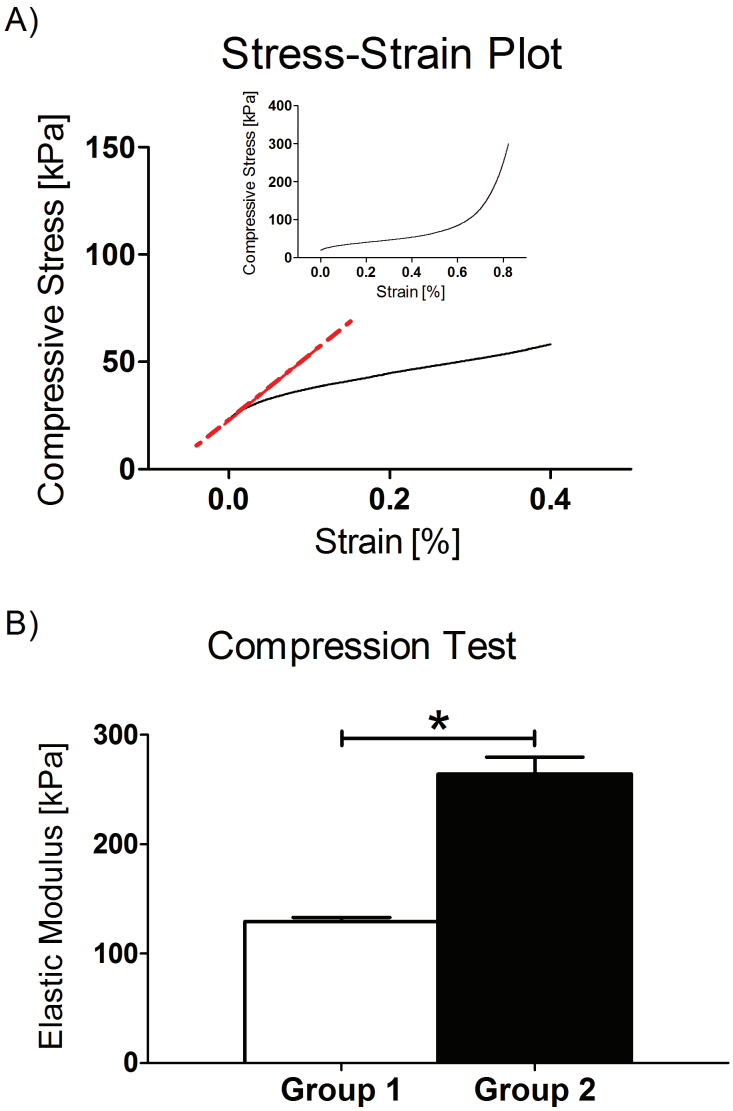

Figure 5.2: (A) Stress–strain plot of a representative compressive mechanical testing for a PdlLA salt-leached sponge scaffold with linear fit slope shown. (B) Elastic moduli of wet scaffolds after immersion in PBS for 30 min. *, $p < 0.05$. Group 1: PdlLA salt-leached sponge; Group 2: PdlLA salt-leached sponge with silk fibroin fibers.

The analysis of the SEM images revealed that the fibers were randomly distributed and well dispersed within the PdlLA sponge.

Micro-CT analysis generated slice information on the scaffolds and color graded images of the pore size distribution. Reconstructed micro-CT 3D images provided a quantitative morphometric analysis of the scaffolds. Accordingly, the porosity and the pore size distribution were determined and are presented inFig. 5.1B and C. The porosities were comparable in the two groups and in excess of 80%. Interestingly, the pore size distribution was also similar and no big differences were observed in the peaks or in the curve profiles of the two groups. Finally, scaffolds with silk fibroin fibers (group 2) had significantly higher degree of anisotropy (Fig. 5.1D) compared to group 1, indicating that group 2 is characterized by a preferential material direction. Stresses and strains were plotted from the compression data.

Compressive moduli were calculated from the slope of the linear fit to the elastic range of the stress-strain curve and the results (Fig. 5.2) demonstrate that the scaffolds with fibers have more than double the elastic modulus of the control scaffolds.

HUVECs proliferation, metabolic activity, distribution and gene expression

$7x10^4$ HUVECs were seeded onto each scaffold and cultured in conditions promoting angiogenesis. Retention and growth of endothelial cells were considered important indications of scaffold properties.

The retention of cells on the two different scaffold groups was comparable (Fig. 5.3A, day 1).

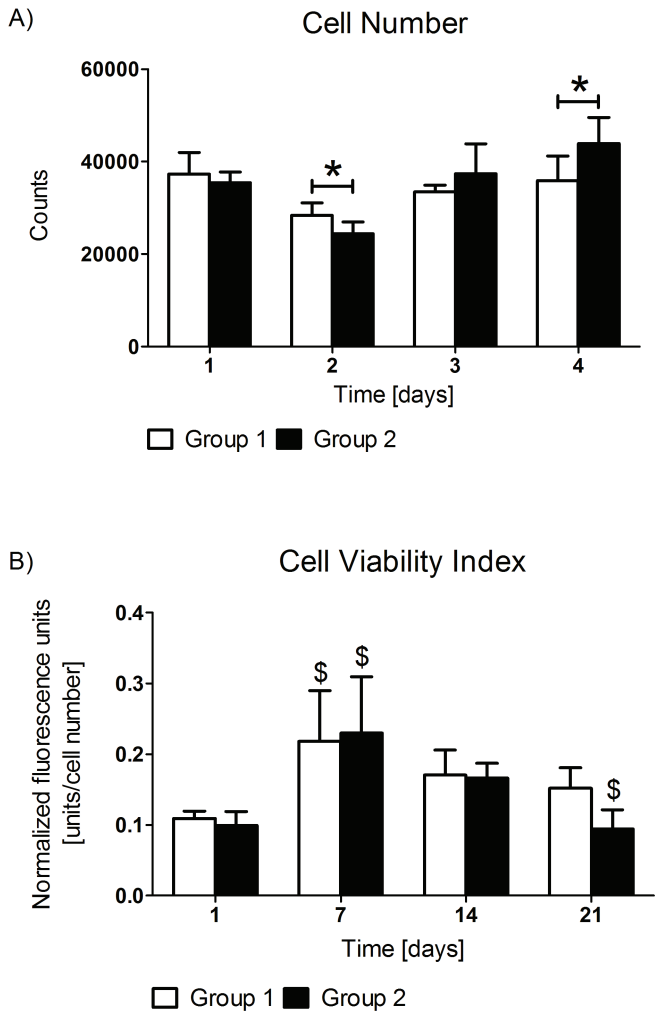

Figure 5.3: (A) HUVEC cell number. *, $p < 0.05$. (B) Viability index for HUVEC cell culture (normalized to cell number). $, $p < 0.05$ vs the same scaffold at the previous time point. Group 1: PdlLA salt-leached sponge; Group 2: PdlLA salt-leached sponge with silk fibroin fibers.

At day 7 there was a decrease in cell number which was probably due to a physiological adaptation to the new environment and group 2 scaffolds were characterized by a lower amount of cells. However, it appears that proliferation was favored in the scaffold with silk fibroin fibers and at 21 days the number of cells was significantly higher in that group.

Cell viability was determined during the cell culture period using the CellTiter-Blue assay The metabolic activity (viability normalized to cell number) was comparable in the cells seeded on the two different scaffolds at each time point (Fig. 5.3B). The

profile was similar in the two groups: an increase in metabolic activity was observed after day 1 with the peak at day 7.

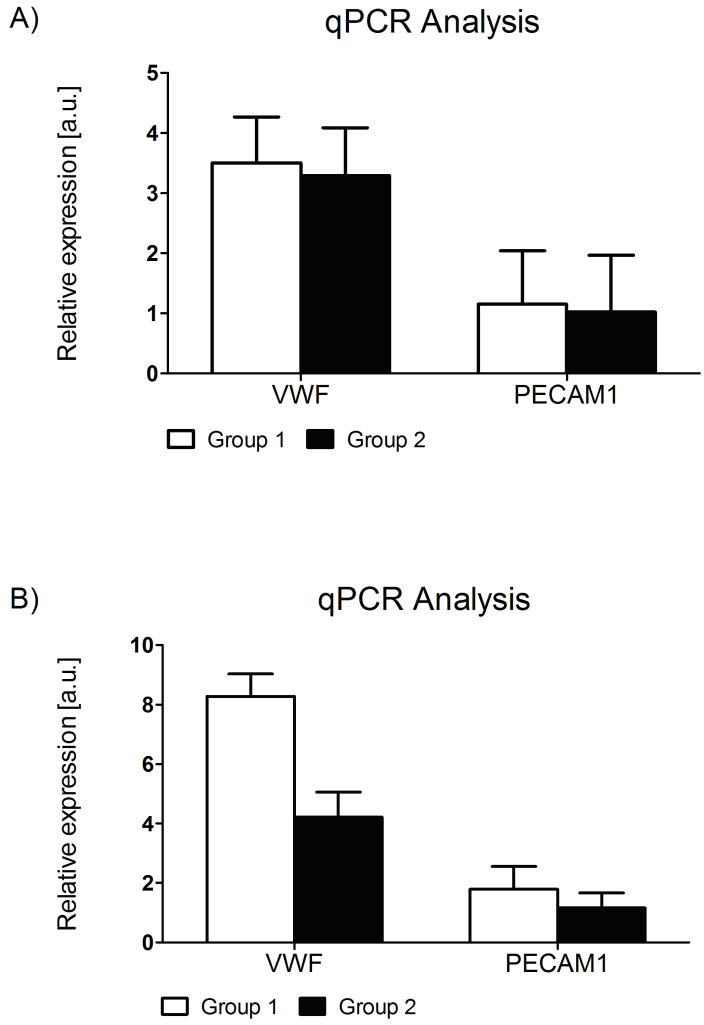

Figure 5.4: RT-qPCR analysis of VWF and PECAM-1 gene expression in cells seeded onto the scaffolds at different time points: (A), 7 days; (B), 21 days. No significative differences are present (n=3). Group 1: PdlLA salt-leached sponge; Group 2: PdlLA salt-leached sponge with silk fibroin fibers.

Reverse transcriptase-quantitative polymerase chain reaction (RT-qPCR) analyses (Fig. 5.4) showed that the gene expression of the cells seeded onto the two different scaffolds at 7 and 21 days was comparable, based on VWF and PECAM-1 mRNA levels. No significant differences in gene expression were observed between the two scaffold groups at either the 7 or 21 day timepoints.

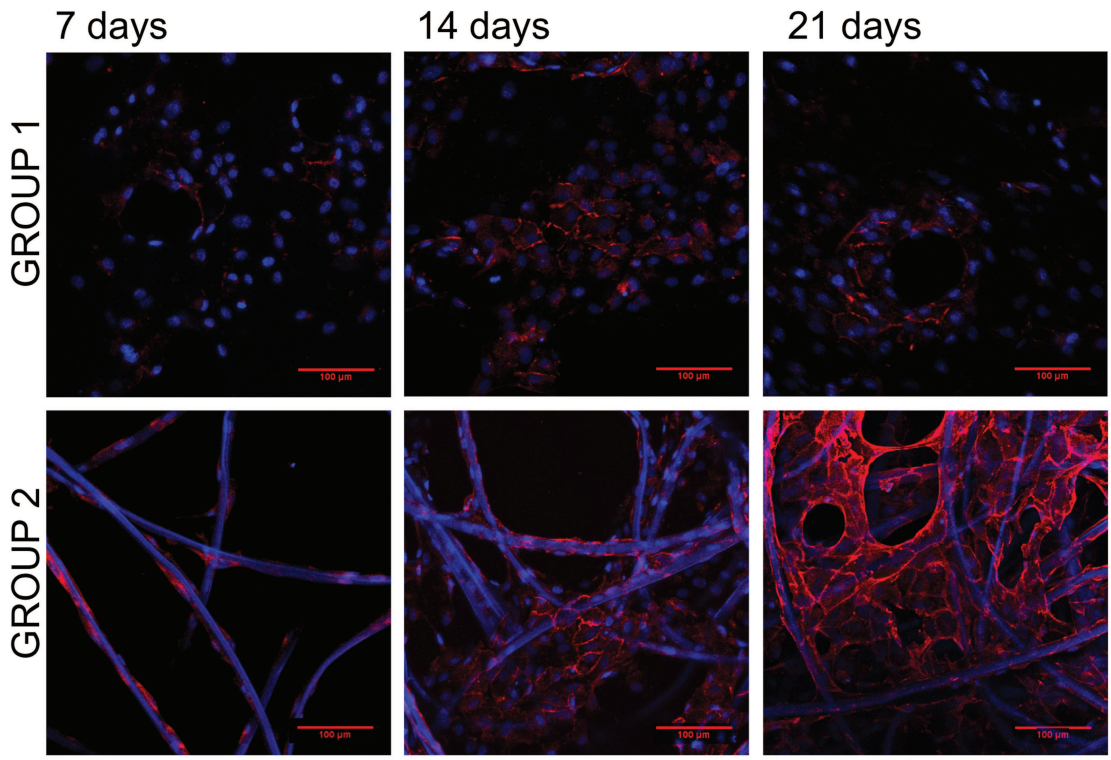

Figure 5.5: Confocal Laser Scanning Microscopy images of HUVEC cells stained for nuclei (DAPI, blue) and PECAM-1 (red). Group 1 and Group 2 at 7, 14 and 21 days after cell seeding are shown. Silk fibroin fibers stain with DAPI. Scale bars = 100 µm. Group 1: PdlLA salt-leached sponge; Group 2: PdlLA salt-leached sponge with silk fibroin fibers.

Confocal microscopy and immunolocalization were used to evaluate cell distribution and PECAM-1 protein expression at cell-cell junctions (Fig. 5.5). Cells attached to both scaffolds. In group 1, cells did not express a strong PECAM-1 signal, and after 21 days it was only present around pore edges. In group 2, cells seemed to prefer to attach to the fibers, then, as their number increased, they colonized not only the fibers but the spaces in between. PECAM-1 expression appeared qualitatively higher with increasing days in culture in scaffolds with silk fibroin fibers.

Subcutaneous model, histology and perfusion

Rats were perfused with a vascular contrast agent to quantify blood vessel ingrowth 3 or 6 weeks after acellular construct implantation. Examination of the explanted samples revealed that scaffolds became vascularized and that scaffold materials were

not completely degraded.

The subcutaneous implants were stained with hematoxylin and eosin (Fig. 5.6A) to show nuclei and possible cellular infiltration.

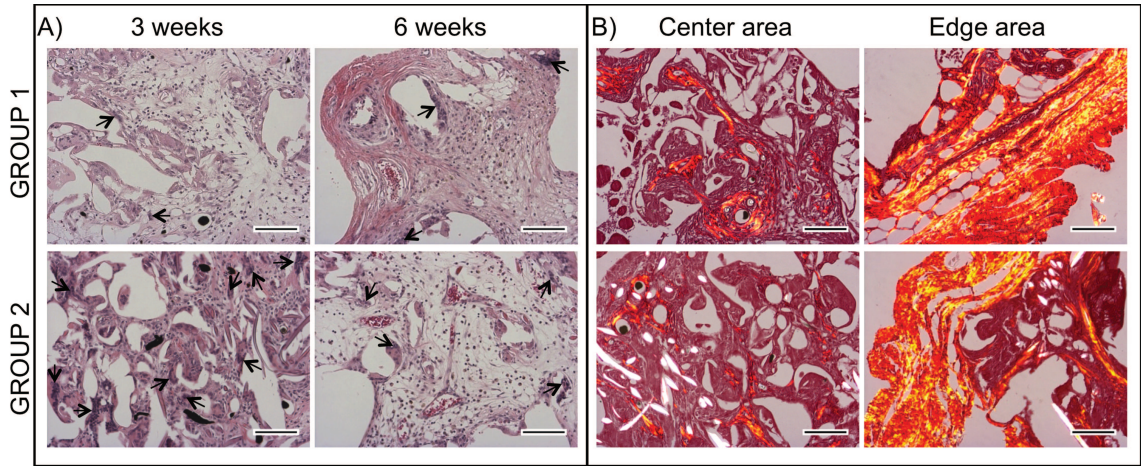

Figure 5.6: Histological images of sections (5 µm) of explanted scaffolds. Left pictures (A) show samples stained with hematoxylin and eosin at 3 and 6 weeks with sample at 3 weeks perfused with vascular contrast agent. Black arrows indicate multinucleated giant cells. Right pictures (B) show samples stained with picrosirius red at 3 weeks. Center area indicates an inner part of the implants, edge area the interface between the implants and newly formed tissue. Scale bars = 100 µm. Vascular contrast agent is also seen in the center area images in B. Group 1: PdlLA salt-leached sponge; Group 2: PdlLA salt-leached sponge with silk fibroin fibers.

Histological analyses showed tissue ingrowth into both the scaffolds. Moreover multinucleated giant cells (macrophages) were visible at the interface between new tissue and the material especially in group 2 at 3 weeks. A comparison of group 1 with group 2 after 3 weeks of culture shows that qualitatively more blood vessels are present in the scaffold with silk fibroin fibers, as evidenced by black spots of perfused contrast agent.

The organization of newly formed collagen matrix was evaluated using picrosirius red staining and polarized light microscopy. In both groups a fibrous capsule formed around the implanted scaffold. The capsule did not block tissue ingrowth into the scaffolds and collagen (birefringent yellow/orange fibers) was partially oriented and aligned in each group.

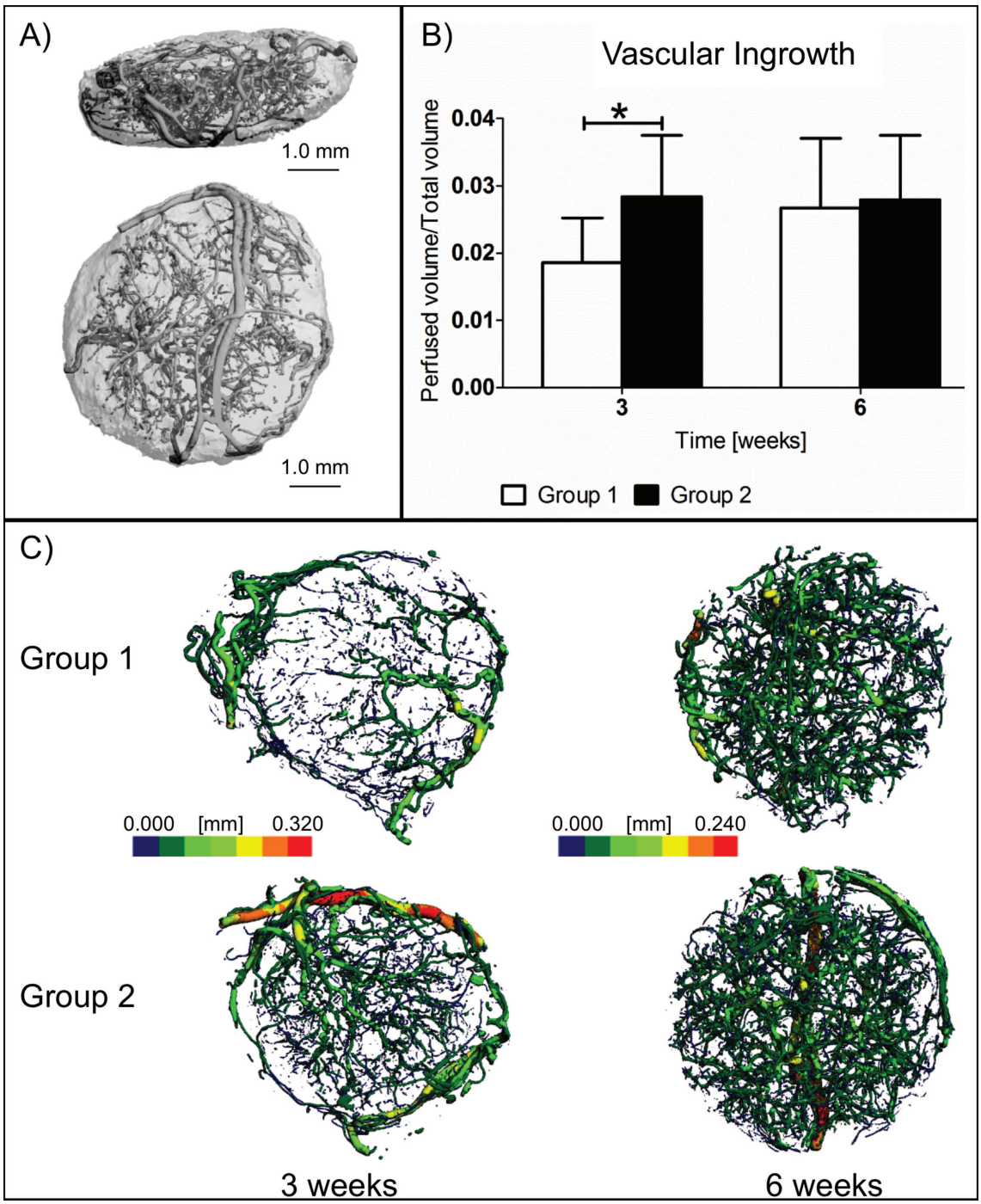

Figure 5.7: (A) Micro-CT images of scaffold implanted subcutaneously in rat perfused with Microfil vascular contrast agent. Vasculature (dark grey) growing into implant area (light grey), (B) Quantification of vascular volume/total scaffold volume. *, $p < 0.05$ (C) Representative scans of blood vessels 3 and 6 weeks after implantation. Color scale bars, defining vessel diameters, range from 0 to 320 µm at 3 weeks to 0 to 240 µm at 6 weeks. Group 1: PdlLA salt-leached sponge; Group 2: PdlLA salt-leached sponge with silk fibroin fibers.

Perfused scaffolds were carefully harvested, cleaning them from the surrounded tissue to restrict evaluation to the vessels inside the scaffold. Fig. 5.7A shows the vessels (dark gray) which have invaded the scaffold area (light gray). Micro-CT analysis revealed a significantly greater vessel volume normalized to scaffold volume in group 2 compared to group 1 at 3 weeks (Fig. 5.7B). At 6 weeks, the vascular volume was comparable in the two groups. In Figure 7C representative scans of perfused constructs of both groups at 3 and 6 weeks after implantation are shown. The diameters of the vessels are displayed on a color scale. As before, there is a greater vascular volume in group 2 at 3 weeks, whereas there is no difference between the groups at 6 weeks.

Finally other morphological parameters such as connectivity, vessel number, and degree of anisotropy were evaluated. The measure of the interconnectedness of the vascular structures (Fig. 5.8A) and the number of distinct vessels (Fig. 5.8B) were not significantly altered by the presence of silk fibroin fibers. However the addition of silk fibroin fibers favored a higher degree of anisotropy, indicating a preferential orientation of the vessels (Fig. 5.8C).

5.5 Discussion

Rapid and sufficient integration of implants with the host vasculature, to ensure an adequate supply of oxygen and nutrients, remains a significant challenge in tissue engineering. This study demonstrates that modification of a baseline scaffold resulted in improved mechanical properties and accelerated tissue integration and vascularization in vivo.

First we demonstrate the ability to generate two different constructs (PdlLA alone or PdlLA with silk fibroin fibers), such that stiffness was increased upon addition of fibers but porosity remained the same. The compression testing results show that the scaffolds with fibers are two-fold stiffer than the PdlLA alone. The increase in apparent elastic modulus achieved in scaffolds with the fibroin fibers could be attributed to their structure, in which triaxial stresses that are established during compression, are also relatively high in tension. Therefore, the addition of an oriented structure, such as the fibroin fibers, could provide benefits in terms of mechanical properties even if positioned randomly or longitudinally to the applied load, as demonstrated in a reticular structure [231].

In culture, we showed that cell proliferation at 21 days was higher for group 2, probably due to the active domains of silk fibroin. In fact, fibroin protein peptides have been demonstrated to enhance cell growth [132]. We also showed that, even if gene expression was unaffected, the adhesion molecule PECAM-1, a well-known endothelial marker, was much more extensively located on the membrane of cells seeded onto the scaffolds with silk fibroin fibers. One explanation may have been related to the amino acid sequences of the fibroin molecule that have been shown to support endothelial cell phenotype and activity [211, 232]. Furthermore, it has to be considered that the gene expression results were normalized to housekeeping genes and, for this reason, the higher cell number of HUVECs supported by the group 2 scaffolds at day 21 would partially explain the more PECAM-1 observed as the cells are more crowded. The immunolocalization of PECAM-1 mechanoreceptor to the cell-cell junction at 21 days suggests a higher degree of organization of the endothelial cells in group 2, proving that scaffold with silk fibroin fibers better support endothelial cells in static culture.

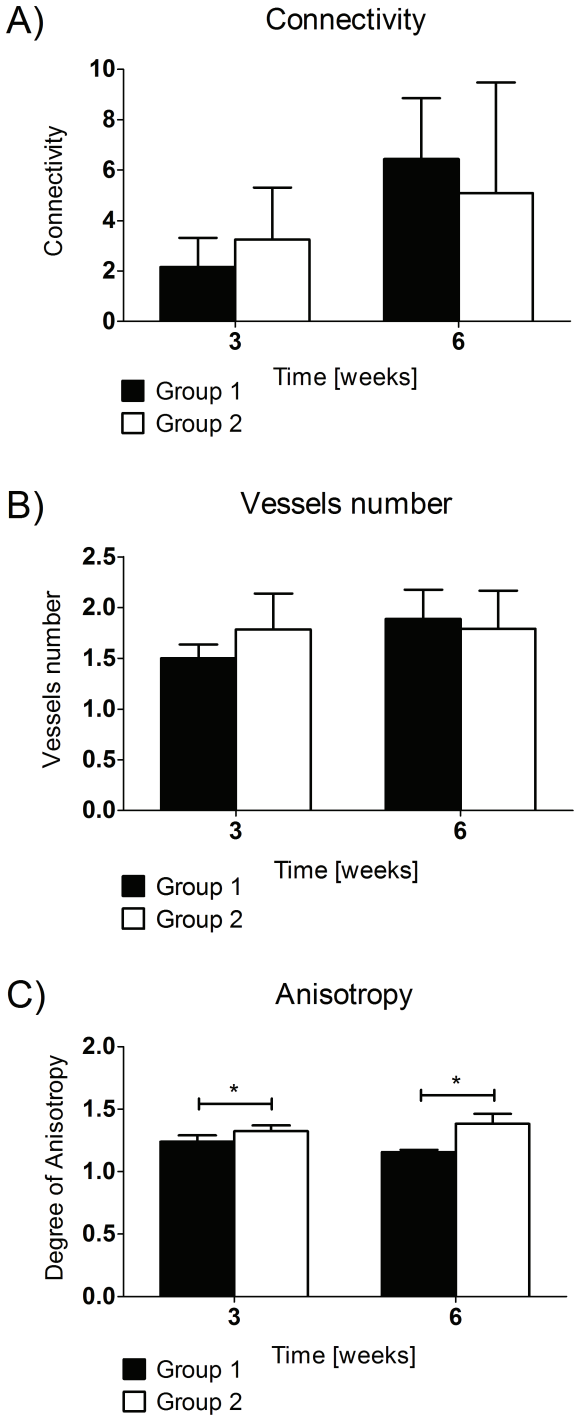

Figure 5.8: (A) Vascular connectivity, (B) Number of vessels and (C) Degree of anisotropy of scaffolds at 3 and 6 weeks after implantation.*, $p < 0.05$. Group 1: PdlLA salt-leached sponge; Group 2: PdlLA salt-leached sponge with silk fibroin fibers.

The vascularization of the scaffolds in vivo is of great importance for understanding the possible applications of this material. Recent studies have underscored how differences in the inflammatory response can lead to differences in tissue repair. Macrophages and multinucleated giant cells play a major role in scaffold vascularization by virtue of their secretion of pro-angiogenic factors [70, 182, 202].

In our study, it is evident that the implantation of both scaffolds caused an inflammatory response, highlighted by the fibrotic capsule encircling all the scaffolds and by the presence of giant multinucleated cells (even more prominent in the scaffolds with silk fibroin fibers). It is a fair assumption that the silk fibroin fibers interacted with macrophages and multinucleated giant cells in order to accelerate the vascularization process at 3 weeks. However, the in vivo perfusion results show that a fully integrated host vasculature formed in the acellular scaffolds of both groups, indicating an earlier and faster integration of scaffolds from group 2.

The other significant parameter different in the two groups is related to vessel anisotropy. In the scaffold with silk fibroin fibers, vessels had a preferred direction in agreement with the scaffold anisotropy. It seems that, even if the fibers had been randomly distributed, the general structure in group 2 shows some level of organization, guiding the orientation of the vessel formation.

5.6 Conclusions

This study demonstrated that adding silk fibroin fibers to a PdlLA salt-leached sponge increased scaffold stiffness, and heightened its capacity to support endothelial cells in vitro and to promote vascularization in vivo. The immunolocalization of PECAM-1 mechanoreceptor to the cell-cell junction at 21 days suggests that scaffold with silk fibroin fibers better support endothelial cells in static culture. Additionally the in vivo perfusion results indicate that a fully integrated host vasculature formed in the acellular scaffolds of both groups, with faster vascularization of the composite scaffolds. Further studies using segmental bone defect models and considering both vascularization and mineralization are warranted to better characterize the role of silk fibroin fibers added to a PdlLA scaffold in the bone healing process.

6 Human Mesenchymal Stem Cells Seeded onto PdlLA Scaffolds: Influence of Addition of Silk Fibroin Fiber and Endothelial Cells

6.1 Abstract

This study investigated the influence of silk fibroin fiber incorporation into a porous salt–leached Poly D, L-Lactic Acid (PdlLA) scaffold on its support of human mesenchymal stem cell (hMSC) and human umbilical vein endothelial cell (HUVEC) cultures. hMSCs alone and in combination with HUVECs were seeded onto PdlLA scaffolds with and without silk fibroin fibers and maintained in osteogenic medium for up to six weeks in vitro. Cell behavior was investigated using indices such as cell viability, proliferation, and alkaline phosphatase activity for a range of time points and harvested scaffolds underwent PECAM-1 and Collagen I immunolocalization and real time RT-PCR analysis for osteogenic and angiogenic gene expression. Our findings suggest that, despite similar porosities exhibited by the PdlLA and PdlLA plus fibroin scaffolds, there were marked differences in cell distribution and function. Endothelial cell localization was strongly associated with fiber presence yet, in the absence of fibers, an early osteogenic differentiation of mesenchymal stem cells was observed in the scaffolds. This study attests the influence of silk-fibroin fibers on the biological attributes of PdlLA salt leached scaffolds and provides information on the inter-relationship between endothelial cells and hMSCs cultured in these environments. The concept of designing composite scaffolds to integrate beneficial

properties of various structures and materials to facilitate appropriate biological responses would seem a promising avenue of research.

6.2 Introduction

Tissue engineering research shows great promise for the treatment of bone defects and fracture non-union. While scaffolds of increasing complexity have been created, the roles of endogenous precursor cells in the vascularization and mineralization processes remain unclear.Osteogenesis is a complex process that involves the well-orchestrated interaction of various cell types [233, 234]. The processes integral to bone formation are thought to be dependent on angiogenesis due to the close interaction between the bone-forming osteoblasts (OBs) and the vessel-forming endothelial cells (ECs) [220, 235, 236, 237].

Several in vitro studies have investigated the interaction between OBs and ECs using co-culture systems as tools for mimicking the complex structures and regulation processes of living tissue[232]. It was demonstrated that direct contact between OBs and ECs is necessary for establishment of a suitable model for studying the interaction between these two cell types, as both direct cell contact and paracrine mechanisms should be considered [235, 236, 238, 239].

The nature of this argument is complex due to the use of different osteoblast cell lines and endothelial cell types [182] which often leads to contradictory results. Nevertheless studies in vitro have shown that endothelial cells regulate the function of osteoblast cells and vice versa [240, 241, 242].

While most authors found that endothelial cells had a positive effect on osteoblast proliferation [240, 242] their influence on osteoblast differentiation was somewhat more controversial [242, 243, 244]. Perhaps of equal importance is the interaction of the bone marrow derived stromal cells with endothelial cells, since these can give rise to osteoblastic precursor cells.

Here we examine the influence of endothelial cells and silk fibroin fibers on the differentiation of MSCs cultured on PDLLA scaffolds in osteogenic culture conditions. To our knowledge, this is the first study to investigate cultures of bone marrow-derived mesenchymal stem cells and endothelial cells on a silk fibroin enhanced PDLLA scaffold. We tested hMSC and hMSC plus HUVECs for the ability to support osteogenic differentiation and development of vascular structures with the goal being to ascer-

tain the influence of endothelial cells and silk fibroin fibers on tissue formation in the scaffolds.

6.3 Materials and Methods

Scaffold production

Two experimental groups were established; Group 1 (PDLLA scaffold only) and Group 2 (PDLLA scaffold with fibroin fibers).

Group 1 was produced by the solvent casting particulate leaching technique. PDLLA (Resomer R207S, Boehringer Ingelheim, Germany) was dissolved in dichloromethane:dimethylforma (70:30 v/v) and a 7% (w/v) solution was prepared. Sieved NaCl particulates, ranging from 425 to 1180 µm, were mixed with PDLLA, obtaining a 1:25 w/w polymer/porogen final concentration. The mixture was air dried (24-36 hours) and immersed in deionized water (dH2O) for 3 days with changes every 6 hours for the removal of the porogen.

Fibers were introduced into the scaffold (Group 2) as described previously [245]. Briefly, the Bombyx mori silkworm cocoons were degummed in order to remove sericin. Degummed silk fibers were then washed several times in distilled water and dried at room temperature. Then 0.05 g of these spread fibers was mixed with sieved NaCl particulates, ranging from 425 to 1180 µm as in Group 1, and the PDLLA solution (as above), obtaining a 1:14 w/w polymer/porogen final concentration. The mixture was air dried (24-36 hours) and immersed in deionized water (dH2O) for 3 days with changes every 6 hours for the removal of the porogen. Before use, scaffolds were cut into discs of 8 mm diameter, sterilized with aqueous ethanol solution 70% (v/v) and dried under a sterile hood at room temperature.

In vitro cell culture

After sterilization, scaffolds were placed in 48 well plates and washed with PBS. Each sample was seeded with 10µl media containing 75,000 Human Mesenchymal Stem Cells (Prockop Laboratory, Texas A&M University, Texas) expanded to passage 3 (not allowed to expand beyond 80% confluency) or 75,000 hMSC plus 75,000 Human Umbilical Vein Endothelial Cells (HUVEC CC-2517, Lonza, Walkersville, MD) expanded to passage 4. After 24 hours, scaffolds were moved to 24 well plates and incubated in MEM alpha medium (Invitrogen). All scaffolds were cultured in MEM alpha medium with 16% (v/v) fetal bovine serum (FBS, Atlanta Biologicals), 100 U Penicillin,100 µg Streptomycin, 2 mM L-glutamine (Invitrogen), 6 mM β-glycerol

phosphate (Sigma), 50 µg/mL ascorbic acid 2-phosphate (Sigma), 1 nM dexamethasone (Sigma) and 50 ng/mL L-thyroxine (Sigma) at 37ºC, 5% CO2. Media were replaced every 48 hours for a total of 42 days. Scaffolds were harvested at different experimental time points.

Proliferation

Cell number over time in culture was determined using a Picogreen DNA quantification assay (Quant-iT PicoGreen dsDNA Assay Kit, Invitrogen, Grand Island, NY). At pre-determined time points, medium was removed from wells and scaffolds washed three times with PBS. 500 µl of 0.05% Triton-X/PBS was used to completely submerge the scaffold before freezing and storing at -20°C until analysis. Each thawed sample was then sonicated for 10 s using a Virsonic ultrasonic cell disrupter (Virtis, Warminster, PA) and centrifuged. Samples (100 µl, in triplicate) were aliquoted into a black 96 well plate and 100 µl PicoGreen working solution added to each well. After 5 minutes the plate was read on a Perkin Elmer HTS 7000 fluorescent plate reader (excitation wavelength: 485 nm, emission wavelength: 535 nm). To calculate DNA concentrations, a calibration curve was generated using the double stranded DNA standard provided with the kit. Results were divided by 7.7 pg DNA, (the average amount of DNA in a cell [175]), to obtain estimates of cell number.

Cell viability

The cellular metabolic activity was measured using the CellTiter Blue assay (Promega, Madison, WI) which is based on the ability of living cells to reduce the non-fluorescent compound resazurin to the fluorescent compound resorufin. The assay was performed according to the manufacturer's instructions. Briefly, the seeded scaffolds were incubated for 3 hours at 37°C with phenol red free culture medium supplemented with Titer Blue diluted 1:5. The resulting fluorescence was read on a fluorescence reader (excitation wavelength: 550 nm; emission wavelength: 595 nm).

ALP activity

The concentration of alkaline phosphatase (ALP) was determined, using the lysates used for DNA quantification. Briefly, the ALP activity of the cells was assessed

by measuring the release of p-nitrophenol (yellow salt) from p-nitrophenyl phosphate. Standards were prepared with a 10mM p-nitrophenol solution, to obtain a standard curve. The color change was measured spectrophotometrically at 405 nm. The amounts of resulting p-nitrophenol released by the cells were quantified by comparison with the standard curve and normalized to the total ng of DNA.

Immunofluorescent localization of PECAM-1 and Collagen I expression

Cells were fixed with formaldehyde (4% w/v in PBS) for 15 min at room temperature, washed with PBS and incubated in blocking buffer (6% BSA / 10% donkey serum / PBS) for an hour. Subsequently the samples were incubated with 1o antibody against Platelet Endothelial Cell Adhesion Molecule (1:100, PECAM-1, Santa Cruz Biotechnology, Inc., Santa Cruz, CA) or human type I collagen (1:100, Meridian Life Science, Saco, ME, USA) overnight at 4°C. After washes in PBS, the samples were incubated in 2o antibody (1:1000, donkey anti-rabbit Alexa Fluor 568, Molecular Probes, Grand Island, NY) for 1.5 h at room temperature. The scaffolds were washed again in PBS and permeabilized with 0.25% Triton-X 100 in PBS for 20 min. This was followed by a brief rinse in PBS and a nuclear counterstain (DAPI, Sigma Aldrich, St Louis, MO), according to the manufacturer's protocol. After the final rinses with PBS, samples were examined by confocal microscopy (Zeiss LSM 510 UV).

RNA isolation and reverse transcriptase–quantitative PCR

ALP (Alkaline phosphatase), COL1A1 (Collagen, type I, alpha 1), RUNX2 (Runt-related transcription factor 2), OC (Osteocalcin), VWF (Von Willebrand Factor) and PECAM-1 gene expression were assessed by RT-qPCR using a Custom PCR Array (RT2 Profiler PCR Array CAPH10845; SA Biosciences, Qiagen, Valencia, CA).

Total RNA from scaffolds (3 replicates for each group) was extracted using the RNeasy MINI kit and QIAshredder columns (Qiagen) according to the manufacturer's instructions. The total RNA was quantified using spectrophotometry (Nanodrop ND-1000,Thermo Scientific, Wilmington, DE) and ranged from 2.8 to 7.5 μg. For best results on the PCR array, all RNA samples were selected for purity using a

A260/A280 UV spectrophotometry ratio $\geq$ 2.00. 250 ng RNA was used for cDNA synthesis, performed using the RT2 First Strand Kit (SA Biosciences, Qiagen) according to the manufacturer's protocol. The cDNA was then amplified using RT2 qPCR Mastermix with RT2 Profiler PCR Arrays (SA Biosciences, Qiagen). The results were normalized to 3 housekeeping genes (HPRT1, GAPDH and RPL13A). Relative gene expression values were analyzed using the RT2 Profiler PCR Array Data Analysis version 3.5 web-based software package.

Micro-CT mineralization analysis

At 3, 4, 5 and 6 weeks, samples were aseptically removed from culture and placed in custom tubes for Micro-CT scanning. Mineralized matrix was determined by using a Viva-CT scanner (Scanco Medical, Bassersdorf, Switzerland) at 55 kVp and 200 ms integration time. The isotropic slice data were obtained and reconstructed into 2D images. These slice images were compiled and analyzed to render 3D images. Regions of interest were globally thresholded based on X-ray attenuation (threshold of 65 with a filter width of 1.0 and a filter support of 0.5). The total volume of the mineralized matrix was thus determined.

Histological analysis

Samples were fixed in 10% NBF. The tissues were processed and paraffin embedded for histological analysis. Sections, cut at 5 µm, were deparaffinized and rehydrated to stain with von Kossa to quantify mineralization (phosphate deposition).

Statistical analysis

The data are expressed as mean $\pm$ standard deviation (mean $\pm$ SD). Statistical analyses were performed using Prism 5 (GraphPad, San Diego, CA). To determine the statistical significance of the results one-way and two-way ANOVA tests were performed (if the interaction term was significant). F-tests of the equality of the variances were conducted with a significance level of 0.05. Significance was assigned at p values less than 0.05. For RT-qPCR analysis, the RT2 Profiler PCR Array Data Analysis version 3.5 web-based software package was used.

6.4 Results and Discussions

Previous studies using scanning electron microscopy and mechanical testing evaluated scaffold morphologies and the compressive modulus, respectively [245].

In this study hMSCs or hMSCs plus HUVECs were seeded onto each scaffold and cultured in conditions promoting osteogenesis for six weeks.

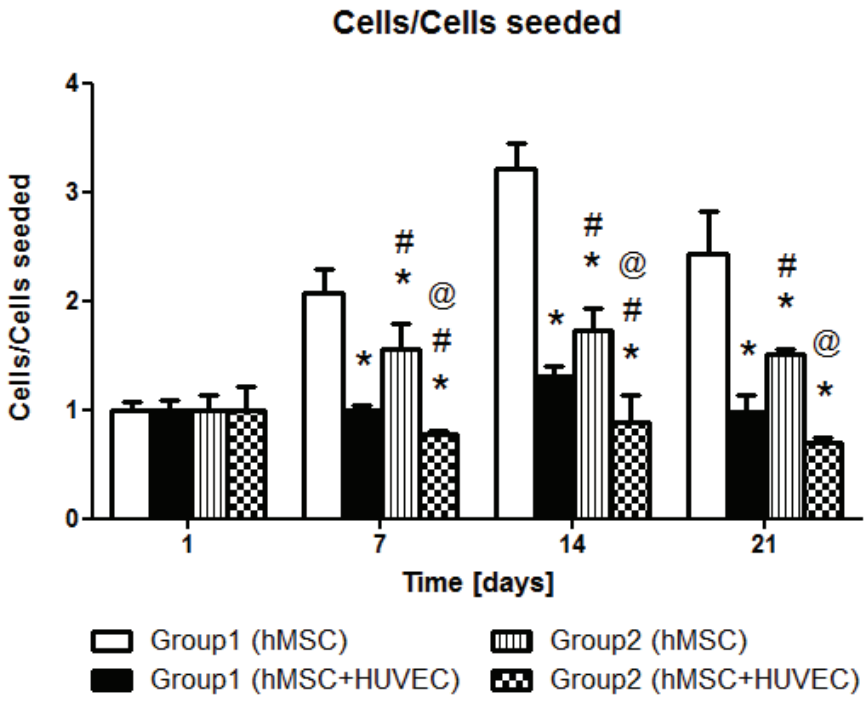

Figure 6.1: Cell number normalized for the number of cells at day 1. *, $p < 0.05$ vs the Group1 (hMSC): #, $p < 0.05$ vs the Group1 (hMSC+HUVEC); @, $p < 0.05$ vs the Group2 (hMSC). Group 1: PdlLA salt-leached sponge; Group 2: PdlLA salt-leached sponge with silk fibroin fibers.

Cell proliferation was evaluated for the first 21 days, normalizing the cell number at given time points by the number of cells at day 1. In Fig. 6.1 the cell number profile is shown. Scaffolds seeded with hMSC show an increase in cell number, especially in Group 1. The number of cells in scaffolds co-cultured with hMSC and HUVECs does not vary with time and in Group 2 it decreases. Group 1 and 2 seeded with hMSCs and HUVECs start with double the number of cells.

The metabolic activity (viability normalized to the cell number) was determined during the cell culture period using the CellTiter-Blue assay (Fig. 6.2). The profile

was comparable during the culture except for Group 1 (with hMSC) at day 1, showing a much higher value.

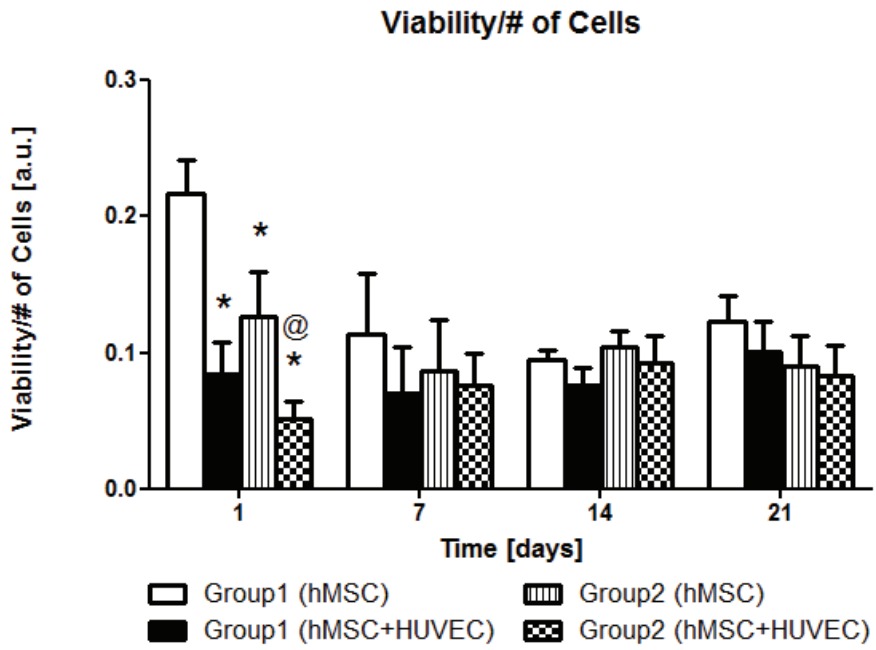

Figure 6.2: Viability index for cell culture (viability normalized to cell number). *, $p < 0.05$ vs the Group1 (hMSC): #, $p < 0.05$ vs the Group1 (hMSC+HUVEC); @, $p < 0.05$ vs the Group2 (hMSC). Group 1: PdlLA salt-leached sponge; Group 2: PdlLA salt-leached sponge with silk fibroin fibers.

The confocal laser microscopy images of Alexa 568 and DAPI to visualize type I collagen organization and nuclei (Fig. 6.3) showed that at day 7 in each of the four samples organized fibers were present. At day 21 collagen type I fibers seemed packed and aligned. However, in Group 2 seeded with hMSCs and HUVECs, type I collagen was not detectable.

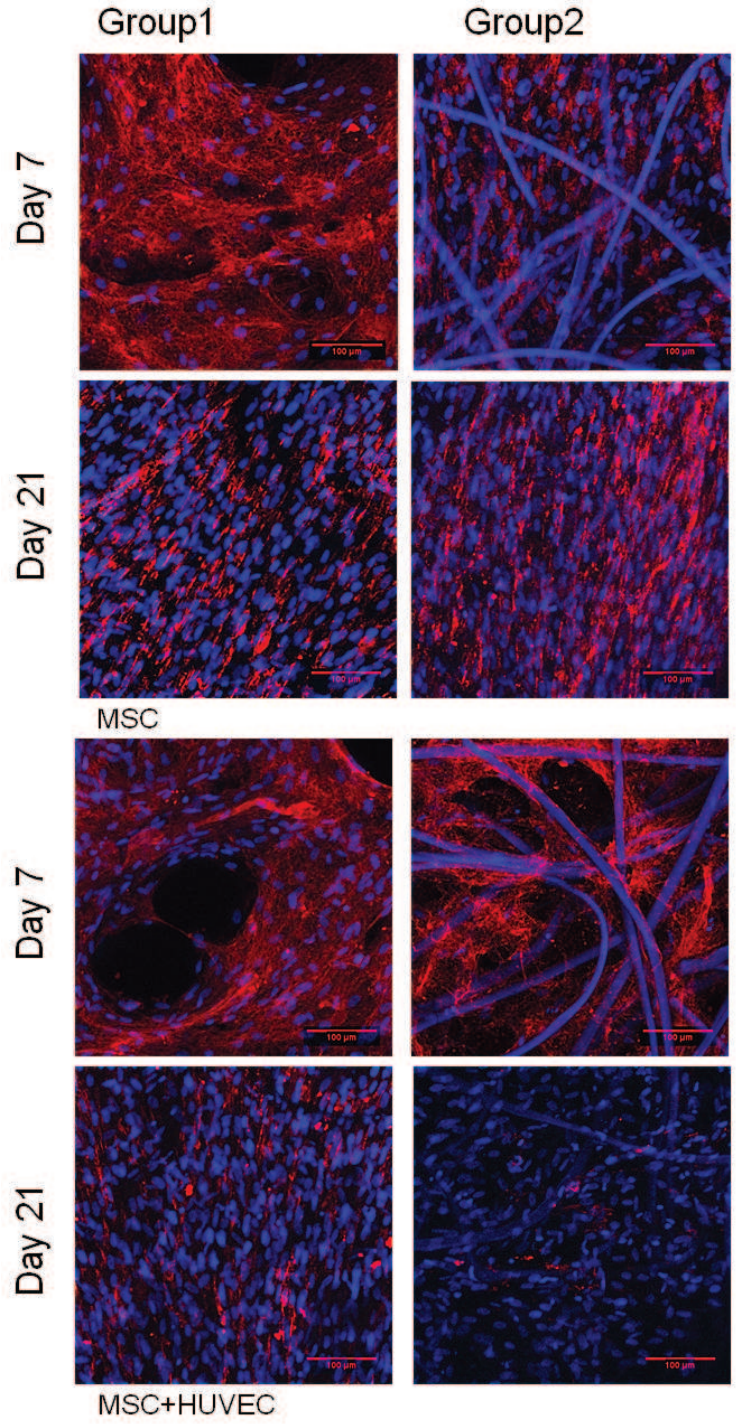

Figure 6.3: Confocal Laser Scanning Microscopy images of the samples stained with a specific antibody for collagen I. Images of 7 and 21 days after cell seeding are reported. Group 1: PdlLA salt-leached sponge; Group 2: PdlLA salt-leached sponge with silk fibroin fibers. Scale bars = 100 µm.

ALP is one of the first functional genes expressed in the process of mineralization and for many, it has become the marker of choice when assessing the phenotype or developmental maturity of cells undergoing osteogenic differentiation. For these reasons the ALP activity of the cells on the scaffolds was measured (Fig. 6.4). In the cells seeded onto Group 1 (with hMSC or with hMSC and HUVECs) the ALP activity was higher, especially at day 21.

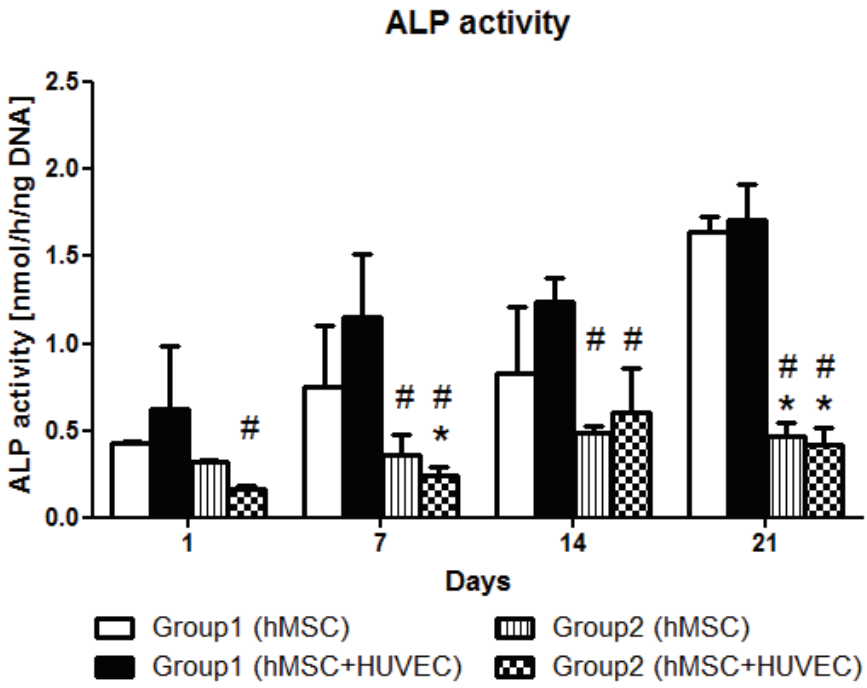

Figure 6.4: ALP activity. *, $p < 0.05$ vs the Group1 (hMSC): #, $p < 0.05$ vs the Group1 (hMSC+HUVEC); @, $p < 0.05$ vs the Group2 (hMSC). Group 1: PdlLA salt-leached sponge; Group 2: PdlLA salt-leached sponge with silk fibroin fibers.

Reverse transcriptase–quantitative PCR was used to verify if at 21 days,, there were differences in the gene expression profiles of cultures on Group 1 scaffolds (Fig. 6.5). Expectedly PECAM and VWF, two typical endothelial markers, were up regulated in the scaffolds with the co-culture but, surprisingly, ALP was up-regulated in the same samples.

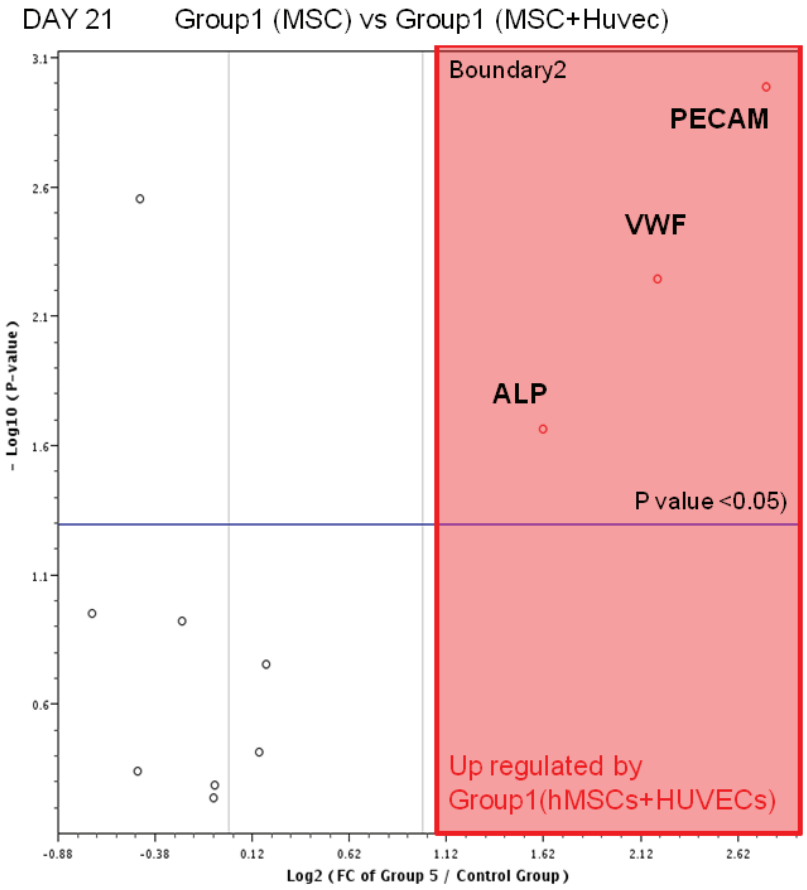

Figure 6.5: Volcano plot with significant gene expression changes between Group 1 scaffolds seeded with hMSCs and Group 1 scaffolds seeded with hMSC and HUVECs. Group 1: PdlLA salt-leached sponge.

Micro-CT was used to measure the total mineralized tissue volume (Fig. 6.6). The results showed that, until week 4, no appreciable mineral deposition was apparent. At week 5 there was an increase especially for Group 1 and at week 6 the higher deposition of mineral was obtained for Group 1 seeded with hMSC and HUVECs.

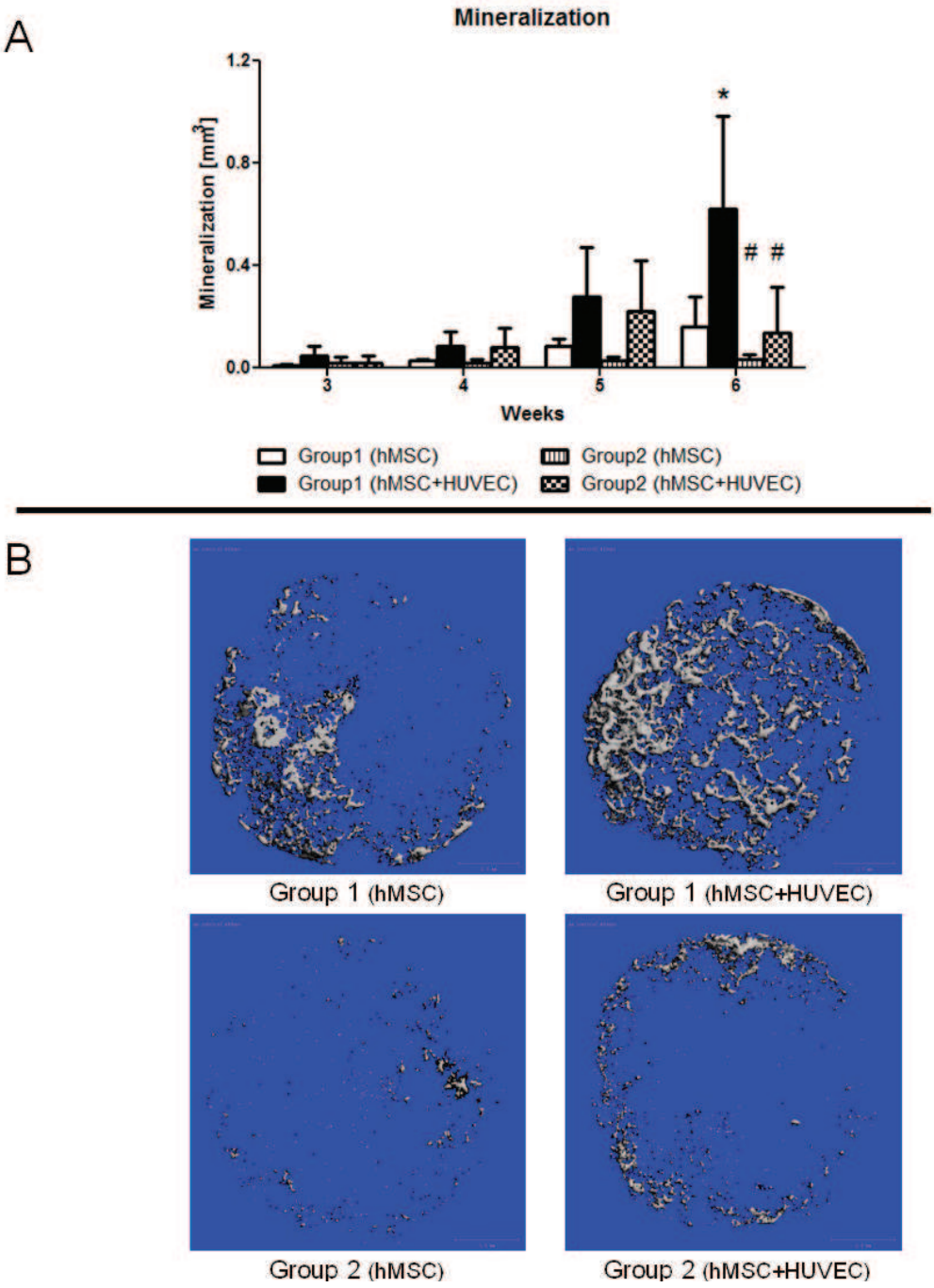

Figure 6.6: (A) Quantification of the mineralization. *, p< 0.05 vs the Group1 (hMSC): #, p< 0.05 vs the Group1 (hMSC+HUVEC); @, p< 0.05 vs the Group2 (hMSC). Group 1: PdlLA salt-leached sponge; Group 2: PdlLA salt-leached sponge with silk fibroin fibers. (B) Micro-CT images of mineralized scaffolds after 6 weeks of cell culture.

To confirm micro-CT results, histology sections were stained with von Kossa. This

reveals phosphate deposition (Fig. 6.7). The images showed (need to orientate people as to where its from) that the phosphate deposition was only detectable in samples from Group 1.

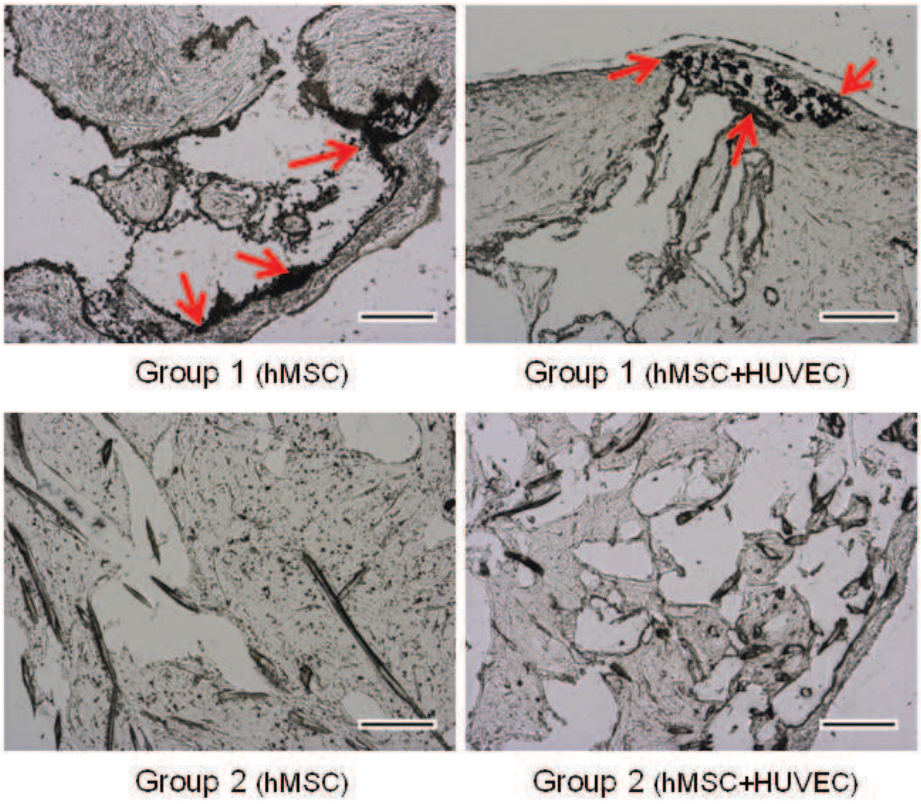

Figure 6.7: Histological images of sections (5 µm) of scaffolds. Samples were stained with von Kossa at 6 weeks. Arrows show granular microdeposits of phosphate. Group 1: PdlLA salt-leached sponge; Group 2: PdlLA salt-leached sponge with silk fibroin fibers. Scale bars = 100 µm.

Reverse transcriptase–quantitative PCR was also used to compare the gene profiles of cells on different scaffolds. Interestingly, the gene expression of the cells in co-cultures seeded on Group 2 scaffolds compared to Group 1 (Fig. 6.8) showed that at day 21, Group 2 endothelial markers (VWF and PECAM) were up-regulated.

This result was confirmed qualitatively by confocal laser microscopy images (Fig. 6.9). In this case we used a specific antibody against PECAM-1. This membrane protein was not detectable in either scaffold at day 21 and at day 7 it was visible only in Group 2.

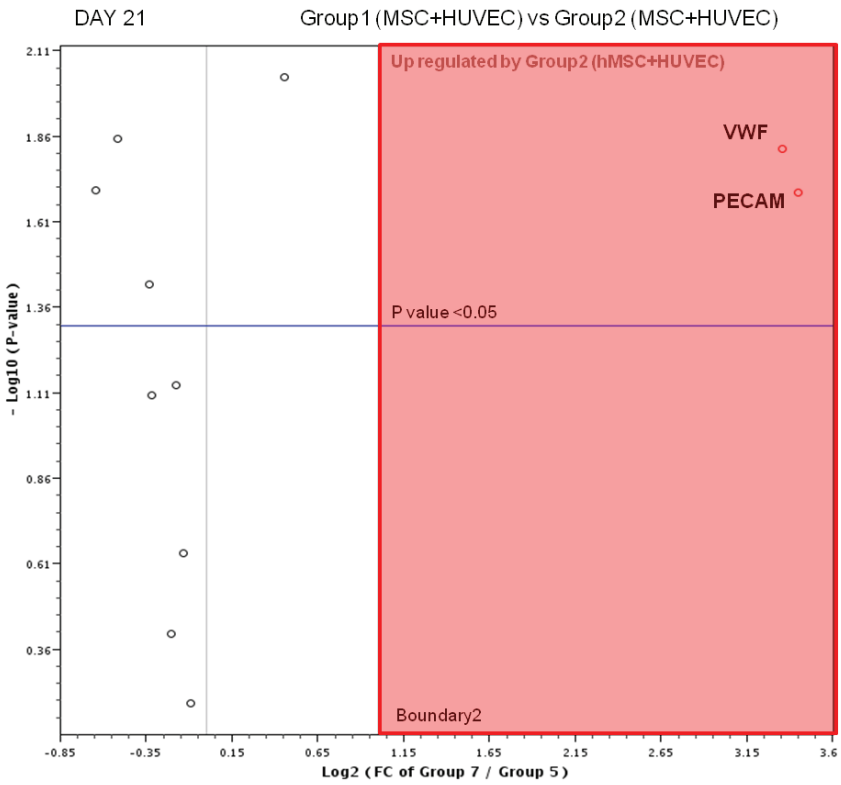

Figure 6.8: Volcano plot with significant gene expression changes between Group 1 scaffolds seeded with hMSCs and HUVECs and Group 2 scaffolds seeded with hMSC and HUVECs. Group 1: PdlLA salt-leached sponge; Group 2: PdlLA salt-leached sponge with silk fibroin fibers.

6.5 Conclusions

The PdlLA scaffolds favor the proliferation of seeded hMSC while the same scaffolds seeded with the co-culture indicate enhanced differentiationby their increased amount of mineralized tissue. With addition of silk fibroin fibers to the scaffold, hMSC differentiation appears inhibited or at least delayed , despite the presence of aligned ECM. Conversely, the same scaffolds support HUVECs in co-cultures, at least at early time points where it was possible to notice a certain degree of organization (Figure 9 with PECAM staining) despite use of osteogenic culture conditions. It is possible that the hMSC differentiated into endothelial cells (alternative source for tissue replacement/vascularisation, Oswald Stem Cells 22:3: 377-384, 2004). These results are of interest because they demonstrate how the addition of endothelial cells can affect hMSC phenotype and that such modifications can be modulated by scaffold composition and structure. In the present study, the introduction of silk fibroin fibers to a PdlLA sponge affected both angiogenesis and osteogenesis, modulating phenotypes of hMSCs and HUVECs. In the future such studies could be extended to a small animal defect model to determine if scaffold composition and co-cultures perform similarly in vivo. If applicable to the bone defect, modulation of the scaffold and cell types could determine whether promotion of angiogenesis or mineralization processes could accelerate the healing process.

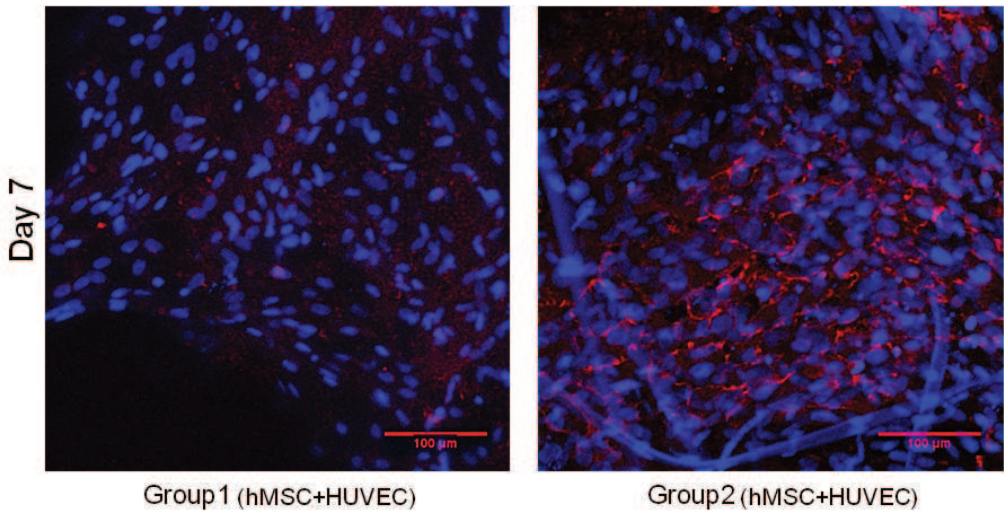

Figure 6.9: Confocal Laser Scanning Microscopy images of cells stained for nuclei (DAPI, blue) and PECAM-1 (red). Group 1 and Group 2 at 7 days after cell seeding are shown. Group 1: PdlLA salt-leached sponge; Group 2: PdlLA salt-leached sponge with silk fibroin fibers. Scale bars = 100 µm.

7 Conclusions

The overall objective of this thesis was to design and evaluate, using different strategies, a novel functional scaffold for a bone tissue engineering application.

The general idea was to mimic the natural ECM. The mature bone is widely considered the 'golden standard' for bone tissue engineering scaffold model. Differently, in all this research work, we move our attention from the final stage of bone healing to an earlier stage, considering the bony callus. It is a temporary tissue, characterized by a collagen network, template for the subsequent healing process that terminates with the mineralized matrix.

We modulated scaffold (made of PdlLA or/and SF) parameters and we correlate them with collagen production and assembling, evaluating which favour ECM mineralization.

In a first approach, we compared scaffolds with ordered and random geometries, produced by a microfabrication system and by solvent casting particulate leaching techniques respectively. The results showed that, even if cells growing and proliferation were comparable, the collagen production and its organization on the scaffolds with a randomly distributed porosity seemed to be more suitable for a bone tissue regeneration application.

We subsequently demonstrated the important role of pore size on cell behaviour and in particular on ECM production and organization.

Once selected a proper pore size and scaffold geometry, we improved the capacity of constructs to be vascularised, introducing SF fibers to the PdlLA sponges for their structural and biological properties.

Finally, working on scaffold structure and composition, we were able to trigger the response of co-cultured cells, influencing and favouring angiogenesis or osteogenesis.

In all the described steps, we put a lot of effort in characterizing the ECM matrix production and organization, finding that evaluation of type I collagen assembling could be considered a useful tool to predict the degree of the final mineralization as

regards the regenerative process.

This work results interesting and innovative because it emphasizes the possibility to correlate the scaffold morphology to type I collagen assembly, which in turn affects the final mineralization process, allowing to evaluate the tissue produced by osteoblasts from the first steps in bone formation. Moreover, we were able to trigger and control some cell behaviours changing construct characteristics.

Further research is required to deeply study the strict relation between type I collagen and mineralization. Additionally, a segmental bone defect models should be considered to characterize the role of silk fibroin fibers during the bone healing process and to determine whether there is correspondence between the results and our in vitro model outcomes.

Bibliography

[1] Schindeler, A, McDonald, M. M, Bokko, P, & Little, D. G. (2008) Bone remodeling during fracture repair: The cellular picture. *Seminars in cell & developmental biology* **19**, 459–66.

[2] Isner, J. M, Vale, P, Symes, J, Losordo, D. W, & Asahara, T. (2001) Angiogenesis and cardiovascular disease. *Dialog Cardiovas Med* **6**, 145–65.

[3] Daley, W. P, Peters, S. B, & Larsen, M. (2008) Extracellular matrix dynamics in development and regenerative medicine. *Journal of cell science* **121**, 255–64.

[4] Hynes, R. O. (2009) The extracellular matrix: not just pretty fibrils. *Science (New York, N.Y.)* **326**, 1216–9.

[5] Lu, P, Takai, K, Weaver, V. M, & Werb, Z. (2011) Extracellular matrix degradation and remodeling in development and disease. *Cold Spring Harbor perspectives in biology* **3**.

[6] Silver, F. H, DeVore, D, & Siperko, L. M. (2003) Invited Review: Role of mechanophysiology in aging of ECM: effects of changes in mechanochemical transduction. *Journal of applied physiology (Bethesda, Md. : 1985)* **95**, 2134–41.

[7] Hynes, R. O & Naba, A. (2012) Overview of the matrisome–an inventory of extracellular matrix constituents and functions. *Cold Spring Harbor perspectives in biology* **4**, a004903.

[8] Frantz, C, Stewart, K. M, & Weaver, V. M. (2010) The extracellular matrix at a glance. *Journal of cell science* **123**, 4195–200.

[9] Lonai, P. (2003) Epithelial mesenchymal interactions, the ECM and limb development. *Journal of anatomy* **202**, 43–50.

[10] Rozario, T & DeSimone, D. W. (2010) The extracellular matrix in development and morphogenesis: a dynamic view. *Developmental biology* **341**, 126–40.

[11] Vakonakis, I & Campbell, I. D. (2007) Extracellular matrix: from atomic resolution to ultrastructure. *Current opinion in cell biology* **19**, 578–83.

[12] Egeblad, M, Rasch, M. G, & Weaver, V. M. (2010) Dynamic interplay between the collagen scaffold and tumor evolution. *Current opinion in cell biology* **22**, 697–706.

[13] Li, L & Xie, T. (2005) Stem cell niche: structure and function. *Annual review of cell and developmental biology* **21**, 605–31.

[14] Tanentzapf, G, Devenport, D, Godt, D, & Brown, N. H. (2007) Integrin-dependent anchoring of a stem-cell niche. *Nature cell biology* **9**, 1413–8.

[15] Taddei, I, Deugnier, M.-A, Faraldo, M. M, Petit, V, Bouvard, D, Medina, D, Fässler, R, Thiery, J. P, & Glukhova, M. A. (2008) Beta1 integrin deletion from the basal compartment of the mammary epithelium affects stem cells. *Nature cell biology* **10**, 716–22.

[16] Stoppato, M, Carletti, E, Maniglio, D, Migliaresi, C, & Motta, A. (2013) Functional role of scaffold geometries as a template for physiological ECM formation: evaluation of collagen 3D assembly. *Journal of tissue engineering and regenerative medicine* **7**, 161–8.

[17] Stoppato, M, Carletti, E, Sidarovich, V, Quattrone, A, Unger, R. E, Kirkpatrick, C. J, Migliaresi, C, & Motta, A. (2013) Influence of scaffold pore size on collagen I development: A new in vitro evaluation perspective. *Journal of Bioactive and Compatible Polymers* **28**, 16–32.

[18] Pellegrini, L, Burke, D. F, von Delft, F, Mulloy, B, & Blundell, T. L. (2000) Crystal structure of fibroblast growth factor receptor ectodomain bound to ligand and heparin. *Nature* **407**, 1029–34.

[19] Ruoslahti, E & Yamaguchi, Y. (1991) Proteoglycans as modulators of growth factor activities. *Cell* **64**, 867–9.

[20] Kainulainen, V, Wang, H, Schick, C, & Bernfield, M. (1998) Syndecans, heparan sulfate proteoglycans, maintain the proteolytic balance of acute wound fluids. *The Journal of biological chemistry* **273**, 11563–9.

[21] Yu, H, Mouw, J. K, & Weaver, V. M. (2011) Forcing form and function: biomechanical regulation of tumor evolution. *Trends in cell biology* **21**, 47–56.

[22] Reilly, G. C & Engler, A. J. (2010) Intrinsic extracellular matrix properties regulate stem cell differentiation. *Journal of biomechanics* **43**, 55–62.

[23] Lopez, J. I, Mouw, J. K, & Weaver, V. M. (2008) Biomechanical regulation of cell orientation and fate. *Oncogene* **27**, 6981–93.

[24] Wolfe, J. N. (1976) Risk for breast cancer development determined by mammographic parenchymal pattern. *Cancer* **37**, 2486–92.

[25] Lieber, M. M. (2006) Towards an understanding of the role of forces in carcinogenesis: a perspective with therapeutic implications. *Rivista di biologia* **99**, 131–60.

[26] Provenzano, P. P & Keely, P. J. (2011) Mechanical signaling through the cytoskeleton regulates cell proliferation by coordinated focal adhesion and Rho GTPase signaling. *Journal of cell science* **124**, 1195–205.

[27] Butcher, D. T, Alliston, T, & Weaver, V. M. (2009) A tense situation: forcing tumour progression. *Nature reviews. Cancer* **9**, 108–22.

[28] Wang, N, Tytell, J. D, & Ingber, D. E. (2009) Mechanotransduction at a distance: mechanically coupling the extracellular matrix with the nucleus. *Nature reviews. Molecular cell biology* **10**, 75–82.

[29] Liu, M, Tanswell, A. K, & Post, M. (1999) Mechanical force-induced signal transduction in lung cells. *The American journal of physiology* **277**, L667–83.

[30] Silver, F. H, Siperko, L. M, & Seehra, G. P. (2003) Mechanobiology of force transduction in dermal tissue. *Skin research and technology : official journal of International Society for Bioengineering and the Skin (ISBS) [and] International Society for Digital Imaging of Skin (ISDIS) [and] International Society for Skin Imaging (ISSI)* **9**, 3–23.

[31] Silver, F. H. (2006) *Mechanosensing and Mechanochemical Transduction in Extracellular Matrix: Biological, Chemical, Engineering, and Physiological Aspects.* (Springer, New York), p. 314.

[32] Miyamoto, S, Teramoto, H, Coso, O. A, Gutkind, J. S, Burbelo, P. D, Akiyama, S. K, & Yamada, K. M. (1995) Integrin function: molecular hierarchies of cytoskeletal and signaling molecules. *The Journal of cell biology* **131**, 791–805.

[33] Plopper, G. E, McNamee, H. P, Dike, L. E, Bojanowski, K, & Ingber, D. E. (1995) Convergence of integrin and growth factor receptor signaling pathways within the focal adhesion complex. *Molecular biology of the cell* **6**, 1349–65.

[34] Huebsch, N & Mooney, D. J. (2009) Inspiration and application in the evolution of biomaterials. *Nature* **462**, 426–32.

[35] Guilak, F, Cohen, D. M, Estes, B. T, Gimble, J. M, Liedtke, W, & Chen, C. S. (2009) Control of stem cell fate by physical interactions with the extracellular matrix. *Cell stem cell* **5**, 17–26.

[36] Moore, S. W. (2003) Scrambled eggs: mechanical forces as ecological factors in early development. *Evolution & development* **5**, 61–6.

[37] Silver, F. H & Bradica, G. (2002) Mechanobiology of cartilage: how do internal and external stresses affect mechanochemical transduction and elastic energy storage? *Biomechanics and modeling in mechanobiology* **1**, 219–38.

[38] Vandenburgh, H, Chromiak, J, Shansky, J, Del Tatto, M, & Lemaire, J. (1999) Space travel directly induces skeletal muscle atrophy. *FASEB journal : official publication of the Federation of American Societies for Experimental Biology* **13**, 1031–8.

[39] Bilezikian, J. P, Raisz, L. G, & Rodan, G. A. (2002) *Principles of Bone Biology.* (Academic Press, San Diego, California) Vol. 338, p. 1696.

[40] Carter, D. R & Hayes, W. C. (1977) The compressive behavior of bone as a two-phase porous structure. *The Journal of bone and joint surgery. American volume* **59**, 954–62.

[41] Karageorgiou, V & Kaplan, D. (2005) Porosity of 3D biomaterial scaffolds and osteogenesis. *Biomaterials* **26**, 5474–91.

[42] Buckwalter, J. A, Glimcher, M. J, Cooper, R. R, & Recker, R. (1996) Bone biology. I: Structure, blood supply, cells, matrix, and mineralization. *Instructional course lectures* **45**, 371–86.

[43] Watanabe, H, Yanagisawa, T, & Sasaki, J. (1995) Cytoskeletal architecture of rat calvarial osteoclasts: microfilaments, and intermediate filaments, and nuclear matrix as demonstrated by detergent perfusion. *The Anatomical record* **243**, 165–74.

[44] Christiansen, P. (1999) Scaling of the limb long bones to body mass in terrestrial mammals. *Journal of morphology* **239**, 167–90.

[45] Cullinane, D. M. (2000) Axial versus Appendicular: Constraint versus Selection1. *American Zoologist* **40**, 136–145.

[46] Sikavitsas, V. I, Temenoff, J. S, & Mikos, A. G. (2001) Biomaterials and bone mechanotransduction. *Biomaterials* **22**, 2581–93.

[47] Manjubala, I, Liu, Y, Epari, D. R, Roschger, P, Schell, H, Fratzl, P, & Duda,

G. N. (2009) Spatial and temporal variations of mechanical properties and mineral content of the external callus during bone healing. *Bone* **45**, 185–92.

[48] Brinckmann, J. (2005) in *Collagen*, eds. Brinckmann, J, Notbohm, H, & Müller, P. K. (Springer), pp. 1–6.

[49] Veit, G, Kobbe, B, Keene, D. R, Paulsson, M, Koch, M, & Wagener, R. (2006) Collagen XXVIII, a novel von Willebrand factor A domain-containing protein with many imperfections in the collagenous domain. *The Journal of biological chemistry* **281**, 3494–504.

[50] Shoulders, M. D & Raines, R. T. (2009) Collagen structure and stability. *Annual review of biochemistry* **78**, 929–58.

[51] Gelse, K. (2003) Collagens-structure, function, and biosynthesis. *Advanced Drug Delivery Reviews* **55**, 1531–1546.

[52] Lodish, H, Berk, A, Zipursky, S. L, Matsudaira, P, Baltimore, D, & Darnell, J. (2000) *Molecular cell biology*. (Freeman, New York).

[53] Berisio, R, Vitagliano, L, Mazzarella, L, & Zagari, A. (2002) Crystal structure of the collagen triple helix model [(Pro-Pro-Gly)(10)](3). *Protein science : a publication of the Protein Society* **11**, 262–70.

[54] Brazel, D, Oberbäumer, I, Dieringer, H, Babel, W, Glanville, R. W, Deutzmann, R, & Kühn, K. (1987) Completion of the amino acid sequence of the alpha 1 chain of human basement membrane collagen (type IV) reveals 21 non-triplet interruptions located within the collagenous domain. *European journal of biochemistry / FEBS* **168**, 529–36.

[55] Ramshaw, J. A, Shah, N. K, & Brodsky, B. (1998) Gly-X-Y tripeptide frequencies in collagen: a context for host-guest triple-helical peptides. *Journal of structural biology* **122**, 86–91.

[56] Astbury, W. T & Bell, F. O. (1940) Molecular Structure of the Collagen Fibres. *Nature* **145**, 421–422.

[57] Pauling, L & Corey, R. B. (1951) The structure of fibrous proteins of the collagen-gelatin group. *Proceedings of the National Academy of Sciences of the United States of America* **37**, 272–81.

[58] Ramachandran, G. N & Kartha, G. (1954) Structure of Collagen. *Nature* **174**, 269–270.

[59] Dee, K. C, Puleo, D. A, & Bizios, R. (2002) *An introduction to tissue-biomaterial interactions*. (Wiley-Liss), p. 248.

[60] Buehler, M. J. (2006) Nature designs tough collagen: explaining the nanostructure of collagen fibrils. *Proceedings of the National Academy of Sciences of the United States of America* **103**, 12285–90.

[61] Fratzl, P. (2008) *Collagen: structure and mechanics*. (Springer).

[62] Gerstenfeld, L. C, Cullinane, D. M, Barnes, G. L, Graves, D. T, & Einhorn, T. A. (2003) Fracture healing as a post-natal developmental process: molecular, spatial, and temporal aspects of its regulation. *Journal of cellular biochemistry* **88**, 873–84.

[63] Le, A. X, Miclau, T, Hu, D, & Helms, J. A. (2001) Molecular aspects of healing in stabilized and non-stabilized fractures. *Journal of orthopaedic research : official publication of the Orthopaedic Research Society* **19**, 78–84.

[64] Lamovec, J, Mozina, E, & Baebler, B. (2003) Hyperplastic callus formation in osteogenesis imperfecta. *Annals of diagnostic pathology* **7**, 231–5.

[65] Shefelbine, S. J, Augat, P, Claes, L, & Simon, U. (2005) Trabecular bone fracture healing simulation with finite element analysis and fuzzy logic. *Journal of biomechanics* **38**, 2440–50.

[66] McKinley, T. (2003) Principles of Fracture Healing. *Surgery (Oxford)* **21**, 209–212.

[67] Einhorn, T. A. (1998) The cell and molecular biology of fracture healing. *Clinical orthopaedics and related research* pp. S7–21.

[68] Kou, P. M & Babensee, J. E. (2011) Macrophage and dendritic cell phenotypic diversity in the context of biomaterials. *Journal of biomedical materials research. Part A* **96**, 239–60.

[69] Sorokin, L. (2010) The impact of the extracellular matrix on inflammation. *Nature reviews. Immunology* **10**, 712–23.

[70] Duffield, J. S. (2003) The inflammatory macrophage: a story of Jekyll and Hyde. *Clinical science (London, England : 1979)* **104**, 27–38.

[71] Johnson, M. R, Boerckel, J. D, Dupont, K. M, & Guldberg, R. E. (2011) Functional restoration of critically sized segmental defects with bone morphogenetic protein-2 and heparin treatment. *Clinical orthopaedics and related research* **469**, 3111–7.

[72] Salgado, A. J, Coutinho, O. P, & Reis, R. L. (2004) Bone tissue engineering: state of the art and future trends. *Macromolecular bioscience* **4**, 743–65.

[73] Griffith, L. G. (2002) Tissue Engineering–Current Challenges and Expanding Opportunities. *Science* **295**, 1009–1014.

[74] Dawson, J. I & Oreffo, R. O. C. (2008) Bridging the regeneration gap: stem cells, biomaterials and clinical translation in bone tissue engineering. *Archives of biochemistry and biophysics* **473**, 124–31.

[75] Langer, R & Vacanti, J. P. (1993) Tissue engineering. *Science (New York, N.Y.)* **260**, 920–6.

[76] Lutolf, M. P, Gilbert, P. M, & Blau, H. M. (2009) Designing materials to direct stem-cell fate. *Nature* **462**, 433–41.

[77] Dutta, R. C & Dutta, A. K. (2010) Comprehension of ECM-cell dynamics: a prerequisite for tissue regeneration. *Biotechnology advances* **28**, 764–9.

[78] Williams, D. F. (2008) On the mechanisms of biocompatibility. *Biomaterials* **29**, 2941–53.

[79] Zhang, S. (2004) Hydrogels: Wet or let die. *Nature materials* **3**, 7–8.

[80] Lee, J, Cuddihy, M. J, & Kotov, N. A. (2008) Three-dimensional cell culture matrices: state of the art. *Tissue engineering. Part B, Reviews* **14**, 61–86.

[81] Drury, J. L & Mooney, D. J. (2003) Hydrogels for tissue engineering: scaffold design variables and applications. *Biomaterials* **24**, 4337–51.

[82] Mason, M, Vercruysse, K. P, Kirker, K. R, Frisch, R, Marecak, D. M, Prestwich, G. D, & Pitt, W. G. (2000) Attachment of hyaluronic acid to polypropylene, polystyrene, and polytetrafluoroethylene. *Biomaterials* **21**, 31–6.

[83] Tang, S & Spector, M. (2007) Incorporation of hyaluronic acid into collagen scaffolds for the control of chondrocyte-mediated contraction and chondrogenesis. *Biomedical materials (Bristol, England)* **2**, S135–41.

[84] Biswas, A, Ovaert, T. C, Slaboch, C, Zhao, H, Bayer, I. S, Biris, A. S, & Wang, T. (2011) Mineral concentration dependent modulation of mechanical properties of bone-inspired bionanocomposite scaffold. *Applied Physics Letters* **99**, 013702.

[85] Rahfoth, B, Weisser, J, Sternkopf, F, Aigner, T, von der Mark, K, & Bräuer, R. (1998) Transplantation of allograft chondrocytes embedded in agarose gel into cartilage defects of rabbits. *Osteoarthritis and cartilage / OARS, Osteoarthritis Research Society* **6**, 50–65.

[86] Benya, P. (1982) Dedifferentiated chondrocytes reexpress the differentiated collagen phenotype when cultured in agarose gels. *Cell* **30**, 215–224.

[87] Shapiro, L & Cohen, S. (1997) Novel alginate sponges for cell culture and transplantation. *Biomaterials* **18**, 583–90.

[88] Zhong, S. P, Teo, W. E, Zhu, X, Beuerman, R, Ramakrishna, S, & Yung, L. Y. L. (2007) Development of a novel collagen-GAG nanofibrous scaffold via electrospinning. *Materials Science and Engineering: C* **27**, 262–266.

[89] Hedén, P, Sellman, G, von Wachenfeldt, M, Olenius, M, & Fagrell, D. (2009) Body shaping and volume restoration: the role of hyaluronic acid. *Aesthetic plastic surgery* **33**, 274–82.

[90] Marcacci, M, Kon, E, Zaffagnini, S, Iacono, F, Filardo, G, & Delcogliano, M. (2006) Autologous Chondrocytes in a Hyaluronic Acid Scaffold. *Operative Techniques in Orthopaedics* **16**, 266–270.

[91] Holzman, S, Connolly, R. J, & Schwaitzberg, S. D. (1994) Effect of hyaluronic acid solution on healing of bowel anastomoses. *Journal of investigative surgery : the official journal of the Academy of Surgical Research* **7**, 431–7.

[92] Mandal, B. B & Kundu, S. C. (2009) Cell proliferation and migration in silk fibroin 3D scaffolds. *Biomaterials* **30**, 2956–65.

[93] Silva, S. S, Motta, A, Rodrigues, M. T, Pinheiro, A. F. M, Gomes, M. E, Mano, J. a. F, Reis, R. L, & Migliaresi, C. (2008) Novel genipin-cross-linked chitosan/silk fibroin sponges for cartilage engineering strategies. *Biomacromolecules* **9**, 2764–74.

[94] Motta, A, Fambri, L, & Migliaresi, C. (2002) Regenerated silk fibroin films: Thermal and dynamic mechanical analysis. *Macromolecular Chemistry and Physics* **203**, 1658–1665.

[95] Unger, R. E, Wolf, M, Peters, K, Motta, A, Migliaresi, C, & James Kirkpatrick, C. (2004) Growth of human cells on a non-woven silk fibroin net: a potential for use in tissue engineering. *Biomaterials* **25**, 1069–75.

[96] Lam, C, Mo, X, Teoh, S, & Hutmacher, D. (2002) Scaffold development using 3D printing with a starch-based polymer. *Materials Science and Engineering: C* **20**, 49–56.

[97] Duarte, A. R. C, Mano, J. a. F, & Reis, R. L. (2009) Preparation of starch-based scaffolds for tissue engineering by supercritical immersion precipitation. *The Journal of Supercritical Fluids* **49**, 279–285.

[98] Yilgor, P, Sousa, R. A, Reis, R. L, Hasirci, N, & Hasirci, V. (2008) 3D Plotted

PCL Scaffolds for Stem Cell Based Bone Tissue Engineering. *Macromolecular Symposia* **269**, 92–99.

[99] Zhang, Y, Huang, Z.-M, Xu, X, Lim, C. T, & Ramakrishna, S. (2004) Preparation of Core-Shell Structured PCL-r-Gelatin Bi-Component Nanofibers by Coaxial Electrospinning. *Chemistry of Materials* **16**, 3406–3409.

[100] Vozzi, G, Flaim, C. J, Bianchi, F, Ahluwalia, A, & Bhatia, S. (2002) Microfabricated PLGA scaffolds: a comparative study for application to tissue engineering. *Materials Science and Engineering: C* **20**, 43–47.

[101] Vozzi, G, Flaim, C, Ahluwalia, A, & Bhatia, S. (2003) Fabrication of PLGA scaffolds using soft lithography and microsyringe deposition. *Biomaterials* **24**, 2533–40.

[102] Kim, S. Y, Kanamori, T, Noumi, Y, Wang, P.-C, & Shinbo, T. (2004) Preparation of porous poly(D,L-lactide) and poly(D,L-lactide-co-glycolide) membranes by a phase inversion process and investigation of their morphological changes as cell culture scaffolds. *Journal of Applied Polymer Science* **92**, 2082–2092.

[103] Yang, F, Cui, W, Xiong, Z, Liu, L, Bei, J, & Wang, S. (2006) Poly(l,l-lactide-co-glycolide)/tricalcium phosphate composite scaffold and its various changes during degradation in vitro. *Polymer Degradation and Stability* **91**, 3065–3073.

[104] Pamula, E & Menaszek, E. (2008) In vitro and in vivo degradation of poly(l-lactide-co-glycolide) films and scaffolds. *Journal of materials science. Materials in medicine* **19**, 2063–70.

[105] Mooney, D. J, Baldwin, D. F, Suh, N. P, Vacanti, J. P, & Langer, R. (1996) Novel approach to fabricate porous sponges of poly(D,L-lactic-co-glycolic acid) without the use of organic solvents. *Biomaterials* **17**, 1417–22.

[106] Lv, Q & Feng, Q. (2006) Preparation of 3-D regenerated fibroin scaffolds with freeze drying method and freeze drying/foaming technique. *Journal of materials science. Materials in medicine* **17**, 1349–56.

[107] Ma, D & McHugh, A. J. (2007) The interplay of phase inversion and membrane formation in the drug release characteristics of a membrane-based delivery system. *Journal of Membrane Science* **298**, 156–168.

[108] Tsivintzelis, I, Pavlidou, E, & Panayiotou, C. (2007) Porous scaffolds prepared by phase inversion using supercritical CO2 as antisolvent. *The Journal of Supercritical Fluids* **40**, 317–322.

[109] Tsivintzelis, I, Pavlidou, E, & Panayiotou, C. (2007) Biodegradable polymer foams prepared with supercritical CO2-ethanol mixtures as blowing agents. *The Journal of Supercritical Fluids* **42**, 265–272.

[110] Liang, D, Hsiao, B. S, & Chu, B. (2007) Functional electrospun nanofibrous scaffolds for biomedical applications. *Advanced drug delivery reviews* **59**, 1392–412.

[111] Li, D & Xia, Y. (2004) Electrospinning of Nanofibers: Reinventing the Wheel? *Advanced Materials* **16**, 1151–1170.

[112] Huang, Z.-M, Zhang, Y.-Z, Kotaki, M, & Ramakrishna, S. (2003) A review on polymer nanofibers by electrospinning and their applications in nanocomposites. *Composites Science and Technology* **63**, 2223–2253.

[113] Cima, M, Sachs, E, Fan, T, Bredt, J. F, Michaels, S. P, Khanuja, S, Lauder, A, Lee, S.-J. J, Brancazio, D, Curodeau, A, & Tuerck, H. (1995) Three-dimensional printing techniques.

[114] Sachs, E. M, Haggerty, J. S, Cima, M. J, & Williams, P. A. (1993) Three-dimensional printing techniques.

[115] Masood, S. (2007) Application of fused deposition modelling in controlled drug delivery devices. *Assembly Automation* **27**, 215–221.

[116] Healy, K. E & Guldberg, R. E. (2007) Bone tissue engineering. *Journal of musculoskeletal & neuronal interactions* **7**, 328–30.

[117] Brekke, J. H & Toth, J. M. (1998) Principles of tissue engineering applied to programmable osteogenesis. *Journal of biomedical materials research* **43**, 380–98.

[118] Tian, L & George, S. C. (2011) Biomaterials to prevascularize engineered tissues. *Journal of cardiovascular translational research* **4**, 685–98.

[119] Novosel, E. C, Kleinhans, C, & Kluger, P. J. (2011) Vascularization is the key challenge in tissue engineering. *Advanced drug delivery reviews* **63**, 300–11.

[120] Tabata, Y. (2009) Biomaterial technology for tissue engineering applications. *Journal of the Royal Society, Interface / the Royal Society* **6 Suppl 3**, S311–24.

[121] Santos, M. I & Reis, R. L. (2010) Vascularization in bone tissue engineering: physiology, current strategies, major hurdles and future challenges. *Macromolecular bioscience* **10**, 12–27.

[122] Phelps, E. A & Garcia, A. J. (2009) Update on therapeutic vascularization strategies. *Regenerative medicine* **4**, 65–80.

[123] Grizzi, I, Garreau, H, Li, S, & Vert, M. (1995) Hydrolytic degradation of devices based on poly(DL-lactic acid) size-dependence. *Biomaterials* **16**, 305–11.

[124] Zhang, X, Espiritu, M, Bilyk, A, & Kurniawan, L. (2008) Morphological behaviour of poly(lactic acid) during hydrolytic degradation. *Polymer Degradation and Stability* **93**, 1964–1970.

[125] Li, S & McCarthy, S. (1999) Further investigations on the hydrolytic degradation of poly (DL-lactide). *Biomaterials* **20**, 35–44.

[126] Carletti, E, Motta, A, & Migliaresi, C. (2011) Scaffolds for tissue engineering and 3D cell culture. *Methods in molecular biology (Clifton, N.J.)* **695**, 17–39.

[127] Böstman, O, Partio, E, Hirvensalo, E, & Rokkanen, P. (1992) Foreign-body reactions to polyglycolide screws. Observations in 24/216 malleolar fracture cases. *Acta orthopaedica Scandinavica* **63**, 173–6.

[128] Lanza, R, Langer, R, & Vacanti, J. P. (2007) *Principles of tissue engineeringle.* (Academic press), p. 1336.

[129] Vepari, C & Kaplan, D. L. (2007) Silk as a Biomaterial. *Progress in polymer science* **32**, 991–1007.

[130] Altman, G. H, Diaz, F, Jakuba, C, Calabro, T, Horan, R. L, Chen, J, Lu, H, Richmond, J, & Kaplan, D. L. (2003) Silk-based biomaterials. *Biomaterials* **24**, 401–416.

[131] Jin, H.-J & Kaplan, D. L. (2003) Mechanism of silk processing in insects and spiders. *Nature* **424**, 1057–61.

[132] Yamada, H, Igarashi, Y, Takasu, Y, Saito, H, & Tsubouchi, K. (2004) Identification of fibroin-derived peptides enhancing the proliferation of cultured human skin fibroblasts. *Biomaterials* **25**, 467–472.

[133] Hollister, S. J, Guldberg, R. E, Kuelske, C. L, Caldwell, N. J, Richards, M, & Goldstein, S. a. (1996) Relative effects of wound healing and mechanical stimulus on early bone response to porous-coated implants. *Journal of orthopaedic research : official publication of the Orthopaedic Research Society* **14**, 654–62.

[134] Block, J. E. (2005) The role and effectiveness of bone marrow in osseous regeneration. *Medical hypotheses* **65**, 740–7.

[135] Schlichting, K, Schell, H, Kleemann, R. U, Schill, A, Weiler, A, Duda, G. N, & Epari, D. R. (2008) Influence of scaffold stiffness on subchondral bone and subsequent cartilage regeneration in an ovine model of osteochondral defect healing. *The American journal of sports medicine* **36**, 2379–91.

[136] Hutmacher, D. W. (2000) Scaffolds in tissue engineering bone and cartilage. *Biomaterials* **21**, 2529–43.

[137] Jones, A. C, Milthorpe, B, Averdunk, H, Limaye, A, Senden, T. J, Sakellariou, A, Sheppard, A. P, Sok, R. M, Knackstedt, M. A, Brandwood, A, Rohner, D, & Hutmacher, D. W. (2004) Analysis of 3D bone ingrowth into polymer scaffolds via micro-computed tomography imaging. *Biomaterials* **25**, 4947–54.

[138] Aydin, H. M, Haj, A. J. E, & Pi, E. (2009) Improving pore interconnectivity in polymeric scaffolds for tissue engineering. *Tissue Engineering* pp. 470–476.

[139] Haaparanta, A.-M, Haimi, S, Ellä, V, Hopper, N, Miettinen, S, Suuronen, R, & Kellomäki, M. (2010) Porous polylactide/beta-tricalcium phosphate composite scaffolds for tissue engineering applications. *Journal of tissue engineering and regenerative medicine* **4**, 366–73.

[140] Schieker, M, Seitz, H, Drosse, I, Seitz, S, & Mutschler, W. (2006) Biomaterials as Scaffold for Bone Tissue Engineering. *European Journal of Trauma* **32**, 114–124.

[141] Zeltinger, J, Sherwood, J. K, Graham, D. A, Müeller, R, & Griffith, L. G. (2001) Effect of pore size and void fraction on cellular adhesion, proliferation, and matrix deposition. *Tissue engineering* **7**, 557–72.

[142] Ishaug-Riley, S. L, Crane-Kruger, G. M, Yaszemski, M. J, & Mikos, a. G. (1998) Three-dimensional culture of rat calvarial osteoblasts in porous biodegradable polymers. *Biomaterials* **19**, 1405–12.

[143] O'Brien, F. J, Harley, B. a, Yannas, I. V, & Gibson, L. J. (2005) The effect of pore size on cell adhesion in collagen-GAG scaffolds. *Biomaterials* **26**, 433–41.

[144] Carletti, E, Endogan, T, Hasirci, N, Hasirci, V, Maniglio, D, Motta, A, & Migliaresi, C. (2011) Microfabrication of PDLLA scaffolds. *Journal of tissue engineering and regenerative medicine* **5**, 569–77.

[145] Eriksson, C, Ohlson, K, Richter, K, Billerdahl, N, Johansson, M, & Nygren, H. k. (2007) Callus formation and remodeling at titanium implants. *Journal of biomedical materials research. Part A* **83**, 1062–9.

[146] Owen, T. A, Aronow, M, Shalhoub, V, Barone, L. M, Wilming, L, Tassi-

nari, M. S, Kennedy, M. B, Pockwinse, S, Lian, J. B, & Stein, G. S. (1990) Progressive development of the rat osteoblast phenotype in vitro: reciprocal relationships in expression of genes associated with osteoblast proliferation and differentiation during formation of the bone extracellular matrix. *Journal of cellular physiology* **143**, 420–30.

[147] Ghosh, S, Viana, J. C, Reis, R. L, & Mano, J. a. F. (2008) Development of porous lamellar poly(L-lactic acid) scaffolds by conventional injection molding process. *Acta biomaterialia* **4**, 887–96.

[148] Garlotta, D. (2002) A Literature Review of Poly (Lactic Acid). *Journal of Polymers and the Environment* **9**, 64–84.

[149] Hong, Z, Reis, R. L, & Mano, J. a. F. (2008) Preparation and in vitro characterization of scaffolds of poly(L-lactic acid) containing bioactive glass ceramic nanoparticles. *Acta biomaterialia* **4**, 1297–306.

[150] Mikos, A. G, Thorsen, A. J, Czerwonka, L. A, Bao, Y, Langer, R, Winslow, D. N, & Vacanti, J. P. (1994) Preparation and characterization of poly(l-lactic acid) foams. *Polymer* **35**, 1068–1077.

[151] Jones, C, Smolinski, D, Keogh, a, Kirk, T, & Zheng, M. (2005) Confocal laser scanning microscopy in orthopaedic research. *Progress in Histochemistry and Cytochemistry* **40**, 1–71.

[152] Dolber, P. C & Spach, M. S. (1993) Conventional and confocal fluorescence microscopy of collagen fibers in the heart. *The journal of histochemistry and cytochemistry : official journal of the Histochemistry Society* **41**, 465–9.

[153] Kano, M, Masuda, Y, Tominaga, T, Hori, T, Kitaichi, T, Yoshizumi, M, & Kitagawa, T. (2001) Collagen synthesis and collagenase activity of cryopreserved heart valves. *The Journal of thoracic and cardiovascular surgery* **122**, 706–11.

[154] SWEAT, F, PUCHTLER, H, & ROSENTHAL, S. I. (1964) Sirius Red F3BA as a stain for connective tissue. *Archives of pathology* **78**, 69–72.

[155] Taatjes, D. J, Wadsworth, M. P, Schneider, D. J, & Sobel, B. E. (2000) Improved quantitative characterization of atherosclerotic plaque composition with immunohistochemistry, confocal fluorescence microscopy, and computer-assisted image analysis. *Histochemistry and cell biology* **113**, 161–73.

[156] Cheng, W, Li, H, & Chang, J. (2005) Fabrication and characterization of β-

dicalcium silicate/poly(d,l-lactic acid) composite scaffolds. *Materials Letters* **59**, 2214–2218.

[157] Draghi, L, Resta, S, Pirozzolo, M. G, & Tanzi, M. C. (2005) Microspheres leaching for scaffold porosity control. *Journal of materials science. Materials in medicine* **16**, 1093–7.

[158] Jing, D, Wu, L, & Ding, J. (2006) Solvent-assisted room-temperature compression molding approach to fabricate porous scaffolds for tissue engineering. *Macromolecular bioscience* **6**, 747–57.

[159] Spiller, K. L, Laurencin, S. J, Charlton, D, Maher, S. a, & Lowman, A. M. (2008) Superporous hydrogels for cartilage repair: Evaluation of the morphological and mechanical properties. *Acta biomaterialia* **4**, 17–25.

[160] Zhu, X, Cui, W, Li, X, & Jin, Y. (2008) Electrospun fibrous mats with high porosity as potential scaffolds for skin tissue engineering. *Biomacromolecules* **9**, 1795–801.

[161] Guan, J, Fujimoto, K. L, Sacks, M. S, & Wagner, W. R. (2005) Preparation and characterization of highly porous, biodegradable polyurethane scaffolds for soft tissue applications. *Biomaterials* **26**, 3961–71.

[162] Hsu, Y. Y, Gresser, J. D, Trantolo, D. J, Lyons, C. M, Gangadharam, P. R, & Wise, D. L. (1997) Effect of polymer foam morphology and density on kinetics of in vitro controlled release of isoniazid from compressed foam matrices. *Journal of biomedical materials research* **35**, 107–16.

[163] Zhang, R & Ma, P. X. (1999) Poly(alpha-hydroxyl acids)/hydroxyapatite porous composites for bone-tissue engineering. I. Preparation and morphology. *Journal of biomedical materials research* **44**, 446–55.

[164] Goegan, P, Johnson, G, & Vincent, R. (1995) Effects of serum protein and colloid on the alamarBlue assay in cell cultures. *Toxicology in vitro : an international journal published in association with BIBRA* **9**, 257–66.

[165] Hughes, L. C, Archer, C. W, & ap Gwynn, I. (2005) The ultrastructure of mouse articular cartilage: collagen orientation and implications for tissue functionality. A polarised light and scanning electron microscope study and review. *European cells & materials* **9**, 68–84.

[166] Othman, S. F, Li, J, Abdullah, O, Moinnes, J. J, Magin, R. L, & Muehleman, C. (2007) High-resolution/high-contrast MRI of human articular cartilage lesions. *Acta orthopaedica* **78**, 536–46.

[167] Welsing, R. T. C, van Tienen, T. G, Ramrattan, N, Heijkants, R, Schouten, A. J, Veth, R. P. H, & Buma, P. (2008) Effect on tissue differentiation and articular cartilage degradation of a polymer meniscus implant: A 2-year follow-up study in dogs. *The American journal of sports medicine* **36**, 1978–89.

[168] Olszta, M. J, Cheng, X, Jee, S. S, Kumar, R, Kim, Y.-Y, Kaufman, M. J, Douglas, E. P, & Gower, L. B. (2007) Bone structure and formation: A new perspective. *Materials Science and Engineering: R: Reports* **58**, 77–116.

[169] Yang, S, Leong, K. F, Du, Z, & Chua, C. K. (2001) The design of scaffolds for use in tissue engineering. Part I. Traditional factors. *Tissue engineering* **7**, 679–89.

[170] Cima, L. G, Langer, R, & Vacanti, J. P. (1991) Polymers for Tissue and Organ Culture. *Journal of Bioactive and Compatible Polymers* **6**, 232–240.

[171] Williams, D. F. (2009) On the nature of biomaterials. *Biomaterials* **30**, 5897–909.

[172] Gamboa-Martinez, T. C, Gomez Ribelles, J. L, & Gallego Ferrer, G. (2011) Fibrin coating on poly (L-lactide) scaffolds for tissue engineering. *Journal of Bioactive and Compatible Polymers* **26**, 464–477.

[173] Salerno, A, Zeppetelli, S, Oliviero, M, Battista, E, Di Maio, E, Iannace, S, & Netti, P. A. (2012) Microstructure, degradation and in vitro MG63 cells interactions of a new poly(e-caprolactone), zein, and hydroxyapatite composite for bone tissue engineering. *Journal of Bioactive and Compatible Polymers* **27**, 210–226.

[174] Setzer, B, Bächle, M, Metzger, M. C, & Kohal, R. J. (2009) The gene-expression and phenotypic response of hFOB 1.19 osteoblasts to surface-modified titanium and zirconia. *Biomaterials* **30**, 979–90.

[175] Forsey, R. W & Chaudhuri, J. B. (2009) Validity of DNA analysis to determine cell numbers in tissue engineering scaffolds. *Biotechnology letters* **31**, 819–23.

[176] Hellemans, J, Mortier, G, De Paepe, A, Speleman, F, & Vandesompele, J. (2007) qBase relative quantification framework and software for management and automated analysis of real-time quantitative PCR data. *Genome biology* **8**, R19.

[177] Wojtowicz, A. M, Ph, D, Templeman, K. L, Sc, B, Hutmacher, D. W, Guldberg, R. E, & Garcia, J. (2010) Runx2 Overexpression in Bone Marrow Stro-

mal Cells Accelerates Bone Formation in Critical-Sized Femoral Defects. **16**, 2795–2808.

[178] Mochida, Y, Parisuthiman, D, Pornprasertsuk-Damrongsri, S, Atsawasuwan, P, Sricholpech, M, Boskey, A. L, & Yamauchi, M. (2009) Decorin modulates collagen matrix assembly and mineralization. *Matrix biology : journal of the International Society for Matrix Biology* **28**, 44–52.

[179] Komori, T. (2010) Regulation of bone development and extracellular matrix protein genes by RUNX2. *Cell and tissue research* **339**, 189–95.

[180] Tsai, S.-W, Cheng, Y.-H, Chang, Y, Liu, H.-L, & Tsai, W.-B. (2010) Type I collagen structure modulates the behavior of osteoblast-like cells. *Journal of the Taiwan Institute of Chemical Engineers* **41**, 247–251.

[181] Galperin, A, Long, T. J, & Ratner, B. D. (2010) Degradable, thermo-sensitive poly(N-isopropyl acrylamide)-based scaffolds with controlled porosity for tissue engineering applications. *Biomacromolecules* **11**, 2583–92.

[182] Unger, R. E, Sartoris, A, Peters, K, Motta, A, Migliaresi, C, Kunkel, M, Bulnheim, U, Rychly, J, & Kirkpatrick, C. J. (2007) Tissue-like self-assembly in cocultures of endothelial cells and osteoblasts and the formation of microcapillary-like structures on three-dimensional porous biomaterials. *Biomaterials* **28**, 3965–76.

[183] Madden, L. R, Mortisen, D. J, Sussman, E. M, Dupras, S. K, Fugate, J. A, Cuy, J. L, Hauch, K. D, Laflamme, M. A, Murry, C. E, & Ratner, B. D. (2010) Proangiogenic scaffolds as functional templates for cardiac tissue engineering. *Proceedings of the National Academy of Sciences of the United States of America* **107**, 15211–6.

[184] Hulbert, S. F, Young, F. A, Mathews, R. S, Klawitter, J. J, Talbert, C. D, & Stelling, F. H. (1970) Potential of ceramic materials as permanently implantable skeletal prostheses. *Journal of biomedical materials research* **4**, 433–56.

[185] Tsuruga, E, Takita, H, Itoh, H, Wakisaka, Y, & Kuboki, Y. (1997) Pore size of porous hydroxyapatite as the cell-substratum controls BMP-induced osteogenesis. *Journal of biochemistry* **121**, 317–24.

[186] Götz, H. E, Müller, M, Emmel, A, Holzwarth, U, Erben, R. G, & Stangl, R. (2004) Effect of surface finish on the osseointegration of laser-treated titanium alloy implants. *Biomaterials* **25**, 4057–64.

[187] Kuboki, Y, Jin, Q, & Takita, H. (2001) Geometry of carriers controlling phenotypic expression in BMP-induced osteogenesis and chondrogenesis. *The Journal of bone and joint surgery. American volume* **83-A Suppl**, S105–15.

[188] Carano, R. A & Filvaroff, E. H. (2003) Angiogenesis and bone repair. *Drug Discovery Today* **8**, 980–989.

[189] Gemmiti, C. V & Guldberg, R. E. (2009) Shear stress magnitude and duration modulates matrix composition and tensile mechanical properties in engineered cartilaginous tissue. *Biotechnology and bioengineering* **104**, 809–20.

[190] Shah, A, Brugnano, J, Sun, S, Vase, A, & Orwin, E. (2008) The development of a tissue-engineered cornea: biomaterials and culture methods. *Pediatric research* **63**, 535–44.

[191] MacNeil, S. (2007) Progress and opportunities for tissue-engineered skin. *Nature* **445**, 874–80.

[192] MACNEIL, S. (2008) Biomaterials for tissue engineering of skin. *Materials Today* **11**, 26–35.

[193] Huang, A. H, Farrell, M. J, & Mauck, R. L. (2010) Mechanics and mechanobiology of mesenchymal stem cell-based engineered cartilage. *Journal of biomechanics* **43**, 128–36.

[194] Clar, C, Cummins, E, McIntyre, L, Thomas, S, Lamb, J, Bain, L, Jobanputra, P, & Waugh, N. (2005) Clinical and cost-effectiveness of autologous chondrocyte implantation for cartilage defects in knee joints: systematic review and economic evaluation. *Health technology assessment (Winchester, England)* **9**, iii–iv, ix–x, 1–82.

[195] Safran, M. R & Seiber, K. (2010) The evidence for surgical repair of articular cartilage in the knee. *The Journal of the American Academy of Orthopaedic Surgeons* **18**, 259–66.

[196] Nomi, M, Atala, A, Coppi, P. D, & Soker, S. (2002) Principals of neovascularization for tissue engineering. *Molecular aspects of medicine* **23**, 463–83.

[197] Cassell, O. C. S, Hofer, S. O. P, Morrison, W. A, & Knight, K. R. (2002) Vascularisation of tissue-engineered grafts: the regulation of angiogenesis in reconstructive surgery and in disease states. *British journal of plastic surgery* **55**, 603–10.

[198] Yu, H, VandeVord, P. J, Mao, L, Matthew, H. W, Wooley, P. H, & Yang,

S.-Y. (2009) Improved tissue-engineered bone regeneration by endothelial cell mediated vascularization. *Biomaterials* **30**, 508–17.

[199] Koike, N, Fukumura, D, Gralla, O, Au, P, Schechner, J. S, & Jain, R. K. (2004) Tissue engineering: creation of long-lasting blood vessels. *Nature* **428**, 138–9.

[200] Hofmann, A, Ritz, U, Verrier, S, Eglin, D, Alini, M, Fuchs, S, Kirkpatrick, C. J, & Rommens, P. M. (2008) The effect of human osteoblasts on proliferation and neo-vessel formation of human umbilical vein endothelial cells in a long-term 3D co-culture on polyurethane scaffolds. *Biomaterials* **29**, 4217–26.

[201] Laschke, M. W, Harder, Y, Amon, M, Martin, I, Farhadi, J, Ring, A, Torio-Padron, N, Schramm, R, Rücker, M, Junker, D, Häufel, J. M, Carvalho, C, Heberer, M, Germann, G, Vollmar, B, & Menger, M. D. (2006) Angiogenesis in tissue engineering: breathing life into constructed tissue substitutes. *Tissue engineering* **12**, 2093–104.

[202] Ghanaati, S, Unger, R. E, Webber, M. J, Barbeck, M, Orth, C, Kirkpatrick, J. a, Booms, P, Motta, A, Migliaresi, C, Sader, R. a, & Kirkpatrick, C. J. (2011) Scaffold vascularization inÂ vivo driven by primary human osteoblasts in concert with host inflammatory cells. *Biomaterials* **32**, 8150–60.

[203] Roche, B, David, V, Vanden-Bossche, A, Peyrin, F, Malaval, L, Vico, L, & Lafage-Proust, M.-H. (2011) Structure and quantification of microvascularisation within mouse long bones: what and how should we measure? *Bone* **50**, 390–399.

[204] Summer-Smith, G. (2002) *Bone in clinical orthopedics*. (Thieme).

[205] Rhinelander, F. W. (year?) Some aspects of the microcirculation of healing bone. *Clinical orthopaedics and related research* **40**, 12–6.

[206] Brown, D. L, Meagher, P. J, Knight, K. R, Keramidaris, E, Romeo-Meeuw, R, Penington, A. J, & Morrison, W. A. (2006) Survival and function of transplanted islet cells on an in vivo, vascularized tissue engineering platform in the rat: A pilot study. *Cell transplantation* **15**, 319–24.

[207] Mertsching, H, Walles, T, Hofmann, M, Schanz, J, & Knapp, W. H. (2005) Engineering of a vascularized scaffold for artificial tissue and organ generation. *Biomaterials* **26**, 6610–7.

[208] Hubbell, J. A. (2003) Materials as morphogenetic guides in tissue engineering. *Current opinion in biotechnology* **14**, 551–8.

[209] Lutolf, M. P & Hubbell, J. A. (2005) Synthetic biomaterials as instructive extracellular microenvironments for morphogenesis in tissue engineering. *Nature biotechnology* **23**, 47–55.

[210] Kim, B.-S & Mooney, D. J. (1998) Development of biocompatible synthetic extracellular matrices for tissue engineering. *Trends in Biotechnology* **16**, 224–230.

[211] Fuchs, S, Motta, A, Migliaresi, C, & Kirkpatrick, C. J. (2006) Outgrowth endothelial cells isolated and expanded from human peripheral blood progenitor cells as a potential source of autologous cells for endothelialization of silk fibroin biomaterials. *Biomaterials* **27**, 5399–408.

[212] Santos, M. I, Fuchs, S, Gomes, M. E, Unger, R. E, Reis, R. L, & Kirkpatrick, C. J. (2007) Response of micro- and macrovascular endothelial cells to starch-based fiber meshes for bone tissue engineering. *Biomaterials* **28**, 240–8.

[213] Unger, R. E, Huang, Q, Peters, K, Protzer, D, Paul, D, & Kirkpatrick, C. J. (2005) Growth of human cells on polyethersulfone (PES) hollow fiber membranes. *Biomaterials* **26**, 1877–84.

[214] Schumann, P, Tavassol, F, Lindhorst, D, Stuehmer, C, Bormann, K.-H, Kampmann, A, Mülhaupt, R, Laschke, M. W, Menger, M. D, Gellrich, N.-C, & Rücker, M. (2009) Consequences of seeded cell type on vascularization of tissue engineering constructs in vivo. *Microvascular research* **78**, 180–90.

[215] Laschke, M. W, Rücker, M, Jensen, G, Carvalho, C, Mülhaupt, R, Gellrich, N.-C, & Menger, M. D. (2008) Incorporation of growth factor containing Matrigel promotes vascularization of porous PLGA scaffolds. *Journal of biomedical materials research. Part A* **85**, 397–407.

[216] Perets, A, Baruch, Y, Weisbuch, F, Shoshany, G, Neufeld, G, & Cohen, S. (2003) Enhancing the vascularization of three-dimensional porous alginate scaffolds by incorporating controlled release basic fibroblast growth factor microspheres. *Journal of biomedical materials research. Part A* **65**, 489–97.

[217] Nomi, M, Miyake, H, Sugita, Y, Fujisawa, M, & Soker, S. (2006) Role of growth factors and endothelial cells in therapeutic angiogenesis and tissue engineering. *Current stem cell research & therapy* **1**, 333–43.

[218] von der Mark, K, Park, J, Bauer, S, & Schmuki, P. (2010) Nanoscale engineering of biomimetic surfaces: cues from the extracellular matrix. *Cell and tissue research* **339**, 131–53.

[219] Shin, H, Jo, S, & Mikos, A. G. (2003) Biomimetic materials for tissue engineering. *Biomaterials* **24**, 4353–4364.

[220] Fuchs, S, Hofmann, A, & Kirkpatrick, C. J. (2007) Microvessel-like structures from outgrowth endothelial cells from human peripheral blood in 2-dimensional and 3-dimensional co-cultures with osteoblastic lineage cells. *Tissue engineering* **13**, 2577–88.

[221] Unger, R. E, Ghanaati, S, Orth, C, Sartoris, A, Barbeck, M, Halstenberg, S, Motta, A, Migliaresi, C, & Kirkpatrick, C. J. (2010) The rapid anastomosis between prevascularized networks on silk fibroin scaffolds generated in vitro with cocultures of human microvascular endothelial and osteoblast cells and the host vasculature. *Biomaterials* **31**, 6959–67.

[222] Unger, R. E, Peters, K, Wolf, M, Motta, a, Migliaresi, C, & Kirkpatrick, C. J. (2004) Endothelialization of a non-woven silk fibroin net for use in tissue engineering: growth and gene regulation of human endothelial cells. *Biomaterials* **25**, 5137–46.

[223] Ghanaati, S, Orth, C, Unger, R. E, Barbeck, M, Webber, M. J, Motta, A, Migliaresi, C, & James Kirkpatrick, C. (2010) Fine-tuning scaffolds for tissue regeneration: effects of formic acid processing on tissue reaction to silk fibroin. *Journal of tissue engineering and regenerative medicine* **4**, 464–72.

[224] Pankajakshan, D & Agrawal, D. K. (2010) Scaffolds in tissue engineering of blood vessels. *Canadian journal of physiology and pharmacology* **88**, 855–73.

[225] Moutos, F. T & Guilak, F. (2008) Composite scaffolds for cartilage tissue engineering. *Biorheology* **45**, 501–12.

[226] Chen, M, Le, D. Q. S, Baatrup, A, Nygaard, J. V, Hein, S, Bjerre, L, Kassem, M, Zou, X, & Bünger, C. (2011) Self-assembled composite matrix in a hierarchical 3-D scaffold for bone tissue engineering. *Acta biomaterialia* **7**, 2244–55.

[227] Bondar, B, Fuchs, S, Motta, A, Migliaresi, C, & Kirkpatrick, C. J. (2008) Functionality of endothelial cells on silk fibroin nets: comparative study of micro- and nanometric fibre size. *Biomaterials* **29**, 561–72.

[228] Ghanaati, S, Barbeck, M, Orth, C, Willershausen, I, Thimm, B. W, Hoffmann, C, Rasic, A, Sader, R. A, Unger, R. E, Peters, F, & Kirkpatrick, C. J. (2010) Influence of β-tricalcium phosphate granule size and morphology on tissue reaction in vivo. *Acta biomaterialia* **6**, 4476–87.

[229] Lin, A. S. P, Barrows, T. H, Cartmell, S. H, & Guldberg, R. E. (2003) Mi-

croarchitectural and mechanical characterization of oriented porous polymer scaffolds. *Biomaterials* **24**, 481–9.

[230] Boerckel, J. D, Uhrig, B. a, Willett, N. J, Huebsch, N, & Guldberg, R. E. (2011) Mechanical regulation of vascular growth and tissue regeneration in vivo. *Proceedings of the National Academy of Sciences of the United States of America* **108**, E674–80.

[231] Sandino, C, Planell, J. a, & Lacroix, D. (2008) A finite element study of mechanical stimuli in scaffolds for bone tissue engineering. *Journal of biomechanics* **41**, 1005–14.

[232] Fuchs, S, Jiang, X, Schmidt, H, Dohle, E, Ghanaati, S, Orth, C, Hofmann, A, Motta, A, Migliaresi, C, & Kirkpatrick, C. J. (2009) Dynamic processes involved in the pre-vascularization of silk fibroin constructs for bone regeneration using outgrowth endothelial cells. *Biomaterials* **30**, 1329–38.

[233] Olsen, B. R, Reginato, A. M, & Wang, W. (2000) Bone development. *Annual review of cell and developmental biology* **16**, 191–220.

[234] Sims, N. A & Gooi, J. H. (2008) Bone remodeling: Multiple cellular interactions required for coupling of bone formation and resorption. *Seminars in cell & developmental biology* **19**, 444–51.

[235] Villars, F, Guillotin, B, Amédée, T, Dutoya, S, Bordenave, L, Bareille, R, & Amédée, J. (2002) Effect of HUVEC on human osteoprogenitor cell differentiation needs heterotypic gap junction communication. *American journal of physiology. Cell physiology* **282**, C775–85.

[236] Finkenzeller, G, Arabatzis, G, Geyer, M, Wenger, A, Bannasch, H, & Stark, G. B. (2006) Gene expression profiling reveals platelet-derived growth factor receptor alpha as a target of cell contact-dependent gene regulation in an endothelial cell-osteoblast co-culture model. *Tissue engineering* **12**, 2889–903.

[237] Zhang, Y, Schedle, A, Matejka, M, Rausch-Fan, X, & Andrukhov, O. (2010) The proliferation and differentiation of osteoblasts in co-culture with human umbilical vein endothelial cells: An improved analysis using fluorescence-activated cell sorting. *Cellular & molecular biology letters* **15**, 517–29.

[238] Villars, F, Bordenave, L, Bareille, R, & Amédée, J. (2000) Effect of human endothelial cells on human bone marrow stromal cell phenotype: role of VEGF? *Journal of cellular biochemistry* **79**, 672–85.

[239] Grellier, M, Ferreira-Tojais, N, Bourget, C, Bareille, R, Guillemot, F, &

Amédée, J. (2009) Role of vascular endothelial growth factor in the communication between human osteoprogenitors and endothelial cells. *Journal of cellular biochemistry* **106**, 390–8.

[240] Bianchi Scarrà, G, Fiorentini, P, Garbarino, G, Bellone, G, Sessarego, M, & Ajmar, F. (1985) Effect of endothelial cell conditioned medium on the growth of human bone marrow fibroblasts. *Journal of cellular physiology* **123**, 343–6.

[241] Villanueva, J. E & Nimni, M. E. (1990) Promotion of calvarial cell osteogenesis by endothelial cells. *Journal of bone and mineral research : the official journal of the American Society for Bone and Mineral Research* **5**, 733–9.

[242] Jones, A. R, Clark, C. C, & Brighton, C. T. (1995) Microvessel endothelial cells and pericytes increase proliferation and repress osteoblast phenotypic markers in rat calvarial bone cell cultures. *Journal of orthopaedic research : official publication of the Orthopaedic Research Society* **13**, 553–61.

[243] Meury, T, Verrier, S, & Alini, M. (2006) Human endothelial cells inhibit BMSC differentiation into mature osteoblasts in vitro by interfering with osterix expression. *Journal of cellular biochemistry* **98**, 992–1006.

[244] Guillotin, B, Bourget, C, Remy-Zolgadri, M, Bareille, R, Fernandez, P, Conrad, V, & Amédée-Vilamitjana, J. (2004) Human primary endothelial cells stimulate human osteoprogenitor cell differentiation. *Cellular physiology and biochemistry : international journal of experimental cellular physiology, biochemistry, and pharmacology* **14**, 325–32.

[245] Stoppato, M, Stevens, H. Y, Carletti, E, Migliaresi, C, Motta, A, & Guldberg, R. E. (2013) Effects of silk fibroin fiber incorporation on mechanical properties, endothelial cell colonization and vascularization of PDLLA scaffolds. *Biomaterials*.

Scientific Production

Manuscripts on International Journals

M. Stoppato, E. Carletti, D. Maniglio, C. Migliaresi, A. Motta: "Functional role of scaffold geometries as a template for physiological ECM formation: evaluation of collagen 3D assembly" *Journal of tissue engineering and regenerative medicine*, 7(2), 161–8.

M. Stoppato, E. Carletti, V. Sidarovich, A. Quattrone, R. E. Unger, C. J. Kirkpatrick, C. Migliaresi, A. Motta: "Influence of Scaffold Pore Size on Collagen I Development: a New In Vitro Evaluation Perspective" *Journal of Bioactive and Compatible Polymers*, 28(1), 16–32.

M. Stoppato, H.Y. Stevens, E. Carletti, A. Motta, C. Migliaresi, R.E. Guldberg: "Effects of silk fibroin fiber incorporation on mechanical properties, endothelial cell colonization and vascularization of PDLLA scaffolds" *Biomaterials*, doi:10.1016/j.biomaterials.2013.02.009

Partecipation to Congresses and Schools

June 7-10 2011

TERMIS EU Chapter meeting 2011 Granada (Spain).

Oral presentation: M. Stoppato, E. Carletti, C. Migliaresi, A. Motta: "Influence of Pores Geometry and Architecture on Collagen 3D Assembling".

Congress proceedings: Histology and Histopathology, vol 26, issue supplement 1, 2011.

July 9-13 2012

Summer School on Biomaterials and Regenerative Medicine: "Bioinspired and biomimetic materials and scaffolds: from nature communication and design strategies" – Riva del Garda (Italy).

Lectures:

M. Stoppato, H.Y. Stevens, E. Carletti, A. Motta, C. Migliaresi, R.E. Guldberg: "Bone tissue engineering and vascularization: the influence of silk fibroin net added to a PDLLA salt leached scaffold ".

M. Stoppato, E. Carletti, V. Sidarovich, A. Quattrone, R. E. Unger, C. J. Kirkpatrick, C. Migliaresi, A. Motta: "ECM Production and Assembly: Effects of Scaffold Morphology".

September 5-8 2012

TERMIS World Congress 2012 Vienna (Austria).

Poster presentation: M. Stoppato, H.Y. Stevens, E. Carletti, A. Motta, C. Migliaresi, R.E. Guldberg: "Influence of Silk Fibroin Fibers on Mechanical and Biological Properties of PDLLA Salt-leached Scaffolds".

Congress proceedings: Journal of Tissue Engineering and Regenerative Medicine, vol 6, issue supplement 1, 2012.

Other activities

May – July 2010

Stage abroad.

Institute of Pathology at The Johannes Gutenberg University – Mainz (Germany).

Advisor: prof. Ronald E. Unger, prof. C. James Kirkpatrick.

September 2011 – March 2012

Research abroad.

Guldberg Lab, Parker H. Petit Institute of Bioengineering and Bioscience, Georgia Institute of Technology – Atlanta (USA).

Advisor: prof. Robert E. Guldberg.

Acknowledgments

In the last three years I had the chance to work in different labs and to know many people.

Hopeful that I won't forget anyone.

BIOtech lab, my home lab.

First, I would love to thank Dr. Antonella Motta, my advisor, who helped and supported me during this incredible experience. Of course I cannot forget Prof. Claudio Migliaresi for creating this lab and for his challenging attitude that forced me to consider and evaluate data and results.

Eleonora. Advisor and FRIEND. Thank you for your guidance both in my work and life.

Cristina. "Amazing colleague". You are the proof that change is possible.

Lucia. Reserved but careful friend.

All the people in this lab who make it such a fun place to work and live.

Elisa, Thiago, Fedrizza and Marta. For sharing PhD moments and many spritz!

Viky. For being so helpful, positive and always smiling.

REPAIR lab at the Institute of Pathology at the University Medical Center of the Johannes Gutenberg (Mainz).

I want to express my gratitude to Prof. C. James Kirkpatrick, Dr Ronald E. Unger and Anne Sartoris for introducing me to the amazing 'endothelial world'. I truly appreciated the scientific environment and the 'German organization'. Thanks to all the people of the lab.

This period would not had been so great without the friendship of some outstanding girls: Amparo, Lour, Susana and Natalia.

Guldberg lab at the Institute of Georgia Technology (Atlanta).

Bob. You have made possible one of the best times of my life. Having had the chance to work in this inspirational lab makes me proud. It is really an amazing environment full of opportunities. I must thank all the colleagues of this lab, really supportive and collaborative.

A special thank to Hazel: unique, sarcastic and wise mentor.

To Jason and Taran, for your friendship, comprehension and chats.

Luckily, I met some great guys even out the Lab.

Ceara. You helped me so much. And make me feel part of your own family!!!!!! Thank you!

Giulia. We shared so many memories in a short time! It was amazing!

Thomas and Aurelien. Turns out French guys can be cool too ;-)!!!!!

Kevin and Anika: best roommates ever!

Next I have to thank my life-long friends.

Boruz, Mene, Marta: a well assembled triad, giants on whose shoulders I stand. People I could always count on. GRAZIE!!!!!

Andrea, Piva, Banti: for the friendship you have provided over the years.

Ele and Nico. Best fellow graduate students I could met!

Ilaria, Soi, Moltrer, Mitch, Vale, Ele and all the UFOs... for being part of my life and sharing great parties, drinks, nights... and much more.

Lastly and mostly, I would like to thank my family.

Mum and dad... for the constant love, support and for providing me with infinite opportunities.

Silvia, Ale, Emma. For your example. And for being so close and really understanding.

Grandma 'nonnaGina'. My angel.

Sandra and Cami. Best aunt and cousin ever!

Rina and Robi. Because you have always been there for me.

Of course I would have to thank many other people.... I know. You know. ;-)